

8-25-2011

A theoretical and experimental analysis of SBS suppression through modification of amplifier seed

Clint M. Zeringue

Follow this and additional works at: https://digitalrepository.unm.edu/ose_etds

Recommended Citation

Zeringue, Clint M.. "A theoretical and experimental analysis of SBS suppression through modification of amplifier seed." (2011).
https://digitalrepository.unm.edu/ose_etds/49

This Dissertation is brought to you for free and open access by the Engineering ETDs at UNM Digital Repository. It has been accepted for inclusion in Optical Science and Engineering ETDs by an authorized administrator of UNM Digital Repository. For more information, please contact disc@unm.edu.

Student Name

Clint Matthew Zeringue

Graduate Unit (Department)

Optical Science and Engineering

This dissertation is approved, and it is acceptable in quality and form for publication:

Approved by the Dissertation Committee:

_____, Chairperson

**A Theoretical and Experimental Analysis of SBS Suppression Through
Modification of Amplifier Seed**

BY

Clint Matthew Zeringue

B.S., Applied Physics, U.S. Air Force Academy, 2005
M.S., Applied Physics, Air Force Institute of Technology, 2006
Ph.D., Optical Science and Engineering, University of New Mexico, 2011

DISSERTATION

Submitted in Partial Fulfillment of the
Requirements for the Degree of

Doctor of Philosophy

Optical Science and Engineering

The University of New Mexico
Albuquerque, New Mexico

May, 2011

DEDICATION

I dedicate this dissertation to my wife Melissa and my parents Barry and Lisa. Their love, encouragement, support, and sacrifices over the years have made this dream possible.

To my supportive and loving wife Melissa, who took this journey with me despite personal sacrifices, for allowing me to follow my life passion, for believing in me when others didn't, and for helping me grow as a person. To my father Barry, who enabled me to have a privileged and loving childhood, for teaching me that being a man, means taking responsibility for ones actions, providing for your family, and always standing up for what you believe in despite what is popular. To my mother Lisa, who loved me unconditionally as a child, and who taught and continues to teach me that humility, compassion, and appreciation are virtues never to be forgotten.

ACKNOWLEDGMENTS

I heartily acknowledge Dr. Iyad Dajani, my advisor and scientific mentor, for nurturing my love of science and for putting in the long hours with me to help create the content in this dissertation. His scientific and professional guidance will remain with me as I continue my career.

I also thank my committee members, Dr. Luke Lester, Dr. Wolfgang Rudolph, and Dr. Alan Paxton, for their valuable recommendations pertaining to this study and assistance in my professional development. Gratitude is extended to the Air Force Research Laboratory, Joint Technology Office (JTO), and Air Force Office of Scientific Research (AFOSR) for funding me to pursue this research.

To Dr. Gerry Moore, research physicist from the Air Force Research Laboratory, for the guidance on constructing the Langevin noise source used in this study. To my co-workers, Christopher Vergien, Craig Robin, and Chunte Lu for the guidance and help with the experimental portions of this work.

And finally to my wife, Melissa, your love is the greatest gift of all.

**A Theoretical and Experimental Analysis of SBS Suppression Through
Modification of Amplifier Seed**

BY

Clint Matthew Zeringue

ABSTRACT OF DISSERTATION

Submitted in Partial Fulfillment of the
Requirements for the Degree of

Doctor of Philosophy

Optical Science and Engineering

The University of New Mexico
Albuquerque, New Mexico

May, 2011

**A Theoretical and Experimental Analysis of SBS Suppression Through
Modification of Amplifier Seed**

By

Clint Matthew Zeringue

B.S., Applied Physics, U.S. Air Force Academy, 2005
M.S., Applied Physics, Air Force Institute of Technology, 2006
Ph.D., Optical Science and Engineering, University of New Mexico, 2011

ABSTRACT

Theoretical and experimental investigations of stimulated Brillouin scattering (SBS) are conducted in Yb-doped fiber amplifiers when the amplifier is simultaneously seeded with multiple distinct frequencies or with a phase modulated signal. To this end, detailed models of the SBS process are developed consisting of both a steady-state approach described mathematically by a coupled set of ordinary differential equations and also transient effects described by a coupled set of partial differential equations.

For the multi-frequency seeded case, the equations are solved in the steady-state limit and include the effects of four-wave mixing (FWM), intrinsic and external thermal gradients, and laser gain. In one configuration of the multi-seeded case, the signals are separated at twice the acoustic frequency of the fiber medium in order to create nonlinear Brillouin gain coupling between the seeds and Stokes signals, which suppresses the SBS process in the highest frequency seed. The concept is theoretically investigated for the two and three seeded cases. It is shown that for this scheme, FWM becomes quite significant making this concept unlikely in a practical application requiring single-frequency output.

Alternatively, a novel concept is developed to suppress SBS in fiber amplifiers that relies on laser gain competition among multiple seeds to create both a favorable thermal gradient and a reduced effective length for the SBS process. In one configuration, the amplifier is simultaneously seeded with a broadband ($\Delta\lambda \sim 0.1nm$) and single-frequency $\Delta\nu \sim 100kHz$ seed. In this case, several experiments are performed to validate the theoretical predictions with experiments leading to a 203 W polarization maintaining (PM), co-pumped monolithic fiber amplifier demonstration. To the best of our knowledge, this output power is the highest reported in the literature to date for such an amplifier.

A time-dependent model of the SBS process initiated from random thermal noise is also developed to study SBS suppression under phase modulated pump conditions. The SBS suppression is characterized for several phase modulation schemes. It is found that the SBS suppression for a white-noise phase modulation (WNS) which broadens the pump spectrum, depends significantly on the length of fiber and only in the long fiber limit follows the often quoted threshold enhancement formula of $P_{th} = P_0 \left(1 + \Delta\nu / \Delta\nu_B\right)$ where P_0 , $\Delta\nu$ and $\Delta\nu_B$ describe the SBS threshold of the single-frequency case, the effective linewidth of the pump, and the spontaneous Brillouin linewidth respectively. In addition, the SBS threshold is characterized as a function of modulation amplitude and frequency for a single-sinusoidal phase modulation scheme.

TABLE OF CONTENTS

LIST OF FIGURES	xi
LIST OF TABLES	xxiii
CHAPTER 1 INTRODUCTION.....	1
1.1 Introduction to nonlinear optics in fibers.....	1
1.2 Dissertation Statement	5
1.3 Stimulated Brillouin Scattering (SBS)	6
1.4 Overview.....	9
1.5 Significance of the Dissertation Study.....	10
1.6 Description of Dissertation Chapters	12
CHAPTER 2 REVIEW OF RELATED LITERATURE	14
2.1 SBS Mitigation in Fibers through Multi-Tone Seeding.....	14
2.2 Time-Dependent Modeling of SBS in Fibers	17
2.3 Modeling SBS Suppression through Phase Modulation in the Fourier Domain ...	18
2.4 Experimental Results of SBS Suppression through Phase Modulation.....	20
CHAPTER 3 MULTI-TONE SEEDING AT TWICE THE BRILLOUIN SHIFT ...	22
3.1 Introduction.....	22
3.2 Theoretical Framework.....	23
3.3 Four-Wave Mixing Effects	29
3.4 Optimization of Seed Ratios	31
3.5 Numerical Results.....	32
3.5.1 Two-Tone Simulations.....	32
3.5.2 Three-Tone Simulations.....	36

3.6 Summary	40
CHAPTER 4 MULTI-TONE SEEDING (LASER GAIN COMPETITION).....	42
4.1 Introduction.....	42
4.2 Numerical Results (Two-Tone Simulations)	43
4.3 Numerical Results (Three-Tone Simulations)	52
4.4 Fiber length and Comparison to Counter-Pumping.....	56
4.5 Seeding with Broad-Band and Narrow-Line Signals.....	59
4.6 Thermal Effects.....	63
4.7 Summary	71
CHAPTER 5 MULTI-TONE SEEDING (EXPERIMENTAL RESULTS)	72
5.1 Introduction.....	73
5.2 Low-Power Demonstration.....	73
5.2.1 Experimental Setup.....	73
5.2.2 Experimental Results and Analysis	74
5.3 High-Power Demonstration	77
5.3.1 Experimental Setup.....	77
5.3.2 Experimental Results and Analysis	80
5.4 Summary.....	85
CHAPTER 6 TIME DEPENDENT SBS WITH PHASE MODULATION.....	87
6.1 Introduction.....	87
6.2 Theoretical Framework.....	88
6.3 Numerical Approach.....	92
6.4 Model Validation	93
6.5 Phase Modulation Schemes and SBS Threshold Effects.....	97
6.5.1 Single-Sinusoidal Modulation	97
6.5.2 White-Noise Modulation	101

6.6 Summary	105
CHAPTER 7 CONCLUSION	107
7.1 Summary	107
7.2 Suggestions for Future Work	109
REFERENCES.....	110

LIST OF FIGURES

Figure 1. An example of total internal reflection in a fiber waveguide. The light propagates down the core of the fiber since the core optical index is larger than the cladding index $n_c > n_{clad}$ 1

Figure 2. An example of a fiber amplifier. The signal light propagates down the core of the fiber and is amplified when the cladding pump light from a laser diode (LD) is absorbed by the Yb ion which re-emits light at the signal wavelength through stimulated emission.....3

Figure 3. Diagram depicting the technological advancements in power scaling single-frequency co-pumped and counter-pumped fiber amplifiers over the last decade. Colored regions depict advancements in SBS mitigation which increase the SBS threshold. The various research institutions responsible for the power level milestones are also labeled.....4

Figure 4. Three wave interaction of the SBS process. An incident field is scattered off an acoustic wave, which generates the Stokes wave that travels in the backward direction.8

Figure 5. Brillouin-scattering scheme with two single-frequency lasers separated by twice the Brillouin frequency shift Ω_B16

Figure 6. Example of a Yb-doped fiber amplifier with laser signal propagating in the core and pump light propagating in the cladding through total internal reflection (TIR).....23

Figure 7. Input Seeds and FWM sidebands23

Figure 8. Yb energy level diagram (left) and emission and absorption cross-sections of Yb-doped silica fiber (right).[30,31]..... 26

Figure 9. The signal power evolution of a two-tone amplifier compared with a single-tone amplifier. The power of the $\lambda = 1068nm$ single-tone case (red) reaches 28 W of output power before the SBS threshold is reached. The total output of the two-tone case with signals oscillating at $\omega_2 = \omega_1 + \Delta\omega$, $\lambda_2 \sim 1067.9nm$ (green) and $[\omega_1, \lambda_1 = 1068nm]$ (blue) was over 80 W. In the two-tone amplifier, the two signals are separated by twice the Brillouin shift ($\Delta\omega = 2\Omega_B \sim 32GHz$, $\Delta\lambda \sim .1nm$), allowing the Stokes light oscillating at $\omega_{s,2}$ generated by the signal oscillating at ω_2 to transfer its energy to the signal light oscillating at ω_1 . The seed ratio for the two-tone case is $P_2 / P_1 = 2$34

Figure 10. The FWM power generated in the inner sidebands $[\omega_3 = \omega_1 + 2\Delta\omega, \lambda_3 \sim 1067.8nm]$ (red) and $[\omega_4 = \omega_1 - \Delta\omega, \lambda_4 \sim 1068.1nm]$ (blue) shown in Figure 7 for the two-tone amplifier. Due to the small wavelength separation FWM is the lowest threshold nonlinear process. $(\Delta\omega = 2\Omega_B \sim 32GHz, \Delta\lambda \sim .1nm)$35

Figure 11. The dependence of total output power for two-tone amplifier on seed power ratio. The two frequencies are separated by twice the Brillouin shift. Here, The seed power ratio is defined as the input power of the higher frequency wave divided by that of the lower frequency $P(\omega_2) / P(\omega_1)$ and the total seed is 2 W..... 35

Figure 12. The signal power evolution of a three-tone amplifier compared with a single-tone amplifier. The power of the $\lambda = 1064nm$ single-tone case (red) reaches 28 W of output power before the SBS threshold is reached. The total output of the three-tone case with signals oscillating at $\omega_3 = \omega_1 + 2\Delta\omega$, $\lambda_3 \sim 1063.8nm$ (black), $\omega_2 = \omega_1 + \Delta\omega$, $\lambda_2 \sim 1063.9nm$ (green) and $[\omega_1, \lambda_1 = 1064nm]$ (blue) was approx. 152 W. In the three-tone amplifier, the three signals are separated by twice the Brillouin shift ($\Delta\omega = 2\Omega_B \sim 32GHz$, $\Delta\lambda \sim .1nm$), allowing the Stokes light oscillating at $\omega_{s,3}$ generated by the signal oscillating at ω_3 and the Stokes light oscillating at $\omega_{s,2}$ generated by the signal oscillating at ω_2 to transfer energy to the signals oscillating at ω_2 and ω_1 respectively. The seed ratios for the three-tone case are: $P_3 / P_1 = 3$ and $P_2 / P_1 = 2$ and the total seed power is 2W.37

Figure 13. Spatial power evolution of the three Stokes waves $\omega_{s,1} = \omega_1 - \Omega_B$ (black), $\omega_{s,2} = \omega_2 - \Omega_B$ (green), and $\omega_{s,3} = \omega_3 - \Omega_B$ (blue). The Stokes waves propagate counter to the laser signals.38

Figure 14. The FWM power generated in the inner and outer sidebands $[\omega_5 = \omega_1 + 3\Delta\omega, \lambda_5 \sim 1063.7nm]$ (solid blue), $[\omega_4 = \omega_1 - \Delta\omega, \lambda_4 \sim 1064.1nm]$ (solid red), $[\omega_7 = \omega_1 + 4\Delta\omega, \lambda_7 \sim 1063.6nm]$ (dashed blue) and $[\omega_6 = \omega_1 - 2\Delta\omega, \lambda_6 \sim 1064.2nm]$ (dashed red) shown in Figure 7 for the three-tone amplifier. Due to the small wavelength separation FWM is the lowest threshold nonlinear process. ($\Delta\omega = 2\Omega_B \sim 32GHz$, $\Delta\lambda \sim .1nm$).39

Figure 15. Surface plot of the total laser output power versus seed power ratios indicating optimal conditions for a total seed power of 2 W for the three-tone case. Here the seed ratios are defined as: $P3 / P1 = P(\omega_3) / P(\omega_1)$ and $P2 / P1 = P(\omega_2) / P(\omega_1)$.40

Figure 16. The sensitivity of SBS to the ratio of the input signals in ‘two-tone’ amplification. The x-axis shows the ratio of power in one input signal (1068nm) to the total input power. The y-axis represents percentage of Stokes power. The total seed power was fixed at 2 W.45

Figure 17. The signal power evolution of a two-tone amplifier compared with a single-tone amplifier using laser gain-competition. The power of the $\lambda = 1064nm$ single-tone case (red) reaches 28 W of output power before the SBS threshold is reached. The total output of the two-tone case with signals oscillating at $\omega_2 = \omega_1 + \Delta\omega$, $\lambda_2 \sim 1064nm$ (green) and $[\omega_1, \lambda_1 = 1068nm]$ (blue) was approx. 54 W. In the two-tone amplifier, the two signals are separated by $(\Delta\omega \sim 1THz, \Delta\lambda \sim 4nm)$. The input seed powers were 1.2 W and 0.8 W for the 1064nm and 1068nm signals respectively.46

Figure 18. Spatial power evolution of the three Stokes waves $[\omega_{S,1} = \omega_1 - \Omega_B, \lambda_1 = 1068nm]$ (blue), $[\omega_{S,2} = \omega_2 - \Omega_B, \lambda_2 = 1064nm]$ (green). The Stokes waves propagate counter to the laser signals.47

Figure 19. The FWM power generated in the inner sidebands $[\omega_3 = \omega_1 + 2\Delta\omega, \lambda_3 \sim 1060nm]$ (red) and $[\omega_4 = \omega_1 - \Delta\omega, \lambda_4 \sim 1072nm]$ (blue) shown in Figure 7 for the two-tone amplifier. $(\Delta\omega = 1THz, \Delta\lambda \sim 4nm)$. Note that the power in these sidebands is one order of magnitude lower than the SBS power.47

Figure 20. The FWM behavior of SBS-suppressed two-tone amplifiers with a) 350 W (left) and b) 550 W (right) of pump power. The FWM power generated in the inner sidebands $[\omega_3 = \omega_1 + 2\Delta\omega, \lambda_3 \sim 1060nm]$ (red) and $[\omega_4 = \omega_1 - \Delta\omega, \lambda_4 \sim 1072nm]$ (blue) shown in Figure 7 for the two-tone amplifier. ($\Delta\omega = 1THz, \Delta\lambda \sim 4nm$). The additional pumping has altered the coherence period relative to that shown in Figure 14 due to SPM and XPM.49

Figure 21. T The signal power evolution of a two-tone amplifier compared with a single-tone amplifier using laser gain-competition. The power of the $\lambda = 1064nm$ single-tone case (red) reaches 28 W of output power before the SBS threshold is reached. The total output of the two-tone case with signals oscillating at $\omega_2 = \omega_1 + \Delta\omega, \lambda_2 \sim 1050nm$ (green) and $[\omega_1, \lambda_1 = 1064nm]$ (blue) was approx. 54 W but in this case over 46 W was generated in the 1064nm signal and represents a 64% enhancement in the SBS threshold relative to the single-tone case. In the two-tone amplifier, the two signals are separated by ($\Delta\omega \sim 3.7THz, \Delta\lambda \sim 14nm$). The input seed power ratio was approximately 9:1 with the 1050nm signal having the higher seed power.50

Figure 22. Total Stokes gain for the 1064 nm light for the two-tone (blue) and single-tone (red) cases. For the two-tone case the pump power is approximately 38 W which generated an output 1064 nm power of approximately 28 W (equal to the output at threshold in the single tone case).51

Figure 23. The FWM power generated in the inner and outer sidebands $[\omega_5 = \omega_1 + 3\Delta\omega, \lambda_5 \sim 1052nm]$ (solid blue), $[\omega_4 = \omega_1 - \Delta\omega, \lambda_4 \sim 1068nm]$ (solid

red), $[\omega_7 = \omega_1 + 4\Delta\omega, \lambda_7 \sim 1048nm]$ (dashed blue) and $[\omega_6 = \omega_1 - 2\Delta\omega, \lambda_6 \sim 1072nm]$ (dashed red) shown in Figure 7 for the three-tone amplifier. Due to the large wavelength separation FWM is much lower than the previous cases considered. $(\Delta\omega \approx 1THz, \Delta\lambda \sim 4nm)$53

Figure 24. The signal power evolution of a three-tone amplifier compared with a single-tone amplifier using laser gain competition. The power of the $\lambda = 1064nm$ single-tone case (red) reaches 28 W of output power before the SBS threshold is reached. The total output of the three-tone case with signals oscillating at $\omega_3 = \omega_1 + 2\Delta\omega, \lambda_3 \sim 1056nm$ (black), $\omega_2 = \omega_1 + \Delta\omega, \lambda_2 \sim 1060nm$ (green) and $[\omega_1, \lambda_1 = 1064nm]$ (blue) was approx. 80 W. In the three-tone amplifier, the three signals are separated by $(\Delta\omega = 1THz, \Delta\lambda \sim 4nm)$. In addition the 1064nm signal output at SBS threshold was over 60 W; more than twice the SBS threshold of the single-tone case. The seed ratios for the three-tone case are: $P_1 : P_2 : P_3 = 1 : 2.7 : 4$.54

Figure 25. The signal power evolution of a three-tone amplifier compared with a single-tone amplifier using laser gain competition. The power of the $\lambda = 1070nm$ single-tone case (red) reaches 28 W of output power before the SBS threshold is reached. The total output of the three-tone case with signals oscillating at $\lambda_3 \sim 1040nm$ (black), $\lambda_2 \sim 1044nm$ (green) and $\lambda_1 = 1070nm$ (blue) was approx. 75 W. In the three-tone amplifier, the 1070nm signal output at SBS threshold was over 60 W: 2.2 times the SBS threshold of the single-tone case.....55

Figure 26. Total Stokes gain for the 1070 nm light for the three-tone (blue) and single-tone (red) cases. For comparison purposes, the pump light for each case was

adjusted such that both case had the same output power at 1070 nm. Note the reduced Stokes gain for the three-tone case, thus allowing for increased pump power.....56

Figure 27. The signal power evolution of a three-tone amplifier compared with a single-tone amplifier using laser gain competition. The power of the $\lambda = 1070nm$ single-tone case (red) reaches 44.5 W of output power before the SBS threshold is reached. The output signals of the three-tone case with signals oscillating at $\lambda_3 \sim 1040nm$ (black), $\lambda_2 \sim 1044nm$ (green) and $\lambda_1 = 1070nm$ (blue) is shown. In the three-tone amplifier, the 1070nm signal output at SBS threshold was approx. 83 W: 1.9 times the SBS threshold of the single-tone case.57

Figure 28. The signal power evolution of a two-tone amplifier and a counter pumped amplifier pumped to the SBS threshold. The pump power in this case was 92 W. Both amplifiers reach an output power of 77 W before the onset of the SBS threshold is reached and rely on SBS suppression through a rapid rise in the signal growth near the output end of the fiber.58

Figure 29. The signal power evolution of a two-tone amplifier compared with a single-tone amplifier using laser gain competition. The power of the $\lambda = 1064nm$ single-tone case (red) reaches 28 W of output power before the SBS threshold is reached. The output signals of the two-tone case with signals oscillating at $\lambda_2 \sim 1040nm$ (green) and $\lambda_1 = 1064nm$ (blue) is shown. In the two-tone amplifier, the 1064nm signal output at SBS threshold was approx. 74 W (2.6 times that of the single-tone case). The 1040 nm light possesses broad linewidth and the 1064 nm light is narrow.60

Figure 30. The signal power evolution of a two-tone amplifier (at optimal efficiency) compared with a single-tone amplifier using laser gain competition. The power of the $\lambda = 1064nm$ single-tone case (red) reaches 28 W of output power before the SBS threshold is reached. The output signals of the two-tone case with signals oscillating at $\lambda_2 \sim 1040nm$ (green) and $\lambda_1 = 1064nm$ (blue) is shown. In the two-tone amplifier, the 1064nm signal output at SBS threshold was approx. 56 W using approx. 200mW of 1064 nm seed.61

Figure 31. The signal power evolution of a two-tone amplifier at 4.5m near maximum efficiency (71%) compared with a single-tone amplifier (efficiency 79%) using laser gain competition. The power of the $\lambda = 1064nm$ single-tone case (red) reaches approx. 40 W of output power before the SBS threshold is reached. The output signals of the two-tone case with signals oscillating at $\lambda_2 \sim 1040nm$ (green) and $\lambda_1 = 1064nm$ (blue) is shown. In the two-tone amplifier, the 1064nm signal output at SBS threshold was approx. 88 W. The 1040 nm light possesses broad linewidth and the 1064 nm light is narrow.62

Figure 32. The signal power evolution of a two-tone amplifier at 3m near maximum efficiency (61%) compared with a single-tone amplifier (67% efficiency) using laser gain competition. The power of the $\lambda = 1064nm$ single-tone case (red) reaches approx. 72 W of output power before the SBS threshold is reached. The output signals of the two-tone case with signals oscillating at $\lambda_2 \sim 1040nm$ (green) and $\lambda_1 = 1064nm$ (blue) is shown. In the two-tone amplifier, the 1064nm signal output at SBS threshold was approx. 122 W. The 1040 nm light possesses broad linewidth and the 1064 nm light is narrow.....63

Figure 33. Skeleton diagram of fiber cross-section detailing the core, cladding, and polymer jacket surrounding a fiber.	69
Figure 34. Spatial evolution of the 1030 nm (Broad Band) and 1080 nm (Narrow-Line) signals. Power is normalized to output power from co-pumped single tone at SBS threshold.....	58
Figure 35. Temperature profiles for different configurations. SBS process turned off for single-tone co-pump to allow for comparable pumping power.	71
Figure 36. Experimental set-up. The 1045 nm laser was built in-house. The system of WDMs is used to combine or to separate the signals.	74
Figure 37. Stokes power vs. 1064 nm light power for single-and two-tone seeding showing increase in SBS threshold. The seed powers for these experiment were 800 mW for the single-tone case and (700/65) mW (high-ratio), (350/65) mW (low-ratio) in the (1045/1064) nm signals respectively.	75
Figure 38. Spectral content of backward light for two-tone configuration for high seed ratio case. Stokes light below the Rayleigh light indicates operation below the SBS threshold.....	76
Figure 39. Power output of 1064 nm signal vs. input pump power for two-tone. Efficiency is comparable to single-tone seeding.	77
Figure 40. Experimental set-up of monolithic two-tone fiber amplifier system. PD 1, PD 2, PD 3, and PD 4 are photodiodes. ISO 1 and ISO 2 are isolators. PM 1, PM 2, and PM 3 are power meters.	78
Figure 41. Reflectivity vs. 1065nm signal output power for monolithic amplifier in different thermal configurations : single tone all on cold spool, 1035 nm two-tone all	

on cold spool, and 1035 nm two tone with 6 m on cold spool and 1 m left to cool in air under ambient conditions (thus utilizing quantum defect heating).....	81
Figure 42 Comparison of output power in the single frequency 1065 nm channel versus launched power for single tone and the two-tone thermal configuration utilizing quantum defect heating. The broadband seed for the latter operated at 1035 nm.	82
Figure 43. Output power as a function of launch power and reflectivity the for cold plate hot plate configuration with the broadband seed operating at 1040 nm.	75
Figure 44. Output power as a function of launch power and reflectivity the for cold plate hot plate configuration with the broadband seed operating at 1035 nm. The theoretical results using the equations developed in Chapter 4 are shown for comparison.	84
Figure 45. Spectral content of the backscattered light at various signal output powers for the hot plate cold plate configuration.....	85
Figure 46. Reflectivity vs. signal output power for two-tone configuration with 1035 nm broad-band signal and hot and cold plate. The numerical simulations of integration of Eqns. (4.1-4.13) are also shown for comparison.	85
Figure 47. Three-wave interaction between optical pump, Stokes, and acoustic wave in an optical fiber	88
Figure 48. Normalized power difference along fiber length for different reflectivity using one-step Euler Method. $\langle R \rangle$ defines the time-averaged reflectivity over several transit times in the long time-limit $\Gamma_B t \gg 1$	94

Figure 49. Normalized power difference along fiber length for different reflectivity using Modified Euler Method. $\langle R \rangle$ defines the time-averaged reflectivity over several transit times in the long time-limit $\Gamma_B t \gg 1$94

Figure 50. Comparison between analytic reflectivity of Eqn. (6.24) for undepleted pump and numerical integration of the equations using a distributing fluctuating noise source. The reflectivity in the case of the numerical integration is averaged over several transit times in the long time limit $\Gamma_B t \gg 1$. The analytic solution shows a strong exponential growth near $G \sim 25$ while the numerical integration shows logarithmic growth over the entire range. These results are in excellent agreement with those discussed in previous works. [13]96

Figure 51. Comparison between analytic linewidth for undepleted pump shown in Eqn. (6.27) and numerical integration of the equations using a distributed fluctuating noise source. The normalized (FWHM = $\Delta\omega / \Gamma$) of the Stokes radiation is computed using the power spectral density of the Stokes field at $z=0$. The analytic solution shows a strong departure from the numerical solution as the single-pass SBS gain is increased. We also observe an asymptotic convergence of the line-width in the numerical solution. These results are in excellent agreement with those discussed in. [13].97

Figure 52. Results of SBS threshold enhancement factor vs. modulation frequency $\nu_{FM} = \omega_{FM} / 2\pi$ for various modulation amplitudes. As expected, the results indicate asymptotic convergence to the theoretical approximation of Eq. (6.30) in the large

modulation frequency limit where the separation between optical modes is large compared to the spontaneous Brillouin linewidth.99

Figure 53. Results of the power spectral density (PSD) of the pump and Stokes fields near SBS threshold for the case $\gamma = 1.435$. with $\omega_{FM} = 2\Gamma_B$ (upper) and $\omega_{FM} = 20\Gamma_B$ (lower) . Both curves are normalized about their respective DC components. The results clearly show that in the small modulation regime interactions among the various sidebands tend to feed the central DC term leading to a higher central Stokes mode. When the modulation frequency is large the Stokes spectrum closely follows that of the pump with three approximately equal side bands.....100

Figure 54. Schematic of white-noise driven phase modulation to broaden and control the linewidth of a laser source. A white noise source is sent through a filter and pass band control to shape the bandwidth of the RF driving signal. The filtered response is amplified and set to match the impedance of the electro-optic modulation (EOM). When the EOM is driven with the noise-filtered signal the laser linewidth is broadened. [56]101

Figure 55. Normalized enhancement factor vs. normalized pump linewidth for fiber lengths ranging from 2m-85m. As the fiber length is increased the enhancement factor closely resembles Eq. (6.35).....104

Figure 56. Normalized slope vs. fiber length. For long fiber lengths the slope asymptotically approaches unity in agreement with Eq. (6.35)..... 104

Figure 57. Experimental data of SBS threshold vs. seed linewidth using Ref [31]. The SBS threshold predicted from Eq. (6.35) is also shown and clearly indicates a severe discrepancy with the experimental data..... 105

LIST OF TABLES

- Table 1. Summary of output power and optical efficiency at SBS threshold for the two-tone and single-tone cases for a 3.0 m, 4.5 m, and 6.0 m fiber length. In all cases the SBS threshold in the 1064 nm signal is higher for the two-tone case. As the fiber is made shorter the optical efficiency is lower for the two-tone case.63
- Table 2. Fiber simulation parameters. These parameters are based on approximate values for fused silica at room temperature and a pump wavelength of 1064nm.....95

1 INTRODUCTION

1.1 INTRODUCTION TO NONLINEAR OPTICS IN FIBERS

An optical fiber is a waveguide which transmits light through a fiber medium. The light is guided inside the fiber through total internal reflection (TIR), which is an optical phenomenon that occurs when light propagating in a medium of high density encounters a boundary of lower density. If the angle of incidence is within a critical angle, the light is completely bent or reflected toward the denser medium; this process continues down the fiber as shown in Figure 1. The manufacturing process of the fiber is such that the core has a higher density than the cladding; or in optical terminology, the core index of refraction is larger than the cladding index of refraction $n_c > n_{clad}$.

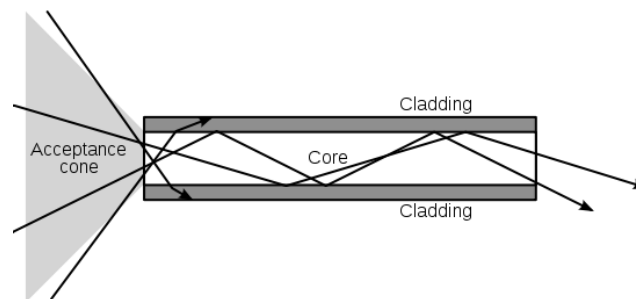


Figure 1. An example of total internal reflection in a fiber waveguide. The light propagates down the core of the fiber since the core optical index is larger than the cladding index $n_c > n_{clad}$.

Nonlinear optics in fibers is the study of phenomenon that occurs when the optical properties of the fiber are modified by the presence of light propagating inside the fiber medium. Nonlinear optical phenomenon is “nonlinear” in the sense that these phenomenon occur when the response of the fiber material is nonlinear with the strength of the optical field propagating in the fiber. To be

precise, the response of the optical medium comes as a result of a change in the polarization $\tilde{P}(t)$ due to the strength of the applied optical field $\tilde{E}(t)$ and is given by [1]:

$$\tilde{P}(t) = \varepsilon_0 \left[\chi^{(1)} \tilde{E}(t) + \chi^{(2)} \tilde{E}^2(t) + \chi^{(3)} \tilde{E}^3(t) + \dots \right] \quad (1.1)$$

where ε_0 is the permittivity of free space and χ is the optical susceptibility. As shown in Eq. (1.1) the polarization is expressed as a power series which describe the various orders of the nonlinear polarization. For example, $\chi^{(1)}$, $\chi^{(2)}$, and $\chi^{(3)}$ describe the first, second, and third order susceptibilities respectively. In general, for condensed matter, the value of the susceptibility decreases with the order and so most nonlinear phenomenon occur in $\chi^{(1)}$, $\chi^{(2)}$, and $\chi^{(3)}$ processes. However, higher order nonlinearities can always occur if the optical field strength is large enough. Some order of magnitude estimates for the first three orders of nonlinearity in condensed matter are: $\chi^{(1)} \sim 1$, $\chi^{(2)} \sim 10^{-12} \text{ m/V}$, and $\chi^{(3)} \sim 10^{-24} \text{ m}^2/\text{V}^2$ [1]. For optical fibers, the real and imaginary parts of the linear susceptibility, $\text{Re}[\chi^{(1)}]$ and $\text{Im}[\chi^{(1)}]$, describe the index of refraction of the fiber medium and amplification or attenuation of the optical field respectively. In regards to amplification, an optical fiber can be made into an optical amplifier by doping the core region of the fiber with a rare-earth ion such as Ytterbium to provide a mechanism for energy to be transferred from one wavelength of light into another through laser gain. A schematic of such a fiber amplifier is shown below in Figure 2. In this case, the signal light and pump light propagate down the fiber in the inner and 1st cladding regions respectively through (TIR). The pump light is typically provided by a laser diode and as this light propagates down the 1st cladding region it is absorbed by the Yb ion which re-emits light at the signal wavelength through stimulated emission. Of course, both the signal and pump light can be attenuated inside the fiber waveguide through absorption processes of the host material such as silica. However, these losses are usually small in fiber amplifiers since the

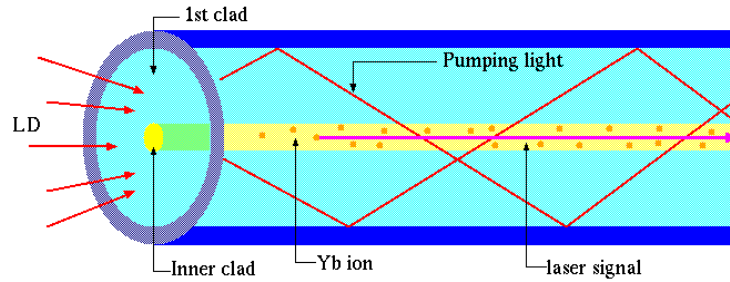


Figure 2. An example of a fiber amplifier. The signal light propagates down the core of the fiber and is amplified when the cladding pump light from a laser diode (LD) is absorbed by the Yb ion which re-emits light at the signal wavelength through stimulated emission.

wavelengths of the pump and signal light are chosen in such a way that the host medium is optically transparent to the signal and pump light.

Most $\chi^{(2)}$ processes in fibers and fiber amplifiers are negligible due to the inversion symmetry of silica glass, which leads to a vanishing $\chi^{(2)}$. In contrast, $\chi^{(3)}$ processes which have non-zero components for centrosymmetric media such as fused silica, dominate nonlinear processes in fibers and fiber amplifiers. One example of the third order nonlinearity in fibers is self-focusing, which can occur as a result of the intensity dependent refractive index. In this case, a beam of light having a nonuniform transverse intensity distribution creates a positive lens in the material. This causes the rays of light to curve toward each other and can result in an optical intensity that is sufficiently large to lead to optical damage of the material. Typically, the damage threshold is not reached in fiber amplifiers because other $\chi^{(3)}$ processes, such as stimulated Raman scattering (SRS) and stimulated Brillouin scattering (SBS), occur before the self-focusing threshold is reached.

In terms of power scaling continuous-wave (CW) fiber amplifiers which possess a very narrow spectral bandwidth ($\Delta\nu \sim \text{MHz}$), SBS is the first nonlinear threshold effect due to its large gain: $g_{\text{SBS}} \sim 5 \times 10^{-11} \text{ m/W}$, more than two orders of magnitude larger than (SRS) gain:

$g_{SRS} \sim 8 \times 10^{-14} \text{ m/W}$ in fused silica [1]. Figure 3 gives an overview of the progress of power scaling single-frequency fiber amplifiers in the last decade for co-pumped and counter-pumped configurations. Here, the terminology of co-pumped and counter-pumped refers to the relative direction of propagation between the pump and signal light in the fiber amplifier.

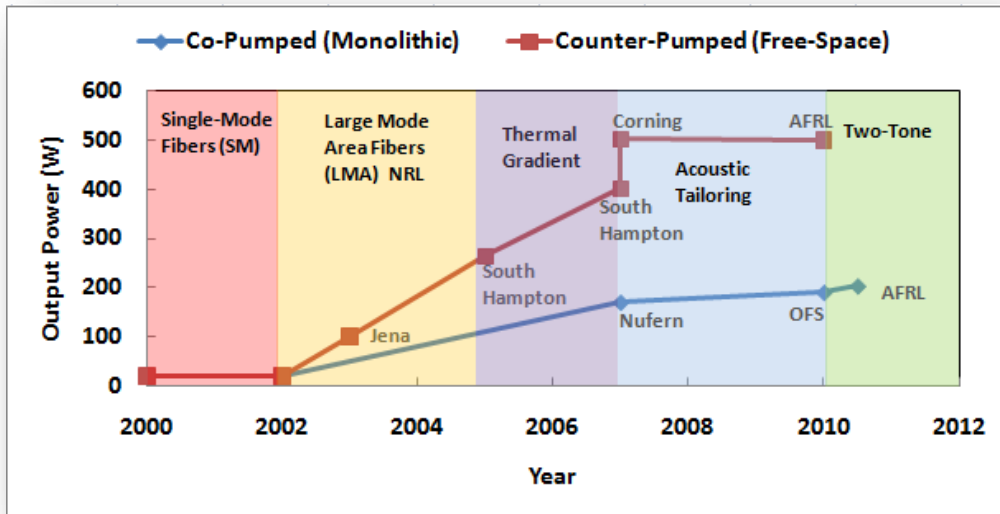


Figure 3. Diagram depicting the technological advancements in power scaling single-frequency co-pumped and counter-pumped fiber amplifiers over the last decade. Colored regions depict advancements in SBS mitigation which increase the SBS threshold. The various research institutions responsible for the power level milestones are also labeled.

The colored regions denote significant milestones in SBS mitigation which increase the SBS threshold through different technologies such as: the development of large mode area (LMA) fibers [2], the use of a thermal gradient on the fiber [3], acoustic tailoring [4,5], and the use of laser gain competition between two signals, which is developed in this work. The fiber amplifiers employing a counter-pumped architecture produce higher output powers due to the SBS suppression that results from the way the signal evolves in the fiber compared to that of a co-pumped fiber amplifier [6]. However, additional aspects of the counter-pumped configuration such as the additional length of

the pump delivery fiber, failure of the pump combiners, and the use of free-space optics can make this configuration less desirable for monolithic (all-fiber) architectures [6]. In order to power scale beyond these levels, techniques such as phase modulation, which broaden the laser linewidth, are becoming a promising technique to scale to the kW level. As such, this work will address phase modulation from a time-dependent perspective to provide valuable insight into the effects of phase modulation on the SBS process. In addition, novel concepts which increase the SBS threshold in single-frequency, co-pumped fiber amplifiers such as those described in this dissertation can help close the power gap between counter and co-pumped amplifier configurations which will lead to a more robust and compact laser.

1.2 DISSERTATION STATEMENT

This dissertation is a theoretical development and experimental verification of the suppression effects on stimulated Brillouin scattering (SBS) in fiber amplifiers due to multi-seeding and phase modulation. A theoretical framework is developed which describes the physics of ytterbium (Yb) doped fiber amplifiers seeded with a collection of continuous-wave (CW) signals of different frequencies. In this framework up to three seed signals are considered. The SBS process is investigated in three different variations of multi-tone seeding. In the first configuration, the amplifier seeds are separated by twice the resonant acoustic frequency of the fiber. The seeds considered are single-frequency with respect to the spontaneous Brillouin linewidth Γ_B ie. $\Delta\nu < \Gamma_B$. The concept was demonstrated as an effective SBS suppressing technique using two signals but with considerable four-wave mixing [7]. This dissertation extends the concept to three signals, provides a theoretical model that supports the experimental results, and explains the effects of four-wave mixing. In the second configuration, the effects of SBS are studied when multiple, single-frequency

seeds of arbitrary frequencies spanning the Yb lasing bandwidth (1030-1080) nm are sent into the amplifier. Finally, in the third configuration the amplifier is co-seeded with a broad-band $\Delta\nu \gg \Gamma_B$ and single-frequency laser of different wavelengths. Low and high power experimental results are presented which support and verify the theoretical conclusions of the latter. The last two configurations demonstrate, for the first time, SBS suppression through laser gain competition.

For the first time, a time-dependent model that describes the SBS suppression effects of phase modulation in fibers is developed in this dissertation. The model solves the triply coupled time-dependent system of partial differential equations describing the three-wave interaction of a pump, Stokes, and acoustic field. The model includes the effects of noise initiation and phase modulation (PM). The effects of SBS suppression through phase modulation are examined. Sinusoidal and white noise modulation schemes are considered. The time-dependent approach serves to fill a research gap in explaining the apparent discrepancy between experiment and theory in the SBS suppression factor of a broadband pump for short fibers. Previous approaches were to solve the equations in the Fourier domain and with an approximation that the fiber length was of the order of kilometers. While this approach is satisfactory for telecommunication applications, in fiber amplifiers the fiber length is typically less than 10 m and previous approaches are inadequate. Unlike the Fourier approach, in which both a pump and SBS differential equation must be solved for each longitudinal mode in the pump spectrum, the time-dependent method only requires integrating three differential equations. Furthermore, the time-dependent model handles high reflectivity regimes.

1.3 STIMULATED BRILLOUIN SCATTERING

Since the invention of the laser, there has been extensive and sustained interest in developing high average power lasers. Recently, rare-earth doped fiber lasers have gained considerable attention

as a means of realizing this goal since they are typically characterized by compact and robust architectures, superior thermal management properties, near diffraction-limited beam quality and high conversion efficiencies. In addition, the rapid progress of high brightness diodes to pump fiber amplifiers have enabled kilowatt class, single transverse mode fiber lasers. [8] In general, high average power fiber lasers require several meters of gain fiber and are characterized by broad linewidths in the range of 10-20 nm. While these lasers offer a considerable benefit in material processing where raw power is sought, their broad linewidths render them ineffective for a range of applications that require single frequency operation such as coherent beam combination, [9] nonlinear frequency conversion [10], adaptive optics [11], and inter-satellite communications. [12] More narrow linewidth lasers may be realized by seeding a fiber amplifier with a master-oscillator or distributed feedback laser (DFB) whereby the final amplification stage inherits the narrow linewidth and frequency stability characteristics of the seed laser. Power scaling in single frequency continuous-wave (CW) fiber amplifiers is primarily limited by the onset of stimulated Brillouin scattering (SBS). Single frequency, in this context, refers to light sources whose linewidth is spectrally narrow compared to the spontaneous Brillouin linewidth. For a fiber amplifier made of fused silica, the spontaneous Brillouin linewidth is approximately 60MHz. The SBS process, depicted in Figure 4, is a third-order nonlinear effect that couples acoustic phonons to the optical field and its associated backscattered Stokes field. The SBS gain coefficient is an intrinsic property of the guiding medium and in silica-based fibers its value is approximately $(1-5) \times 10^{-11} m/W$, making it the lowest threshold nonlinear process in single frequency CW fiber amplifiers. In comparison, the next lowest threshold phase-matched process is stimulated Raman scattering (SRS) which has a peak gain coefficient in silica fibers of less than $10^{-13} m/W$; two-three orders of magnitude lower than the SBS gain coefficient.

The SBS process is started from spontaneous scattering of the signal light from thermally excited acoustic waves, or in the low-temperature regime, from quantum noise associated with the fiber medium. [13,14,15]

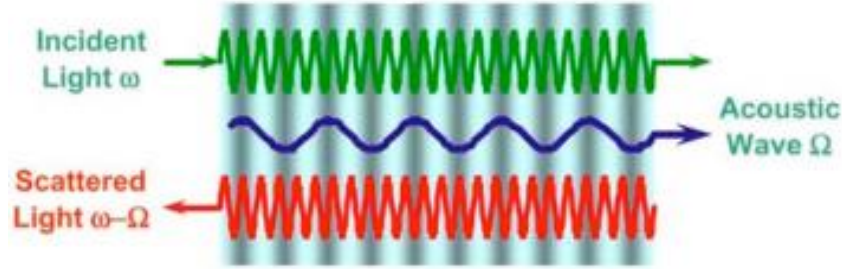


Figure 4. Three wave interaction of the SBS process. An incident field is scattered off an acoustic wave, which generates the Stokes wave that travels in the backward direction.

The scattered Stokes light is zero in the forward direction, non-zero at $\theta \neq 0^\circ$, and maximum at $\theta = 180^\circ$. [1] The SBS process is characterized by conservation of momentum and energy: $\vec{q} = \vec{k}_L - \vec{k}_S$ and $\hbar\omega_S = \hbar\omega_L - \hbar\Omega_B$ where k_L, k_S , and q are the laser, Stokes, and acoustic wavevectors respectively which are related to their respective angular frequencies $\omega_L = ck_L/n$, $\omega_S = ck_S/n$, and $\Omega_B = vq$. Here n is the index of refraction of the medium, c is the speed of light, and v is the velocity of sound in the medium. When an incident beam is launched into the fiber medium spontaneous Brillouin scattering will develop leading to backward traveling Stokes light. The incident laser field and resulting Stokes field interact leading, through electrostriction, to variations in density and pressure in the fiber and consequently further amplification of the acoustic and Stokes waves. While the initial process is spontaneous, a resonance condition quickly develops in time since only those Stokes frequencies within the spontaneous acoustic bandwidth Γ_B have appreciable SBS gain. If the intensity of the incident laser field is high enough, the Stokes field becomes so large that an exponential rise in the backward

power is observed known as the SBS threshold. Operation of the amplifier near or beyond this point is problematic due to high-energy pulsations within the fiber medium capable of reaching the threshold intensity for optical damage to fused silica at approximately $3\text{GW}/\text{cm}^2$. [1] To that end, suppression of SBS in fiber amplifiers remains a major challenge and novel SBS suppressing concepts such as the one developed in this dissertation help pave the path forward.

1.4 OVERVIEW

This dissertation is an attempt to address several questions related to SBS in fiber amplifiers that are seeded with multiple signals or when a single seed is phase modulated. To that end, detailed models of the SBS process are developed throughout this dissertation. The models consist of steady state and transient differential equations that describe the SBS process. In the multi-tone case, the differential equations are solved in the steady state. The effects of four-wave mixing, intrinsic and external thermal gradients, and laser gain are also included. In the configuration where the signals are separated at twice the Brillouin shift the seed ratio required to maximize SBS suppression is developed. The effects of four-wave mixing provide insight into the practicality of using this concept as an effective means of suppressing the SBS process. The major questions that are answered as they relate to this concept are: the optimal seed ratios and expected SBS enhancement for N tones and the magnitude of the four-wave mixing for the two and three seed cases. Another major question this dissertation addresses is if laser gain competition between one or more signals within the fiber can reduce the SBS process. To that end, this dissertation is the first demonstration of SBS suppression via laser gain competition. The theoretical details, requirements on wavelength and seed ratio, and the expected SBS suppression of this concept are discussed in Chapter 4. Experimental results and comparison to theory are presented in Chapter 5.

Finally, in Chapter 6 a time-dependent SBS model is developed to study the SBS effects of phase modulation. The time-dependent approach is developed to address ongoing concerns about the discrepancy between the expected SBS threshold under broadband pumping conditions and experimental results in short fibers. In addition to resolving this discrepancy, the SBS threshold for several different modulation schemes is characterized.

1.5 SIGNIFICANCE OF THE DISSERTATION STUDY

This study is being conducted for several reasons. First, this dissertation advances knowledge of SBS in multiple wavelength amplifiers and phase modulated amplifiers. Second, it is the first investigation of SBS suppression through phase modulation using a time-dependent approach. Finally, this dissertation demonstrates a novel concept of SBS suppression through laser gain competition; leading to the best of our knowledge the highest reported power for a co-pumped, single-frequency Yb-doped fiber amplifier.

The SBS suppression due to a fiber simultaneously illuminated with multiple single-frequency signals with equal wavelength separation was studied previously in passive fibers. [16,17] The study was limited to long fibers and also fails to describe a unique case of SBS suppression by seeding with multiple signals at twice the Brillouin shift. In this dissertation we advance knowledge of the SBS process in this area by extending the study to active fibers. In particular, the case of multiple wavelengths in Yb doped fiber amplifiers is considered. Contrary to previous studies, no assumptions are made about the fiber length. We also incorporate an additional term to describe non-linear coupling between multiple Stokes waves separated at twice the Brillouin shift.

Phase modulation of a pump spectrum can create a multiple wavelength spectrum. To that end, the previous study described above is adequate in describing the suppression of SBS for a phase modulated pump beam in long fibers or when the separation between wavelengths is large. [17]

However, most fiber amplifiers are only several meters long making this approximation invalid. In addition, previous approaches fall short of describing the SBS suppression for several signals separated within the Brillouin line width. The differential equation system describing a multi-wavelength pump spectrum and the SBS process has also been considered in the Fourier domain. However, these studies ignore the phase-mismatched terms resulting from cross-interactions between Stokes waves for the same reasons mentioned above (ie. long fibers and large wavelength separation). Furthermore, the system of differential equations in the Fourier domain is large since one must solve a differential equation for each pump and Stokes wavelength in the spectrum. This dissertation extends knowledge in this area by considering the effects of phase modulation on SBS suppression using a time-dependent approach. In this way, only three differential equations are solved and no assumptions are made on the fiber length or wavelength separation. This allows the effects of phase modulation on the SBS process to be studied in short fibers and when the phase modulation scheme creates closely spaced modes.

Another significant achievement of this dissertation is the development and verification of a novel SBS mitigation concept using laser gain competition. Only a handful of SBS mitigation concepts for fibers have been discovered over the last thirty years. While these concepts such as thermal gradients, acoustic tailoring, phase modulation, and applying stress enhance the SBS threshold in fibers they cannot necessarily be used in conjunction. On the contrary, SBS mitigation through laser gain competition may be paired with all known SBS mitigation strategies. To that end, the concept developed in this dissertation is well suited for power scaling narrow-line fiber amplifiers.

In summary, a detailed analysis of multi-tone amplification and the SBS process is presented which extends previous studies to incorporate an active lasing medium. Phase modulation effects on

the SBS process is studied for the first time using a time-dependent approach, which eliminates previous approximations for long fibers and large wavelength separations. Finally, a novel SBS mitigation concept that uses competition between laser gain is developed in this dissertation. For these reasons this dissertation makes a significant contribution to the field of SBS in fiber amplifiers.

1.6 DESCRIPTION OF DISSERTATION CHAPTERS

This dissertation is organized into seven chapters. The second chapter is a review of literature related to this dissertation. The results of previous studies of SBS effects on multi-wavelength pumps are summarized. This section also includes an examination of previous approaches to modeling SBS in the time-domain. Phase modulation studies carried out in the Fourier domain are also reviewed in this section. Chapter Two ends with a brief overview of past experimental results of SBS suppression through phase modulation. Chapter Three examines the SBS process when multiple signals separated at twice the Brillouin shift are sent into a fiber amplifier. The theoretical framework for modeling multiple seeds in a fiber amplifier is presented. This chapter also discusses the theoretical optimal seed ratios for up to N tones. For this special case of multi-tone seeding, the suppression effects of SBS and considerations of FWM are also characterized in this chapter. Chapter Four presents the first demonstration of SBS suppression in multiple-wavelength fiber amplifiers through laser gain competition. First, an overview of the theoretical concept is presented with the intention of introducing the reader to this novel concept. Second, optimization of the seed ratios for maximum SBS suppression is discussed. Chapter Five presents the experimental results and verification of SBS suppression through laser gain competition. The experimental setup, procedures, and results of low and high power experiments are demonstrated in this chapter. The experiments also consider SBS suppression effects when the two-tone concept is used in conjunction with intrinsic and external thermal gradients. Chapter Six

introduces the time-dependent approach to modeling phase modulation and the effect on the SBS process in fibers. The theoretical framework and numerical approach to solving the system of differential equations is presented first. Next, the numerical models are verified using several validation criteria. SBS suppression is then characterized using the time-dependent model for several different types of phase modulation schemes. Chapter Seven summarizes the major findings of this study. A synopsis of the SBS suppression effects in multi-wavelength fiber amplifiers is presented along with a recap of the SBS suppression concept through laser gain competition. This chapter also summarizes the major conclusions of the effects of phase modulation using a time-dependent approach. Finally, the benefits and future work of this dissertation are discussed.

2 REVIEW OF RELATED LITERATURE

2.1 SBS MITIGATION IN FIBERS THROUGH MULTI-TONE SEEDING

SBS mitigation effects in a fiber seeded with multiple signals was explored theoretically and verified experimentally in 1987 by Litchman et. al. [16] This study explored the effects of SBS in a passive fiber excited by two pump frequencies in the steady-state regime. The motivation of this work was to find the dependence of the SBS gain on the frequency separation Ω between the two pump modes. The main conclusion of this work was that the SBS gain vs. frequency separation of the two pumps depended on the relative magnitude between the coherence length $L_{coh} = \pi c / \Omega$ and the SBS gain length $L_{ch} \sim 1/g_o(I_1 + I_2)$ of the fiber. Here, I_1 and I_2 are the intensities of the two pump fields and g_o is the small signal SBS gain coefficient.

In the regime where $L_{coh} \ll L_{ch}$, the effect of interactions between the two Stokes modes may be neglected. For this case, the two Stokes modes act independently with each of there pump modes and the SBS gain of each is reduced according to the separation between the two optical pumps. In addition, in the large separation limit where $\Omega/\Gamma_B \gg 1$, the normalized SBS gain (normalized to that of the single frequency case with the same total intensity: $I = I_1 + I_2$) of each Stokes frequencies approaches 1/2. This means that if the fiber is seeded with two signals each at the SBS threshold I_{th} : $I_{th} = I_1 = I_2$, the total power transmitted before the onset of SBS is twice that of the same fiber seeded with a single tone. These results can be generalized for a fiber seeded with N signals. In the general case, the total output power obtainable before the SBS threshold is reached is N times greater than that of the same fiber seeded with the a single frequency of the same total intensity.

In the opposite limit where $L_{coh} \gg L_{ch}$ cross interactions among the Stokes modes dominate the process. For the case of the SBS generator, in which the Stokes wave is growing from noise inside the fiber, the results indicate that in the large separation limit $\Omega/\Gamma_B \gg 1$, the SBS gain is equal to the SBS gain of a single frequency pump having the same total intensity $I = I_1 + I_2$. To that end, the SBS gain reduction as described in the previous case is overcome by the perfect phase matching between the phases of the two Stokes frequencies. This means that, in this regime, there is no benefit in terms of SBS suppression to seeding with multiple signals compared to that of a single seed.

A final, and somewhat surprising, conclusion drawn from this work is that the SBS gain for the two-seeded pump case may be as large as 1.5 times that of a single seeded fiber with the same total intensity. Such high gain occurs in the regime $L_{ch}/L_{coh} < 0.15$ and when $\Omega/\Gamma_B \ll 1$. This regime is characterized by strong cross gain interactions and non-perfect phase matching among the various Stokes frequencies. It is important to note that this work was the first to demonstrate that the power limitations of SBS for a single seeded fiber could be increased using multiple signals. In this way, the total power could be increased since each signal could be made to reach its SBS threshold independently. However, the SBS threshold of each signal is still the same as the single-tone case; the difference is that the total output power at the SBS threshold of either signal is larger.

Recently, in 2004, Weßels et. al demonstrated an SBS gain reduction and subsequent increase in the SBS threshold of an individual signal for a special case of a two-tone seeded fiber. [7] In this case, a fiber is simultaneously seeded with two lasers separated in wavelength by twice the acoustic frequency $\Omega_b \sim 16GHz$ in a 72m long fused silica fiber. The scheme is depicted in Figure 5.

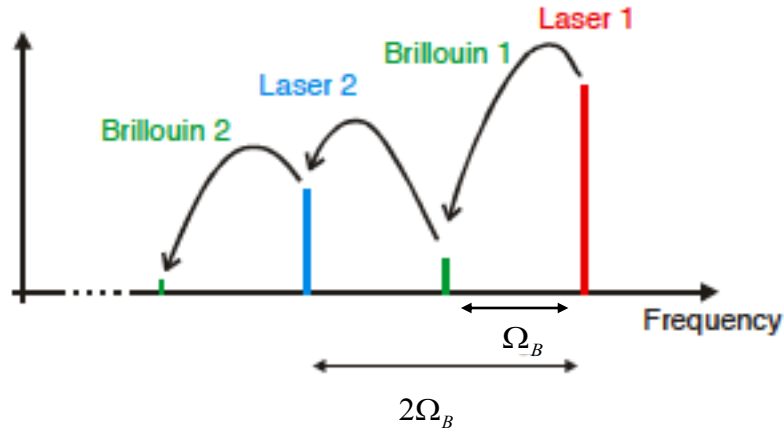


Figure 5. Brillouin-scattering scheme with two single-frequency lasers separated by twice the Brillouin frequency shift Ω_B .

Here the Stokes from Laser 1, denoted as Brillouin 1, has a subsequent Stokes that couples power into Laser 2 since it is separated at twice the Brillouin shift from Laser 1. Additionally, the Stokes of Brillouin 1 is traveling in the forward direction and thus is intrinsically phase matched to Laser 2. To that end, the Stokes from Laser 1 transfers a portion of its power into Laser 2. The work showed that if Laser 1 was seeded with twice the power of Laser 2, a reduction of 2 in the SBS gain could be achieved such that the SBS threshold of Laser 1 was twice that of the single tone case. One major drawback of this concept was the generation of four-wave mixing (FWM) due to interactions between the two pumps signals. In this work six additional side bands were observed in the output spectra indicating a significant portion of the output was contained in the sidebands due to mixing between the two single-frequency sources. Contrary to Litchman's analysis, this concept did demonstrate an SBS suppression of an individual frequency when a fiber is co-seeded with several signals.

2.2 TIME-DEPENDENT MODELING OF SBS IN FIBERS

The time-dynamics of the SBS process in a passive fiber was studied previously by Boyd et. al. [13] One of the most significant results of this study was the mathematical formulation of the acoustic noise source responsible for initiating the SBS process. Boyd et. al formulated the noise term using statistical properties of a Langevin process where the strength of the fluctuations was proportional to the intrinsic properties of the fiber. Specifically, Boyd was able to describe how SBS is initiated by spatially distributed thermal fluctuations of the density of the fiber medium. By initiating the SBS process from noise, Boyd et. al were able to predict intensity fluctuations in the output Stokes and predict the spontaneous Brillouin linewidth. In addition to being the first time-dependent study of the triply-coupled nonlinear differential equations describing the SBS process, the results of this study led to several major findings. First, it was shown how various approaches to the initiation of the SBS process compared with each other. The initiation processes considered were: an undepleted pump approximation with a distributed fluctuating source, a localized nonfluctuating source, a distributed fluctuating source (numerical integration of time dependent equations), and a localized fluctuating source. The localized models of (Zeldovich, Pilipetskii, and Shkunov) were found to be in good qualitative but not quantitative agreement. [18] It was also shown that models which use a non-fluctuating noise source to start the SBS overestimate the reflectivity of the SBS process since a fluctuating input will always experience smaller time-averaged gain than a stationary one. In addition, this study showed gain narrowing of the Stokes output spectrum with increasing SBS gain. Finally, Boyd's study formulated an analytic expression showing how the SBS reflectivity depends on the single-pass SBS gain through the medium in the undepleted pump approximation with a distributed fluctuating noise source. The latter finding is

useful in comparing the accuracy (at low reflectivity) of SBS models developed to study the SBS process in the high gain limit.

2.3 MODELING SBS SUPPRESSION THROUGH PHASE MODULATION IN THE FOURIER DOMAIN

One approach to modeling SBS suppression through phase modulation is to solve the system describing the interaction between the pump, Stokes, and acoustic field in the Fourier domain. Litchman, Waarts, and Friesem considered this approach in 1988 to describe the SBS suppression from three phase modulation schemes relevant to the telecommunication industry: Phase-Shift Keying (PSK), Amplitude-Shift Keying (ASK), and Frequency-Shift Keying (FSK). [17] The authors assumed that the pump and Stokes fields were a superposition of longitudinal modes with a frequency separation Ω . The expressions for the SBS gain were developed under the assumption that the fiber length was long and/or the separation between longitudinal modes was large: $\frac{n_o \Omega L}{c} \gg 1$. Here n_o is the linear index of refraction of the fiber medium. The assumption is valid in many practical fiber optic communications systems, since, in these systems $L > 1km$ and $\Omega > 10MHz$. Under this assumption, Litchman et. al argued that the non phase-matched terms inside the differential equation describing the evolution of the Stokes amplitude changed sign many times so their net contribution was negligible. The results were extended to include a continuous pump spectrum where the total Stokes gain G is given by:

$$G(\omega_s) = g \Gamma_B L_{eff} \int_{-\infty}^{\infty} \frac{I_L(\omega) d\omega}{\Gamma_B^2 + (\omega - \omega_s - \Omega_a)^2} \quad (2.1)$$

Here, g is the SBS gain coefficient, Γ_B is the spontaneous Brillouin linewidth (HWHM), $\Omega_a = 2n_o v_a / c$ is the resonance frequency of the acoustic medium, ω_s is the frequency of the Stokes

signal, L_{eff} is the effective length of the SBS process [19], and $I_L(\omega)$ describes the pump intensity spectrum. By substituting the resultant Fourier transforms of the time-dependent functions describing ASK, PSK, and FSK, into Eq. (2.1) the authors were able to obtain analytic expressions for the carrier gain of each modulation scheme. The authors only considered the carrier SBS gain because, for each of these modulation schemes, the optical power in the side bands is always smaller than the carrier itself. While the approach taken in this work is valid for long fibers and/or large frequency separation, it is important to realize that in cases where the fiber length is short, or the frequency separation is small the approach taken by Lichtman et. al is inadequate. Other notable works considering the SBS process in the Fourier domain, under similar assumptions to that above, are the works of Minardo, Testa, Zeni, and Bernini who considered the effects of intensity and phase modulation for Brillouin-based distributed sensing. [20,21] In these analyses, only a single monochromatic sinusoidal modulation function was considered and the modeled fibers were still relatively long $L > 30m$. Nevertheless, the authors were able to show general agreement between the Stokes spectrum and their theoretical predictions. Recently, Kovalev, Kotova, and Harrison considered the effects of the pump spectrum on the group index of the fiber for slow light applications. [22] Contrary to the aforementioned works, the only approximation made in this study was that the pump was undepleted. Still, the work was limited in that although the general treatment was formulated, further approximations were made requiring the growth of the Stokes field in z to be small. In this approximation, the gain narrowing of the Stokes field described previously in the time-dependent approach cannot be explained. However, the main thesis of the work was to investigate the possibility that the group index of the fiber medium could be modified in the presence of a modulated pump field through SBS. With the undepleted approximation for the Stokes field, the authors claimed that spectral broadening of the pump results in only a minute

increase of the spectral width of the material's excitation in SBS. To that end, the main conclusion was that phase modulation could not be effective in modifying the group index of the medium for a Stokes pulse injected into the fiber. The latter claim is currently an ongoing debate in the application of slow light using the SBS process. [23,24,25]

2.4 EXPERIMENTAL RESULTS OF SBS SUPPRESSION THROUGH PHASE MODULATION

Phase modulation has been used as an effective means of suppressing the SBS process. In 1994, Willems, Muys, and Leong demonstrated SBS suppression for two types of modulation schemes: a single sinusoidal phase modulation and optical frequency dithering [26]. While both concepts effectively broaden the linewidth, the main difference is that the single sinusoidal modulation scheme produces a discrete set of sidebands in the optical spectrum while the dithering technique broadens the linewidth in a continuous manner. In their experiments, the modified spectrum was launched into a 24 km passive fiber and the SBS threshold, defined at 0.2 dB Relative Intensity Noise (RIN), was measured. In the single sinusoidal case, measurements were performed for different modulation depths while in the frequency dithered scheme the SBS threshold was compared for different linewidths. They found excellent agreement between the measured SBS threshold and their corresponding theoretical enhancement factors [27,28]:

$$\Delta P_{SBS}^{th}(\beta) = \max_{k \in \{0,1,2,\dots\}} J_k^2(\beta) \quad (2.2)$$

and

$$\Delta P_{SBS}^{th}(\Delta\nu_D) = 1 + \Delta\nu_D / \Delta\nu_B. \quad (2.3)$$

Here, Eqs. (2-2) and (2-3) describe the theoretical enhancement of the single-sinusoidal and frequency dithering phase modulation techniques respectively. β is the modulation depth of the single sinusoidal modulation function, $J_k(\beta)$ is the Bessel function of the 1st kind of order k , and

$\Delta\nu_D, \Delta\nu_B$ represent the measured pump linewidth and spontaneous Brillouin linewidth, respectively. It should be noted that in Eq. (2-2) the SBS threshold increase depends on the maximum sideband k . One should use caution in the application of Eq. (2.2) and Eq. (2.3) since these formulas were derived during the telecom industry for long fibers and/or large separation between the frequency components in the pump spectrum. At that time most fibers were very long thus a study of the effects for shorter fibers was not interesting. As will be shown in this dissertation, these formulas inaccurately predict the SBS enhancement in short fibers or in modulation schemes where the frequency separation is close to the spontaneous Brillouin linewidth. In 2001, Yang et. al experimentally demonstrated that for a single sinusoidal modulation scheme the expected SBS threshold increase was 5 dB. [29] More recently in 2009, Liu, Lü, Dong, and Li investigated the SBS enhancement with a multi-frequency phase modulation scheme. [30] In their work, the SBS threshold was improved by over 10 dB using 4 single sinusoidal modulation-driving functions with different modulation depths and phases. In 2010, Goodno et. al explored the SBS suppressive factor for different pump linewidths. [31] A crucial difference to the work of Willems, Muys, and Leong was that in this case the fiber length was much shorter $L < 10m$. In this work, a 1.4 kW narrow linewidth ($\Delta\nu > 20GHz$) was developed by increasing the pump linewidth using phase modulation. In their study of the SBS threshold vs. linewidth, the enhancement factor was much less than that given by Eq. (2.3). For example, a pump linewidth of 11 GHz should increase the SBS threshold by approximately 200 in accordance with Eq. (2.3) for a spontaneous Brillouin linewidth of 57 MHz (typical of fused silica). This is nearly a factor of 20 above their experimental observations. This discrepancy is resolved later in this dissertation by simulating linewidth broadening with phase modulation using a time-dependent SBS model.

3 MULTI-TONE SEEDING AT TWICE THE BRILLOUIN SHIFT

3.1 INTRODUCTION

A promising technique that can be used to suppress the SBS process in fibers involves the simultaneous illumination of the fiber by two co-propagating narrow linewidth seed lasers with frequencies ω_2 and ω_1 whose frequency separation is twice the spontaneous Brillouin shift. [7] The scheme is shown in Figure 5. The higher frequency seed generates a Stokes wave at frequency $\omega_s = \omega_2 - \Omega_B$, which travels in the backward direction. This Stokes wave then generates its own Stokes wave at frequency $\omega'_s = \omega_s - \Omega_B$, which travels in the forward direction and with the same frequency as the second seed laser ω_1 since $\omega_2 - \omega_1 = 2\Omega_B$. The indirect nonlinear coupling between ω_s and ω_1 suppresses the SBS process of the seed at ω_2 . It was shown experimentally that with a 2:1 ratio between the higher frequency and lower frequency seeds, the total output power could be increased by a factor of 3 before the onset of stimulated Brillouin scattering [7]. However, one major drawback of this technique is the generation of a significant amount of power in four-wave mixing (FWM) sidebands. In silica-based fibers, the FWM gain coefficient is approximately 2×10^{-13} m/W. This value is appreciably lower than the SBS gain coefficient, but unlike SBS the driving terms are composed of degenerate products of the signal fields. Furthermore, the lack of perfect phase-matching in FWM is less pronounced here due to the small wavelength separation of ~ 32 GHz.

In this chapter, the concept is investigated theoretically in Yb-doped high power fiber amplifiers and also extended to model three-tone amplification. As shown in Figure 6, these amplifiers consist of a fused silica fiber with a Yb:doped core and inner and outer claddings to guide the pump and signal light respectively. In this case, the signals propagate in the core of the

fiber and the pump light is guided in the 1st cladding region. In order to model this technique, a comprehensive symbolic and numerical model that can solve for single-, two-, and three-tone seeding is constructed. The model is built using Mathematica since this software is well suited to handle problems requiring both symbolic and numerical manipulations.

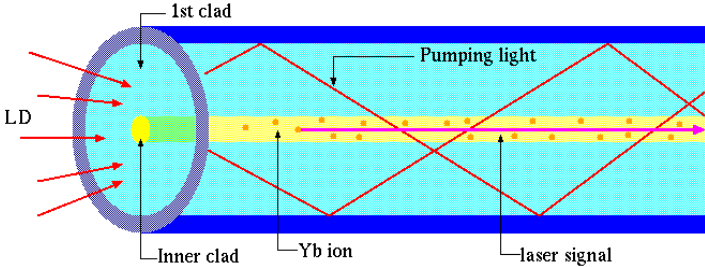


Figure 6. Example of a Yb-doped fiber amplifier with laser signal propagating in the core and pump light propagating in the cladding through total internal reflection (TIR).

3.2 THEORETICAL FRAMEWORK

Consider the three seed inputs to oscillate at frequencies ω_1, ω_2 , and ω_3 . Let the frequency separation be equal and given by $\Delta\omega$. Since in this case FWM effects are significant, up to 4 FWM sidebands are included as can be seen in Figure 7. In addition, the Stokes light at each of the signal seeds is also considered.

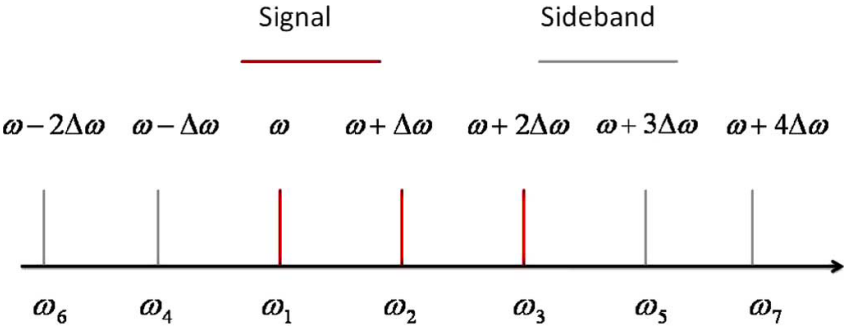


Figure 7. Input seeds and FWM sidebands.

The evolution of the electric field of each frequency component can be described using the nonlinear wave equation:

$$\nabla^2 E_i - \frac{n_i^2}{c^2} \frac{\partial^2}{\partial t^2} E_i = \frac{1}{\epsilon_0 c^2} \frac{\partial^2}{\partial t^2} P_i^{(nl)} \quad (3.1)$$

where the subscript i represents the frequency component of the electric field, $P_i^{(nl)}$ is the nonlinear polarization, and n_i is the linear index of refraction. The nonlinear polarization for the laser signals is due partly to SBS and FWM. Furthermore, these signals can undergo amplification or loss due to population inversion in the active core and this laser action can also be mathematically incorporated into the nonlinear polarization. The three backward traveling Stokes waves experience gain through the SBS process as well as laser gain or loss. Here, the interest is in amplifier action near or below the SBS threshold and since the total FWM at this threshold is estimated to be an order of magnitude lower or more than the total signal power, the interaction of the FWM sidebands and any Stokes light is neglected. Following coupled mode theory [32], the frequency components of the electric field may be expressed in the following form:

$$E_i(\mathbf{r}, t) = \sum (1/2) A_{i,j}(z) \phi_{i,j}(x, y) \exp[i(\beta_{i,j} - \omega_i t)] + c.c. \quad (3.2)$$

where j represents the mode, $A_{i,j}$ is the amplitude, $\beta_{i,j}$ is the propagation constant, and $\phi_{i,j}(x, y)$ is the transverse profile. This analysis is focused on the nonlinear coupling of the lowest-order modes of the various optical waves since large-mode-area (LMA) fibers are typically coiled to induce appreciable bend losses in the higher-order modes. One may then drop the subscript j from Eq. (3.2) and it is understood that the equations that follow describe the lowest-order mode for each frequency component. Furthermore, since the frequency separation among the waves is much smaller than the optical frequency, the modal profiles of all waves are set to be equal. The following equation

describes in compact form the evolution of the two lower frequency signals, which in accordance with Figure 7 correspond to ω_1, ω_2 :

$$\frac{dA_i}{dz} = \frac{g_i}{2} A_i - \frac{g_B \epsilon_o c n_i k_{ao}}{4} \left(|A_{i,S}|^2 - \alpha |A_{i+1,S}|^2 \right) A_i + \frac{i \omega_i n^{(2)} k_{pm} f_i}{c} \quad (3.3)$$

where g_i , $n^{(2)}$, and g_B are the laser gain, nonlinear index of refraction, and the SBS gain coefficient, respectively and where $A_{i,S}$ is the Stokes wave. Note that the nonlinear indices of refraction and also the SBS gain coefficients are taken as equal for each frequency as dispersive effects for these parameters are negligible. The nonlinear index of refraction $n^{(2)}$ is related to the linear index of refraction n through: $n^{(2)l} = (2\mu_0 c \cdot n^{(2)}) / n$ where $n^{(2)l} = 3 \times 10^{-20} m^2 / W$ [33]. The effective linear index of refraction is related to the propagation constant and may be approximated as: $\beta_i = n_i \omega_i / c$, where n_i is the effective index of refraction computed using the Sellmeier equation for fused silica. Furthermore, it is assumed that the linear index of refraction is approximately equal for a signal wave and its Stokes light. The third term in Eq. (3.3) describes the coupling from the Stokes of the frequency ω_{i+1} into the optical field associated with the frequency ω_i in accordance with Figures 5 and 7. Recall, that the SBS suppressing nature of this approach is that the frequency separation among the optical fields is set to twice the Brillouin shift (resonance acoustic frequency) of the fiber medium such that $\Delta\omega = 2\Omega_B$. The terms contained in f_i account for FWM and are described in section 3.4. The overlap integral for FWM, κ_{pm} , and the overlap integral for the acoustic and optical wave interaction, κ_{ao} , are given by:

$$\kappa_{pm} = \kappa_{ao} = \frac{\iint |\varphi|^4 dx dy}{\iint |\varphi|^2 dx dy} \quad (3.4)$$

The Yb:doped fiber laser gain is modeled by assuming a quasi-two-level system and is given by:

$$g_i = \frac{\iint (N_2 \sigma_i^{(e)} - N_1 \sigma_i^{(a)}) |\phi|^2 dx dy}{\iint |\phi|^2 dx dy}, \quad (3.5)$$

where N_2 and N_1 are the population densities of the upper and lower energy manifolds, respectively, and where $\sigma_i^{(e)}$ and $\sigma_i^{(a)}$ represent the emission and absorption cross sections for ω_i , respectively. Figure 8 shows the energy level diagram and emission and absorption cross sections for a Yb: doped silica fiber [36,37]. The integration in the numerator of Eqs. (3.4) and (3.5) is carried out within the core. Algebraic expressions for N_2 and N_1 in terms of pump, signal, Stokes, and FWM waves can be obtained from the steady state solutions to the rate equations [35]:

$$N_o = N_1(z) + N_2(z), \quad (3.6)$$

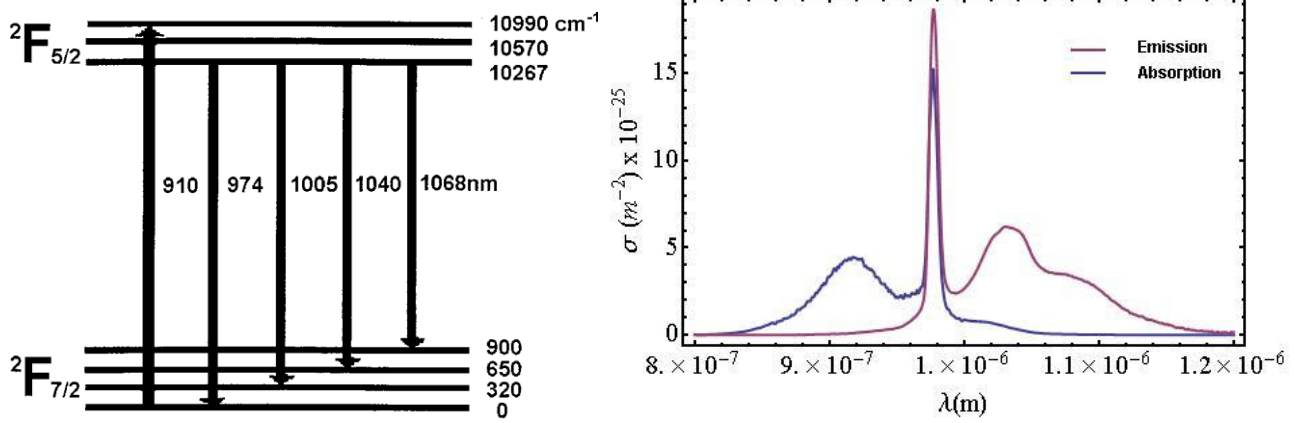


Figure 8. Yb energy level diagram (left) and emission and absorption cross-sections of Yb-doped silica fiber (right). [30,31]

$$N_2(z) = \frac{\sum_{i=1}^7 \frac{\tau \sigma_i^{(a)}}{\hbar \omega_i} I_i + \sum_{i=1}^3 \frac{\tau \sigma_{i,S}^{(a)}}{\hbar \omega_{i,S}} I_{i,S} + \frac{\tau \sigma_p^{(a)}}{\hbar \omega_p} I_p}{\sum_{i=1}^7 \frac{\tau (\sigma_i^{(a)} + \sigma_i^{(e)})}{\hbar \omega_i} I_i + \sum_{i=1}^3 \frac{\tau (\sigma_{i,S}^{(a)} + \sigma_{i,S}^{(e)})}{\hbar \omega_{i,S}} I_{i,S} + \frac{\tau (\sigma_p^{(a)} + \sigma_p^{(e)})}{\hbar \omega_p} I_p + 1} N_0 \quad (3.7)$$

where N_0 represents the density of Yb ions in the fiber core, τ is the lifetime of the upper laser level, and the subscripted I 's represent the intensities of the various waves: $I_i = 2\varepsilon_0 cn |A_i|^2$. The intensity of the pump, which is taken to propagate in the same direction as the seeds, evolves according to:

$$\frac{dI_p}{dz} = \frac{d_{core}^2}{d_{clad}^2} (N_2 \sigma_p^{(e)} - N_1 \sigma_p^{(a)}) I_p \quad (3.8)$$

where as shown in Figure 6, d_{core} and d_{clad} are the diameters of the core and the cladding, respectively. The evolution of the field amplitude of the highest frequency wave is given by:

$$\frac{dA_3}{dz} = \frac{g_3}{2} A_3 - \frac{g_B \varepsilon_0 c n_3 \kappa_{ao}}{4} |A_{3,S}|^2 A_3 + \frac{i \omega_3 n^{(2)} \kappa_{pm}}{c} f_3 \quad (3.9)$$

where g_3 is the laser gain for signal ω_3 and has a similar form to Eq. (3.5), and where f_3 and n_3 are the FWM terms and the linear index of refraction, respectively. The Stokes light is initiated from noise and travels counter to the signal waves. The spatial evolution of the field amplitudes of the two Stokes waves corresponding to $A_{i,S}, i = 2, 3$ can be expressed in compact form as:

$$\frac{dA_{i,S}}{dz} = -\frac{g_{i,S}}{2} A_{i,S} - \frac{g_B \varepsilon_0 c n_i \kappa_{ao}}{4} (|A_i|^2 + \alpha |A_{i-1}|^2) A_{i,S} \quad (3.10)$$

where the Stokes laser gain has a similar form to Eq. (3.5). The evolution of the amplitude of the Stokes wave corresponding to $A_{1,S}$ is given by:

$$\frac{dA_{1,S}}{dz} = -\frac{g_{1,S}}{2} A_{1,S} - \frac{g_B \varepsilon_0 c n_1 \kappa_{ao}}{4} |A_1|^2 A_{1,S}. \quad (3.11)$$

The boundary conditions for the signal, FWM, and Stokes fields are:

$$A_i(z=0) = \begin{cases} A_i^0 & i = 1, 2, 3 \\ 0 & otherwise \end{cases} \quad (3.12)$$

$$A_{i,S}(z=L) = 10^{-6} A_i(L) \quad (3.13)$$

The Stokes wave, is initiated from noise at the opposite end of the fiber and travels in

the backward direction. Note that the noise contribution is incorporated into Eq. (3.13) as we employ a localized source model as proposed by Zel'dovich et al. [18] Eq. (3.13) physically represents the approximation that the distributed acoustic noise present in the fiber may be localized at the end of the fiber by estimating the number of photons present due to the signal intensity at the output end. For a uniform temperature distribution this approximation is highly accurate. However, as will be shown later in this dissertation, when the effects of temperature gradients are modeled with the SBS process, the noise must be taken as a distributed source since hotter sections of the fiber contain more thermal noise. [13] It should be noted that since the boundary conditions in Eqns. (3.12-3.13) are on opposite ends of the integration domain, the system is a two-point boundary problem. In order to solve this system a shooting method technique is employed to match the known boundary conditions at the input and output ends of the fiber. To be precise, the boundary value problem is such that laser signals and the co-propagating pump are known at $z = 0$, while the Stokes signals are initiated from noise at $z = L$. The sidebands signals are set to zero at $z = 0$. To that end, the system of ODE's are solved using the explicit Runge-Kutta Four (RK4) method in an iterative fashion until the boundary conditions $z = L$ are satisfied to within 0.01 %.

The numerical solver is subjected to several tests in order to verify both its numerical accuracy and to confirm that it captures the correct physics. One set of tests simulated a passive fiber with the SBS gain neglected. In this case, our simulations agreed with the expected results with regards to FWM, including the square sinusoidal behavior with distance in the case of phase mismatch and the quadratic behavior in the case of perfect phase-matching at low seed powers (low conversion efficiency). Furthermore, the total energy of the seeds and the sidebands was shown to be numerically conserved to better than one part in 10^6 . Another set of tests simulated a passive fiber with SBS gain but no FWM. Calculations of SBS thresholds compared well to those reported in the

literature and to the well-known approximation of the SBS threshold in a passive fiber [53]: $P_{th} \sim [21 - 25]A_{eff} / g_B L_{eff}$, where A_{eff} and L_{eff} are the effective core area and effective length of the fiber respectively. Furthermore, it was verified that the difference in optical powers between the signals and Stokes fields, $\sum_i P_i - \sum_i P_{i,S}$, was constant along the length of the fiber to better than one part in 10^6 .

3.3 FOUR-WAVE MIXING EFFECTS

The system of equations discussed in section 3.2 represents a two-point boundary consisting of an 11x11 system of nonlinear differential equations describing the optical fields and one algebraic equation, which describes the population inversion. The total number of FWM terms represented by f_i is 128. This can be determined from computing the total pertinent number of possible combination of four-wave interactions. For each of the signal waves, there are 20 distinct FWM terms of which 7 terms represent self-phase modulation (SPM) and cross-phase modulation (XPM). The FWM terms for the signal waves are of the following form:

$$\begin{aligned}
f_1 = & |A_1|^2 A_1 + 2 \sum_{i \neq 1} |A_i|^2 A_1 + A_2^2 A_3^* \exp[i(2\beta_2 - \beta_3 - \beta_1)z] \\
& + 2A_1^* A_2 A_4 \exp[i(\beta_2 + \beta_4 - 2\beta_1)z] \\
& + 2A_2^* A_3 A_4 \exp[i(\beta_3 + \beta_4 - \beta_2 - \beta_1)z] \\
& + 2A_5^* A_2 A_3 \exp[i(\beta_2 + \beta_3 - \beta_1 - \beta_5)z] + \dots
\end{aligned} \tag{3.14}$$

$$\begin{aligned}
f_2 = & |A_2|^2 A_2 + 2 \sum_{i \neq 2} |A_i|^2 A_2 + 2A_1 A_2^* A_3 \exp[i(\beta_1 + \beta_3 - 2\beta_2)z] \\
& + A_1^2 A_4^* \exp[i(2\beta_1 - \beta_4 - \beta_2)z] \\
& + 2A_1^* A_3 A_4 \exp[i(\beta_3 + \beta_4 - \beta_1 - \beta_2)z] \\
& + A_3^2 A_5^* \exp[i(2\beta_3 - \beta_5 - \beta_2)z] \\
& + 2A_1 A_3^* A_5 \exp[i(\beta_1 + \beta_5 - \beta_2 - \beta_3)z] + \dots
\end{aligned} \tag{3.15}$$

$$\begin{aligned}
f_3 = & |A_3|^2 A_3 + 2 \sum_{i \neq 3} |A_i|^2 A_3 + A_2^2 A_1^* \exp[i(2\beta_2 - \beta_1 - \beta_3)z] \\
& + 2A_1 A_2 A_4^* \exp[i(\beta_1 + \beta_2 - \beta_3 - \beta_4)z] \\
& + 2A_1 A_2^* A_5 \exp[i(\beta_1 + \beta_5 - \beta_2 - \beta_3)z] \\
& + 2A_2 A_3^* A_5 \exp[i(\beta_2 + \beta_5 - 2\beta_3)z] + \dots
\end{aligned} \tag{3.16}$$

The first two terms on the right hand side of Eqns. (3.14)-(3.16) represent SPM and XPM. The third term represents direct interactions among the signal waves, while the rest of the terms represent interactions with the sidebands. Note that for brevity only direct interactions with the inner sidebands are written explicitly in the equations above, although in the simulations the full set of FWM interactions are considered.

For each of the two inner sidebands ($i = 4, 5$), there are 18 distinct FWM terms including 7 SPM and XPM terms and two driving terms containing products of the amplitudes of the signal waves only. The SPM, XPM, and driving terms for f_4 and f_5 appearing in the inner sideband field evolution equations are given below:

$$\begin{aligned}
f_4 = & |A_4|^2 A_4 + 2 \sum_{i \neq 4} |A_i|^2 A_4 + A_1^2 A_2^* \exp[i(2\beta_1 - \beta_2 - \beta_4)z] \\
& + 2A_1 A_2 A_3^* \exp[i(\beta_1 + \beta_2 - \beta_3 - \beta_4)z] + \dots
\end{aligned} \tag{3.17}$$

$$\begin{aligned}
f_5 = & |A_5|^2 A_5 + 2 \sum_{i \neq 5} |A_i|^2 A_5 + A_3^2 A_2^* \exp[i(2\beta_3 - \beta_2 - \beta_5)z] \\
& + 2A_1^* A_2 A_3 \exp[i(-\beta_1 + \beta_2 + \beta_3 - \beta_5)z] + \dots
\end{aligned} \tag{3.18}$$

For the right hand side of each equation, the first term results in SPM, the second set of terms results in XPM, and the third and fourth terms are the driving terms. Recalling that for relatively low conversion efficiency FWM is proportional to the cubic of the signal powers, one would expect in the case of small wavelength separation considerable power to be generated in the inner sidebands.

For each of the two outer sidebands ($i = 6, 7$), there are 16 distinct FWM terms including 7 SPM and XPM terms and one driving term containing products of the amplitudes of the signal waves only:

$$f_6 = |A_6|^2 A_6 + 2 \sum_{i \neq 6} |A_i|^2 A_6 + A_1^2 A_3^* \exp[i(2\beta_1 - \beta_3 - \beta_6)z] \quad (3.19)$$

$$f_7 = |A_7|^2 A_7 + 2 \sum_{i \neq 7} |A_i|^2 A_7 + A_1^* A_3^2 \exp[i(-\beta_1 + 2\beta_3 - \beta_7)z] \quad (3.20)$$

Mathematica is used to generate all 128 FWM terms in symbolic form, which are then imported into our numerical two-point boundary problem solver. It is worthwhile to point out here that the symbolic and numerical code can also be used to simulate single, and two-tone amplification for this case by setting one/two of the input seed signals to zero.

3.4 OPTIMIZATION OF SEED RATIOS

In Ref. [7] it was estimated and proven experimentally that for optimal SBS suppression the seed ratio between the higher and lower frequencies should be 2:1. It should be clear from Figure 5 that in order to maximize the effect of power transfer between the Stokes of the higher frequency signals into the lower frequency optical signals, one must seed harder in the higher frequency signals (ie. $E_{i+1}(z=0) > E_i(z=0)$). However, if the seed ratio is too large, the SBS gain in the higher frequency signal will be substantially larger than the others leading to minimal power enhancement. In the opposite limit, where the higher frequency seed is seeded too low the SBS gain of the lower frequency signal will be too large. Thus, in order to maximize the SBS suppression the seed ratios should be chosen such that the SBS gain for each signal is the same. This optimized case can be estimated by considering a passive fiber and neglecting the FWM terms. Expressing the input ratios

of the signals shown in Figure 7 as $r = P_1 / P_2$, $q = P_2 / P_3$, and using the undepleted pump limit, the small signal SBS gain for the three Stokes waves is:

$$G_{3,S} = \frac{g_B \epsilon_0 c n \kappa_{ao} |A_3|^2}{4} (1 - q)(L - z), \quad (3.21)$$

$$G_{2,S} = \frac{g_B \epsilon_0 c n \kappa_{ao} |A_3|^2}{4} q(1 - r)(L - z), \quad (3.22)$$

$$G_{1,S} = \frac{g_B \epsilon_0 c n \kappa_{ao} |A_3|^2}{4} r q(L - z). \quad (3.23)$$

Therefore, it is straightforward to show from Eqn. (3.21)-(3.23) that for this variant of three-tone amplification, the optimal ratio of the three input seeds should be close to 3:2:1 in order of higher to lower frequency. Based on this analysis, one would then expect the total power to be 6 times more than the single-tone amplification case. In general, for N-tone amplification, the ratio should be close to $N : N - 1 : N - 2 \dots$, though one would expect some departure from this ratio due to FWM and laser effects.

3.5 NUMERICAL RESULTS

3.5.1 TWO-TONE SIMULATIONS

In this section a 25/400 μm Yb-doped gain fiber is used to theoretically investigate the two-tone suppressing technique implemented experimentally by Weßels et al. [7] The dopant level N_0 is taken to be $1.2 \times 10^{26} / \text{m}^3$ (typical of a standard 25/400 Yb-doped fiber with 2.4dB/m absorption at 976nm). The cross-sections are taken from experimental values [37] and the lifetime τ of the upper level is $8.0 \times 10^{-4} \text{s}$. As previously mentioned, the LMA fiber is assumed to be coiled so that the power in the higher-order fiber modes can be neglected. The peak Brillouin gain is taken as $g_B = 5 \times 10^{-11} \text{m} / \text{W}$ and a 6.5 m long fiber is considered. This technique relies on selecting the two

input frequencies to be equal to twice the Brillouin shift Ω_B , i.e. twice the frequency of the phonon field. In optical fibers, this value is approximately 32 GHz ($\Delta\lambda_B \sim 0.1nm$). The wavelengths selected for the two seeds were close to 1068 nm, while the pump wavelength for this amplifier is chosen to be $\lambda_p = 976nm$. In this case, only the two inner sidebands are considered. In accordance with Figure 7, these sidebands oscillate at $\omega_4 = \omega_1 - \Delta\omega$ and $\omega_3 = \omega_1 + 2\Delta\omega$, where $\Delta\omega = \omega_2 - \omega_1 = 32GHz$. As described in section 3.4, in order to achieve the largest suppression of SBS, the SBS small signal gain for each of the Stokes fields has to be approximately equal. In this case, the optimal seed ratio $r = P_1 / P_2$ is 1/2, i.e. the input power of ω_2 is twice that of ω_1 . This is the same power ratio used by Wessels et al. and is further borne out by the numerical simulations presented below. In addition, the SBS threshold considered here is defined when either of the two signals reaches a reflectivity of 1%, i.e. $R_i = 100 \times P_{s,i}(0) / P_i(L) = 1\%$, where $P_{s,i}$ and P_i describe the powers of the Stokes and signals respectively.

The amplified powers are shown in Figure 9 with the single-seed case also shown for comparison. The maximum total power out of this two-tone amplifier was greater than 80 W, an approximately three-fold increase in total power over the single seed case. Furthermore, the total power output in one of the signals was twice that of the single tone case. This is close to the improvement noted in the experimental results of Ref. [7]. The nonlinear effects in this amplifier are shown in Figure 10. The FWM effects are significant in the case, but they are still roughly a factor of 10 less than what was previously experimentally observed. [7] This is due mainly to the much shorter length of this Yb-doped amplifier compared to the km long fiber considered in the previous Weßels experiment.

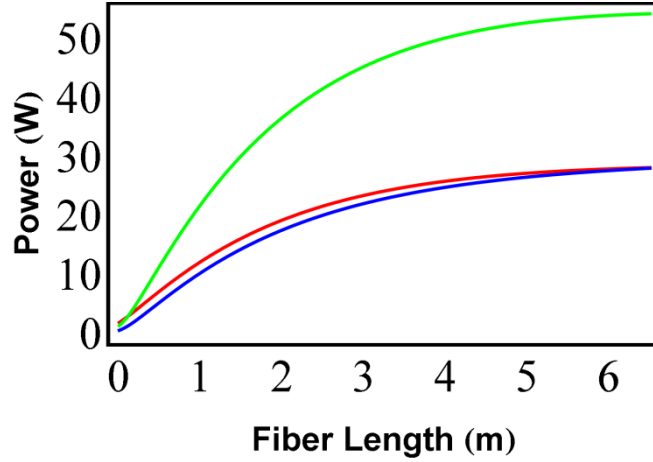


Figure 9. The signal power evolution of a two-tone amplifier compared with a single-tone amplifier. The power of the $\lambda = 1068nm$ single-tone case (red) reaches 28 W of output power before the SBS threshold is reached. The total output of the two-tone case with signals oscillating at $\omega_2 = \omega_1 + \Delta\omega$, $\lambda_2 \sim 1067.9nm$ (green) and $[\omega_1, \lambda_1 = 1068nm]$ (blue) was over 80 W. In the two-tone amplifier, the two signals are separated by twice the Brillouin shift ($\Delta\omega = 2\Omega_B \sim 32GHz$, $\Delta\lambda \sim .1nm$), allowing the Stokes light oscillating at $\omega_{s,2}$ generated by the signal oscillating at ω_2 to transfer its energy to the signal light oscillating at ω_1 . The seed ratio for the two-tone case is $P_2 / P_1 = 2$.

Additional aspects of this case of two-tone amplification, such as the optimal 2:1 ratio, were also considered. Keeping track of the total output power, the input seed ratio was varied from 1:1 up to 3:1 with a total seed power of 2W. For these simulations, the total seed power remained constant but pump power was varied until the SBS threshold was reached. The results of this investigation are shown in Figure 11. As shown in Figure 11, there is actually a broad range of input ratios spanning approximately 1.8 to 2.3 that effectively mitigate SBS by providing an output power that is within 5% of the maximum achievable power output.

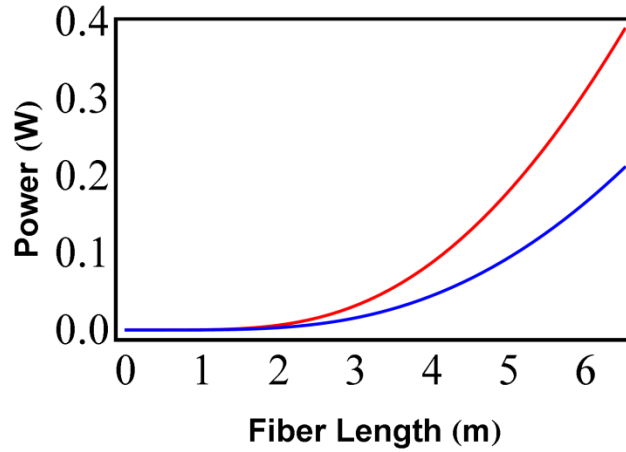


Figure 10. The FWM power generated in the inner sidebands $[\omega_3 = \omega_1 + 2\Delta\omega, \lambda_3 \sim 1067.8nm]$ (red) and $[\omega_4 = \omega_1 - \Delta\omega, \lambda_4 \sim 1068.1nm]$ (blue) shown in Figure 7 for the two-tone amplifier. Due to the small wavelength separation FWM is the lowest threshold nonlinear process. ($\Delta\omega = 2\Omega_B \sim 32GHz, \Delta\lambda \sim .1nm$).

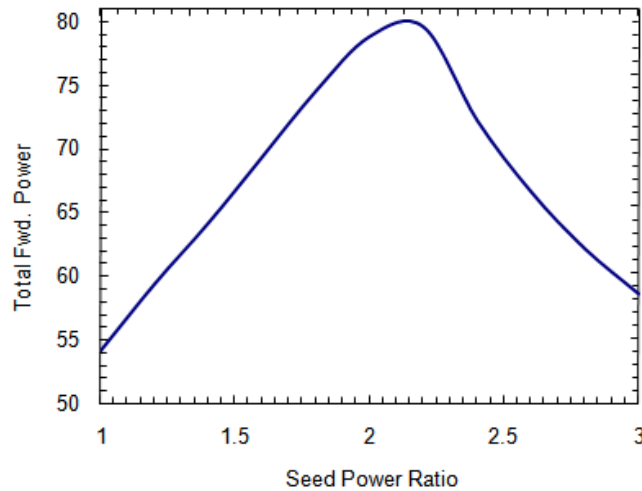


Figure 11. The dependence of total output power for two-tone amplifier on seed power ratio. The two frequencies are separated by twice the Brillouin shift. Here, The seed power ratio is defined as the input power of the higher frequency wave divided by that of the lower frequency $P(\omega_2) / P(\omega_1)$ and the total seed is 2 W.

Furthermore, the optimal seed ratio is close to the theoretical approximation of 2:1 where the slight discrepancy is due to laser gain, pump depletion, and FWM effects which were not considered in the derivation of Eqns. (3.21)-(3.23).

3.5.2 *THREE-TONE SIMULATIONS*

In this section, Weßels SBS mitigating concept [7] is extended to three-tones. The fiber parameters are the same as those listed in the preceding section with the exception that here the seeds are chosen near 1064 nm to investigate the concept at a different wavelength. Additionally, the full four sidebands shown in Figure 7 were considered. For one set of simulations, the fiber is seeded with a total of 2 watts with input ratios close to the optimal condition, i.e. (3:2:1). In order to reach the SBS threshold, the input pump power was set at 184 W. As a working definition, again the SBS threshold here is defined as occurring when the Stokes light due to any one of the signals reaches 1% of the corresponding laser light. The results are shown in Figure 12. For comparison purposes, the case of one tone seeding pumped to the SBS threshold (approx. 28 W) using 32 W of pump power is also shown. The total output power of the three-tone amplification (approx. 152 W) is slightly higher than 5.4 times the output power from single-tone amplification (approx. 28 W). Based on the Eqns. (3.21)-(3.23), one would expect the total power to be closer to 6 times more. However, these equations do not account for FWM, which is substantial in this case. As a comparison, for two-tone amplification presented in the preceding section, the total power was approximately three times more. Due to the depletion of the highest frequency Stokes light via the added coupling to the middle signal light (ω_2) (see Figures 5 and 7.), the highest frequency signal light (ω_3) (see Figures 5 and 7) generates the highest output power at approximately 2.5 times that of the single-tone amplification.

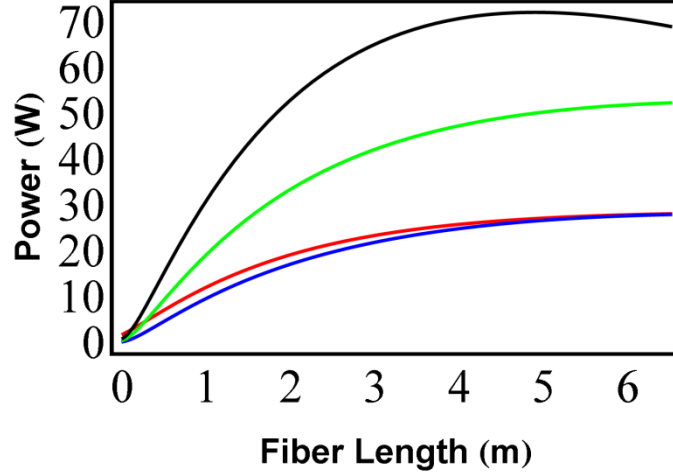


Figure 12. The signal power evolution of a three-tone amplifier compared with a single-tone amplifier. The power of the $\lambda = 1064nm$ single-tone case (red) reaches 28 W of output power before the SBS threshold is reached. The total output of the three-tone case with signals oscillating at (black), $\omega_2 = \omega_1 + \Delta\omega$, $\lambda_2 \sim 1063.9nm$ (green) and $[\omega_1, \lambda_1 = 1064nm]$ (blue) was approx. 152 W. In the three-tone amplifier, the three signals are separated by twice the Brillouin shift ($\Delta\omega = 2\Omega_B \sim 32GHz$, $\Delta\lambda \sim .1nm$), allowing the Stokes light oscillating at $\omega_{s,3}$ generated by the signal oscillating at ω_3 and the Stokes light oscillating at $\omega_{s,2}$ generated by the signal oscillating at ω_2 to transfer energy to the signals oscillating at ω_2 and ω_1 respectively. The seed ratios for the three-tone case are: $P_3 / P_1 = 3$ and $P_2 / P_1 = 2$ and the total seed power is 2W.

For two-tone amplification, the output of the highest frequency light was approximately twice as much as single-tone amplification. The rollover in the ω_3 output shown in Figure 12 is due to FWM as energy depletion due to this effect exceeded laser gain for that particular signal beyond the rollover point. The power output at ω_2 is twice the one tone case, while the output at ω_1 is approximately equal to it. The three Stokes waves are shown in Figure 13. Since for this set of simulations the amplifier is operating near threshold, the Stokes waves exhibit a sharp increase in strength near $z = 0$.

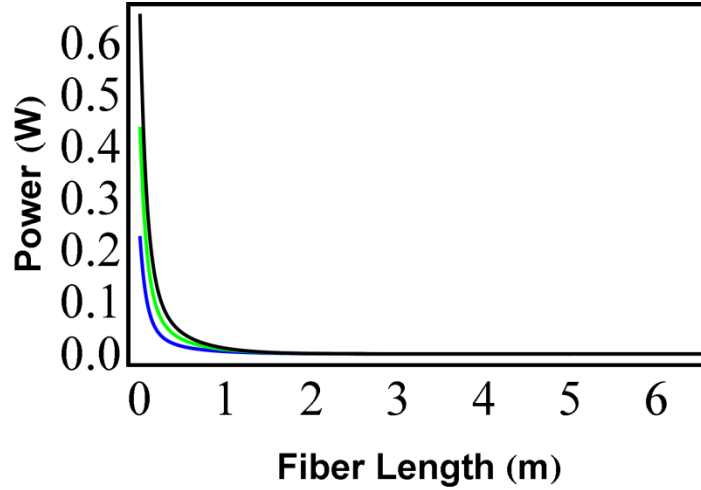


Figure 13. Spatial power evolution of the three Stokes waves $\omega_{S,1} = \omega_1 - \Omega_B$ (black), $\omega_{S,2} = \omega_2 - \Omega_B$ (green), and $\omega_{S,3} = \omega_3 - \Omega_B$ (blue). The Stokes waves propagate counter to the laser signals.

The FWM powers as a function of the fiber length are shown in Figure 14. Due to the small wavelength separation, the amount of FWM power is substantial in the inner sidebands and approximately an order of magnitude less in the outer sidebands. Therefore, for this particular variant of three-tone amplification, FWM is more dominant than SBS effects and is much higher than was previously found for two-tone amplification in section 3.5.1. As mentioned above, this is due to the increased number of driving terms in the three-tone case. The high level of FWM makes the implementation of this three-tone amplification in high power amplifiers impractical in the absence of specially designed dispersive fibers.

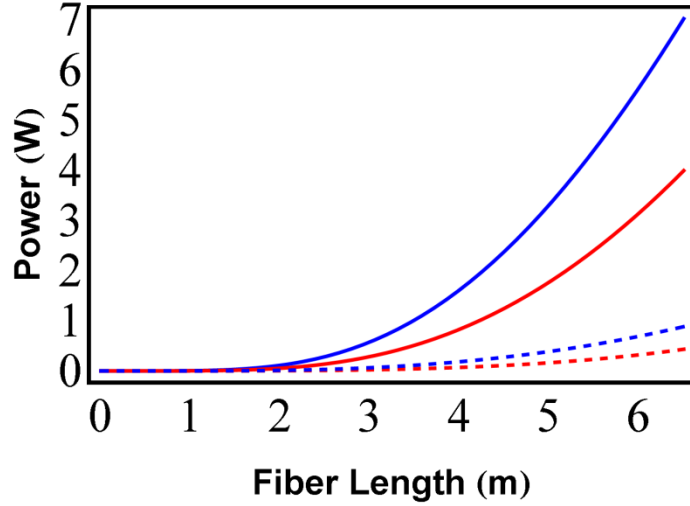


Figure 14. The FWM power generated in the inner and outer sidebands $[\omega_5 = \omega_1 + 3\Delta\omega, \lambda_5 \sim 1063.7nm]$ (solid blue), $[\omega_4 = \omega_1 - \Delta\omega, \lambda_4 \sim 1064.1nm]$ (solid red), $[\omega_7 = \omega_1 + 4\Delta\omega, \lambda_7 \sim 1063.6nm]$ (dashed blue) and $[\omega_6 = \omega_1 - 2\Delta\omega, \lambda_6 \sim 1064.2nm]$ (dashed red) shown in Figure 7 for the three-tone amplifier. Due to the small wavelength separation FWM is the lowest threshold nonlinear process. ($\Delta\omega = 2\Omega_B \sim 32GHz$, $\Delta\lambda \sim .1nm$).

The optimal ratio condition for this technique was also investigated by running a set of simulations covering a sizable range of input seed ratios. This was accomplished by holding the total input seed power at 2 W for each set of input ratios while the pump power was increased until the SBS threshold was reached. The optimal ratio was found to be approximately 3.6: 2.2: 1, although as can be seen from Figure 15 there is a fairly large range of tunability that can get to within 10% of the maximum achievable power. Again, the departure of this numerically determined optimal ratio from the ratio derived previously (3:2:1) can be traced to the neglect of laser gain and FWM in the simplified analytical model.

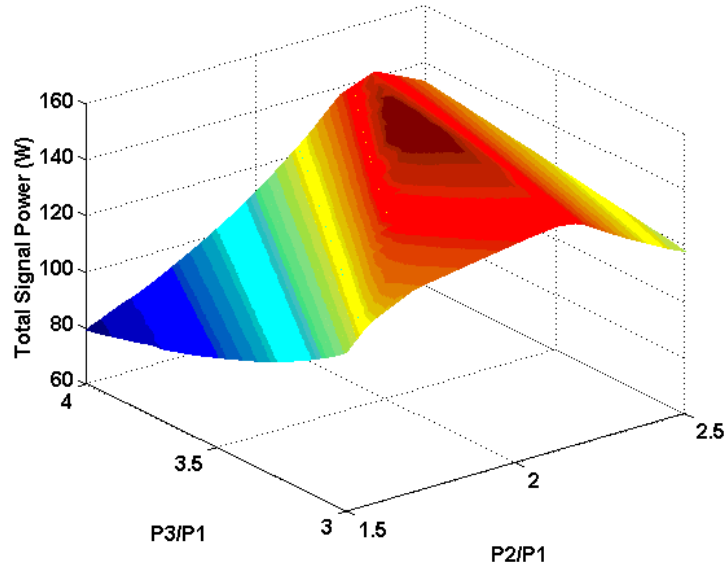


Figure 15. Surface plot of the total laser output power versus seed power ratios indicating optimal conditions for a total seed power of 2 W for the three-tone case. Here the seed ratios are defined as: $P3 / P1 = P(\omega_3) / P(\omega_1)$ and $P2 / P1 = P(\omega_2) / P(\omega_1)$.

3.6 SUMMARY

A theoretical investigation that rigorously formulated the problem of a Yb-doped amplifier seeded with multiple laser frequencies separated at twice the Brillouin shift was performed. In this model, stimulated Brillouin scattering and four-wave mixing were included. Two cases were considered and were shown to enhance the total output power and the output power of the highest frequency signal: 1) a two-tone scheme and 2) a three seeded case. In both cases the enhancement power was close to the theoretical predictions and in the former in agreement with experimental results [7]. In addition, the optimal seed ratios for both cases were derived and validated numerically by solving the system of $N \times N$ differential equations. The results showed a slight discrepancy from the theoretical predictions due to the neglect of FWM and laser gain from the theoretical approximation. Nevertheless, this model serves as a powerful tool to simulate SBS suppression for a

fiber amplifier seeded with multiple signals separated at twice the Brillouin shift. In addition, FWM was shown to be significant as the number of input seeds was increased from 2 to 3, thus identifying a possible limitation to the effectiveness of this concept in fiber amplifiers not specifically designed to mitigate FWM, i.e. dispersive fibers.

4 MULTI-TONE SEEDING (LASER GAIN COMPETITION)

4.1 INTRODUCTION

The SBS mitigation technique discussed in Chapter 3 resulted in an increased SBS threshold for one of the seed signals through additional interactions among the input and Stokes signals, but also transferred large amounts of power into numerous FWM-generated sidebands. This broadening of the optical power spectrum precludes the application of this method to fiber laser applications that require well-defined spectra such as electronically phased coherent arrays[9,38,39] and spectral beam combination [40,41]. In addition, the maximum optical efficiency of the highest output signal in the two-tone technique described in Chapter 3 is ~67%. In this chapter a new variant of multi-tone seeding is presented in which the separation between the signals is so large that FWM is negligible and the optical efficiency can exceed 80%. Additionally, since the wavelengths are separated by more than 4 nm current dichroic technologies may be used to achieve single-frequency output. In the previous approach, this is not easy to achieve since the wavelength separation is on the order of 32 GHz. In this case, the SBS suppressing mechanism is a result of laser gain competition between the signals propagating in the active fiber medium. Due to its suppression of FWM and the ability to achieve only one frequency at the output end of the amplifier, this is much more suited for use in laser applications requiring single frequency spectral output.

In the following sections, this novel concept is investigated theoretically in Yb-doped high power fiber amplifiers for two and three seeded configurations. The equations describing this concept are the same as those described in Chapter 3 with the exception that, in this case, the third term in Eqs. (3.3) and (3.10) is non-existent. Recall that this term describes the interaction between the input and Stokes fields for a precise frequency separation of twice the Brillouin shift: $\Delta\omega = 2\Omega_B$ (~32 GHz). Although, this separation does define the maximum SBS suppression for the technique,

SBS suppression is still observed as long as the frequency separation lies within the range $(2\Omega_B - \Gamma_B, 2\Omega_B + \Gamma_B)$, where Γ_B (~ 60 MHz) is the spontaneous Brillouin bandwidth. [7] In the technique presented in this chapter, the minimum wavelength separation considered is 4 nm (well outside range quoted above) and thus there is no coupling between the input and Stokes fields. Two variants of SBS suppression through laser gain competition will be explored: an amplifier seeded with multiple single-frequency signals and an amplifier seeded with a combination of single-frequency and broad-band signals. Here, the terminology single-frequency and broad-band refer to signals where the spectral width is much smaller and much larger than the spontaneous Brillouin bandwidth, respectively. In the latter case, the linewidth of the broad-band laser signal is assumed to be sufficiently large such that the SBS process for that signal may be neglected.

In addition, this chapter shows that, with a large enough separation, the FWM terms described in Chapter 3 become negligible up to 100's of watts of output power. In this approximation, the equations described in Chapter 3 are transformed into power equations and additional terms are added that describe the effects of thermal gradients on the SBS process. These terms are necessary to accurately model the SBS suppression from laser gain competition in amplifiers seeded with multiple signals. As will be shown, the effects of laser gain competition between the signals create a favorable thermal gradient inside the fiber, which leads to even further SBS suppression.

4.2 NUMERICAL RESULTS (TWO-TONE SIMULATIONS)

The large wavelength separation case of two-tone seeding is modeled for a gain fiber with parameters based on Nufern's 25/400 μm LMA Yb-doped fiber. The dopant level N_0 is taken to be $1.2 \times 10^{26} / \text{m}^3$ (derived from the manufacturer quoted 2.4 dB/m absorption at 976 nm). The cross-sections are taken from experimental values [37] and the lifetime τ of the upper level is $8.0 \times 10^{-4} \text{ s}$.

The numerical aperture (NA) for this fiber is 0.06 and, as previously mentioned, the LMA fiber is assumed to be coiled so that the power in the higher-order fiber modes can be neglected. Since dispersion effects in the nonlinear index of refraction are negligible, for all waves we use $n^{(2)l} = 3 \times 10^{-20} m^2 / W$, where $n^{(2)l}$ is related to the non-linear index of refraction $n^{(2)}$ used in Chapter 3 by $n^{(2)l} = (2\mu_0 c \cdot n^{(2)}) / n$. We take a value of the group velocity dispersion, $\beta^{(2)}$ of 15 ps²/km as computed from the fitted experimental measured dispersion of bulk-fused silica at 1.0 μm region [42]. This is done to estimate the values of the phase matching terms in our coupled system. The 8x8 coupled system of equations as described in Chapter 3 is solved numerically using the same technique described previously (Section 3.4. p. 39): RK4 in conjunction with a shooting method.

Numerous runs were completed to validate the power improvement available for ‘two-tone’ amplification in the case of wavelength separation $\Delta\lambda = 4nm$. For the first test, 6.5 meters fiber segment was seeded with a 1.2 W 1064 nm signal and a 0.8 W 1068 nm signal using a 976nm pump. This particular ratio of seed powers was selected to optimize total output power. If the ratio of the input powers is not chosen carefully, one of the seeds can become more quickly amplified; this ‘robs’ the other input signal of its gain and ensures that the intensity of the quickly amplified signal will increase enough to reach the SBS threshold well below the maximum possible total output power. Figure 16 shows that the percent of SBS at constant pumping level near threshold can vary dramatically with the power ratio of the seed inputs. Here the total seed power was fixed at 2W. It should be pointed out here that the optimal ratio does not follow the ratios in the Weßels et al. technique, as this technique differs in the mechanisms leading to SBS suppression. To be clear, there is no obvious simple analytical form for the optimal ratio for the large wavelength separation case as this ratio will be dependent on the choice of the wavelengths, pump intensity, fiber core size, and fiber length.

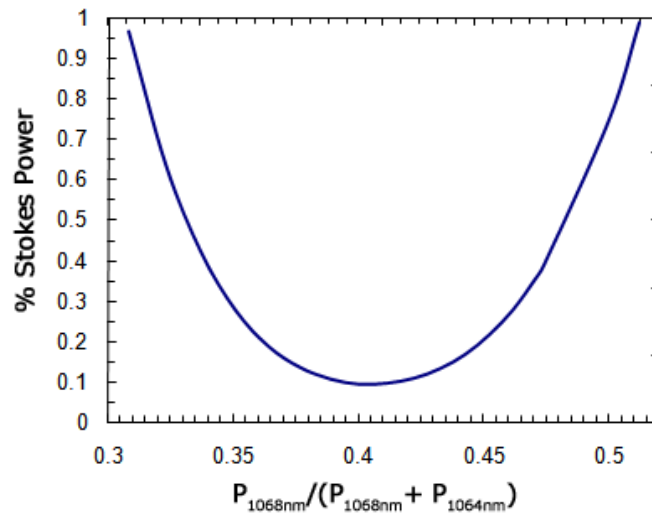


Figure 16. The sensitivity of SBS to the ratio of the input signals in ‘two-tone’ amplification. The x-axis shows the ratio of power in one input signal (1068nm) to the total input power. The y-axis represents percentage of Stokes power. The total seed power was fixed at 2 W.

The case of a single 2.0 W 1064 nm seed was also modeled for comparison. In these model runs, the power from a 976nm pump was increased for each seed method until the SBS threshold was reached. For clarity, a working definition of the SBS threshold is adopted where the generated SBS power from a signal, that is, from a single 1064 nm seed or either of the ‘two-tone’ seeds, reached 1% of the output power for that amplified signal. The results of the model runs at this defined SBS threshold are shown in Figures. (17-19).

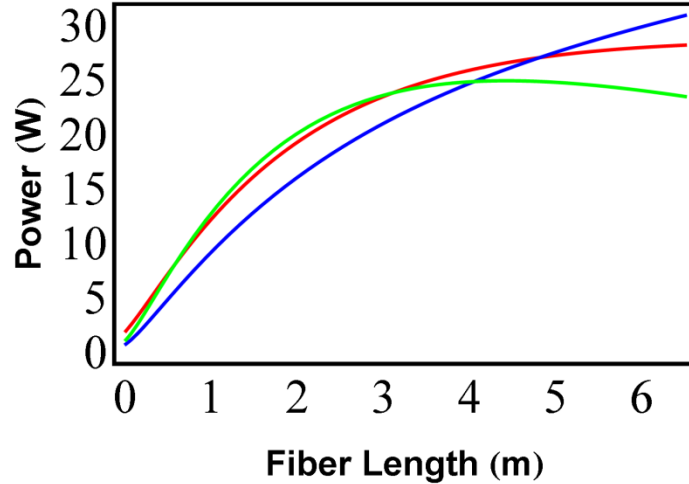


Figure 17. The signal power evolution of a two-tone amplifier compared with a single-tone amplifier using laser gain-competition. The power of the $\lambda = 1064nm$ single-tone case (red) reaches 28 W of output power before the SBS threshold is reached. The total output of the two-tone case with signals oscillating at $\omega_2 = \omega_1 + \Delta\omega$, $\lambda_2 \sim 1064nm$ (green) and $[\omega_1, \lambda_1 = 1068nm]$ (blue) was approx. 54 W. In the two-tone amplifier, the two signals are separated by $(\Delta\omega \sim 1THz, \Delta\lambda \sim 4nm)$. The input seed powers were 1.2 W and 0.8 W for the 1064nm and 1068nm signals respectively.

The typical single seed amplification reached SBS threshold at 33 W of pump power for an amplified power of approximately 28 W; the two-tone case reached its SBS threshold at 62 W of pump power. Here the output power of the 1064nm signal was approximately 24.5 W and 30 W for the 1068 nm signal for a total exceeding 54 W. Thus, the total amplified power from the two-tone amplifier was almost twice the single seed case with minimal FWM while maintaining the overall optical efficiency and suppressing SBS. Note from Figures 18 and 19, FWM is an order of magnitude lower than SBS. Furthermore, it can be inferred that the coherence lengths of the two FWM sidebands are different. This is due to laser gain in the sidebands as well as SPM and XPM effects.

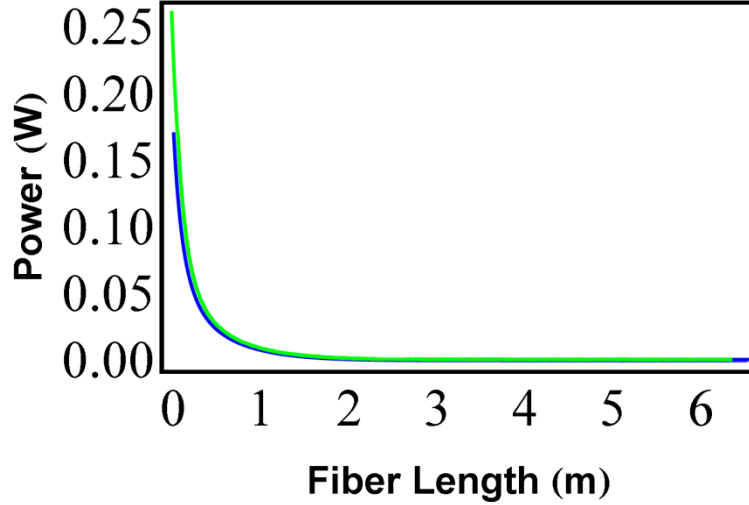


Figure 18. Spatial power evolution of the three Stokes waves $[\omega_{S,1} = \omega_1 - \Omega_B, \lambda_1 = 1068nm]$ (blue), $[\omega_{S,2} = \omega_2 - \Omega_B, \lambda_2 = 1064nm]$ (green). The Stokes waves propagate counter to the laser signals.

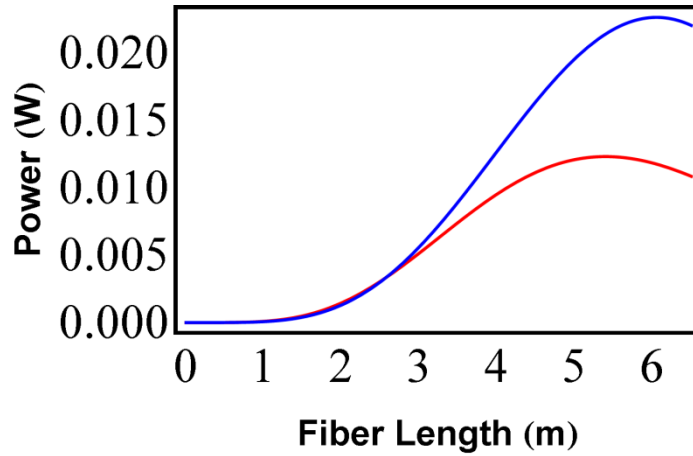


Figure 19. The FWM power generated in the inner sidebands $[\omega_3 = \omega_1 + 2\Delta\omega, \lambda_3 \sim 1060nm]$ (red) and $[\omega_4 = \omega_1 - \Delta\omega, \lambda_4 \sim 1072nm]$ (blue) shown in Figure 7 for the two-tone amplifier. ($\Delta\omega = 1THz, \Delta\lambda \sim 4nm$). Note that the power in these sidebands is one order of magnitude lower than the SBS power.

Referring to Figure 17, it is worthwhile to mention here that at some point along the fiber, the 1064 nm light will experience negative laser gain. This will be explained further in this chapter.

Since considerable effort has recently been devoted to building high power narrow-linewidth amplifiers [43,44,45], the possible use of this technique in conjunction with other SBS-suppressing

techniques was also examined. For these cases, an SBS suppressing fiber was used in order to test regimes where FWM was the lowest threshold nonlinear effect and thus would impose an upper limit on achievable power. The two-tone amplifier (with a 4nm wavelength separation) was modeled with 350 W and 550 W of pump power corresponding to an approximately SBS gain reduction factor of 6 and 10, respectively. This mirrors the possible suppression available with fibers constructed to specific acoustic guiding properties [43,44,45]. The laser efficiencies of these model runs were approximately equal to the previous simulations. The FWM was comparable to SBS at 350 W, but exceeded it at 550 W. Note from Figure 20, that the coherence length of the FWM sidebands has decreased from the previous simulations (see Figure 19) due to the increased SPM and XPM effects. All of this suggests that at a wavelength separation of 4 nm, this technique can be applied to amplifiers with outputs near 550 W while keeping FWM to reasonably low levels (1-10W).

Returning back to the initial amplifier configuration (with the SBS gain suppressing factor turned off), the wavelength separation of the two input signals was increased and decreased. For these tests, the pump power was held constant at approximately 60W which was near our defined SBS threshold for $\Delta\lambda = 4nm$. For $\Delta\lambda < 3nm$ the FWM increased considerably and became comparable to the Stokes light. For $\Delta\lambda > 10nm$, the FWM was extremely small. Most remarkably for this wavelength separation, considerable enhancement (~64%) in the power output of the lower laser frequency was obtained. For example, at $\Delta\lambda = 14 nm$ and input seeds with wavelengths 1064 nm and 1050 nm, 46 W of output power was obtained for the 1064 nm light.

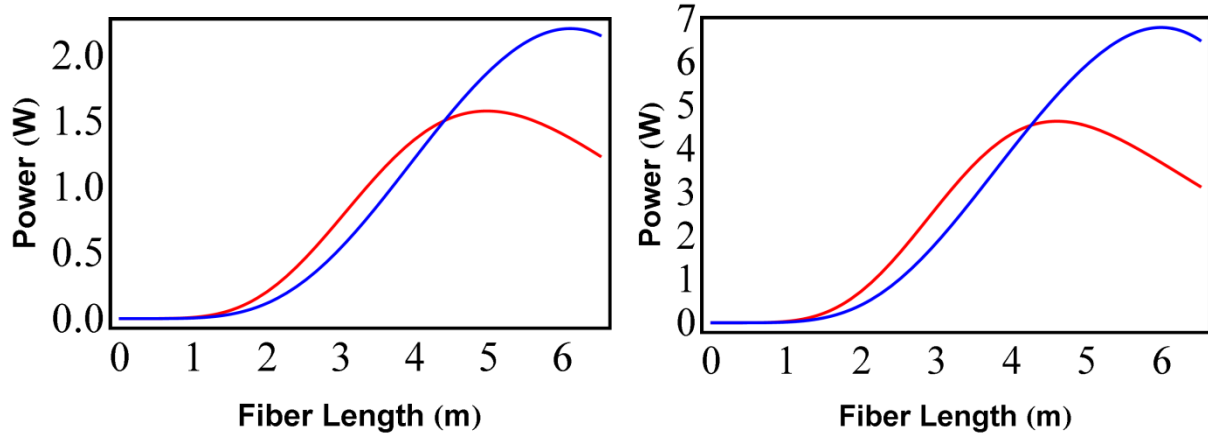


Figure 20. The FWM behavior of SBS-suppressed two-tone amplifiers with a) 350 W (left) and b) 550 W (right) of pump power. The FWM power generated in the inner sidebands $[\omega_3 = \omega_1 + 2\Delta\omega, \lambda_3 \sim 1060nm]$ (red) and $[\omega_4 = \omega_1 - \Delta\omega, \lambda_4 \sim 1072nm]$ (blue) shown in Figure 7 for the two-tone amplifier. $(\Delta\omega = 1THz, \Delta\lambda \sim 4nm)$. The additional pumping has altered the coherence period relative to that shown in Figure 19 due to SPM and XPM.

The power ratio needed to obtain this output was approximately 9:1 with the 1050 nm having the higher input power. The 46 W output power represented a 64% enhancement over a 1064 nm single tone amplifier as shown in Figure 21. Higher power output in one of the tones is possible to the point where almost all the output power would be in a single frequency. This can be achieved through an optimal ratio of seed and wavelength separation, or by selecting a more suitable fiber configuration; the details will be discussed further in this chapter. Note that the 1050 nm signal reaches its maximum value at a distance shorter than the midway point of the fiber. This is due to the higher pump power, the skewed input seed power ratio, and the higher emission cross section of the 1050 nm light as compared to that of 1064 nm light. As the two laser signals propagate down the fiber, the population density of the upper level state, N_2 , decreases.

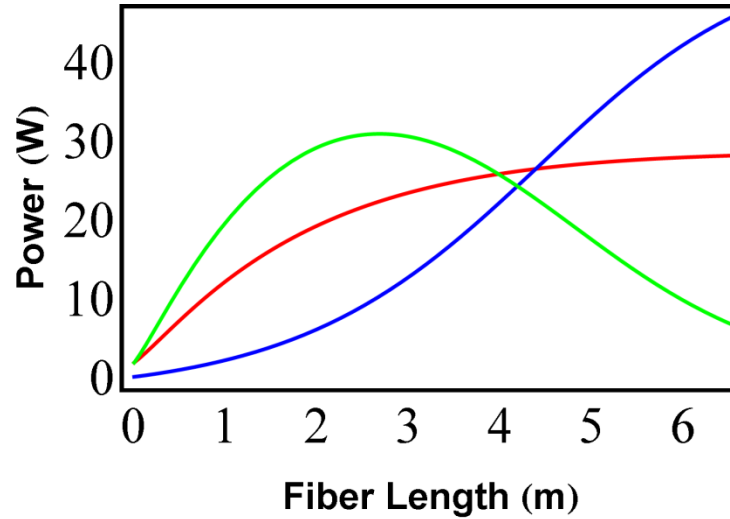


Figure 21. The signal power evolution of a two-tone amplifier compared with a single-tone amplifier using laser gain-competition. The power of the $\lambda = 1064\text{nm}$ single-tone case (red) reaches 28 W of output power before the SBS threshold is reached. The total output of the two-tone case with signals oscillating at $\omega_2 = \omega_1 + \Delta\omega$, $\lambda_2 \sim 1050\text{nm}$ (green) and $[\omega_1, \lambda_1 = 1064\text{nm}]$ (blue) was approx. 54 W but in this case over 46 W was generated in the 1064nm signal and represents a 64% enhancement in the SBS threshold relative to the single-tone case. In the two-tone amplifier, the two signals are separated by $(\Delta\omega \sim 3.7\text{THz}, \Delta\lambda \sim 14\text{nm})$. The input seed power ratio was approximately 9:1 with the 1050nm signal having the higher seed power.

Immediately past the point where the maximum power for the 1050 nm light is obtained, the population inversion is such that the 1050 nm light will experience negative laser gain. The 1064 nm, light which has an appreciably lower absorption cross section, will, however, continue to experience positive laser gain. As a consequence, power transfer occurs from the 1050 nm light and into the 1064 nm light. The SBS threshold is raised because the spatially integrated Stokes light gain for the two-tone 1064 nm light will be close to the 1064 nm single tone case even though more 1064 nm output power is obtained in the former. This is made possible because, for a significant portion of the fiber, the power in the 1064 nm light for the two tone case is less than that for the single tone case as can be seen from Figure 21. Here, the total gain for the electric field amplitude of the Stokes light as a function of position is examined. Referring to Eq. (3.10) in Chapter 3, this total gain is due

to the total of the laser and Brillouin gain. It is worthwhile to point out here that the amplitude gain is half that of the intensity or power gain. Figure 22 represents a comparison of the amplitude gain for the two-tone case pumped such that the power output at 1064 nm is equal to the power output in a single tone amplifier at threshold. Note that the spatially integrated Stokes gain for two-tone is reduced significantly, thus allowing for higher pumping power and consequently higher output at 1064 nm. While some 1050 nm light is unabsorbed in the fiber for the simulation discussed above, this technique represents a novel way to increase the power in CW narrow linewidth Yb-doped amplifiers. Later in this chapter it will be shown that the unabsorbed auxiliary signal light can be minimized by appropriate choice of seed ratio and proper selection of wavelengths.

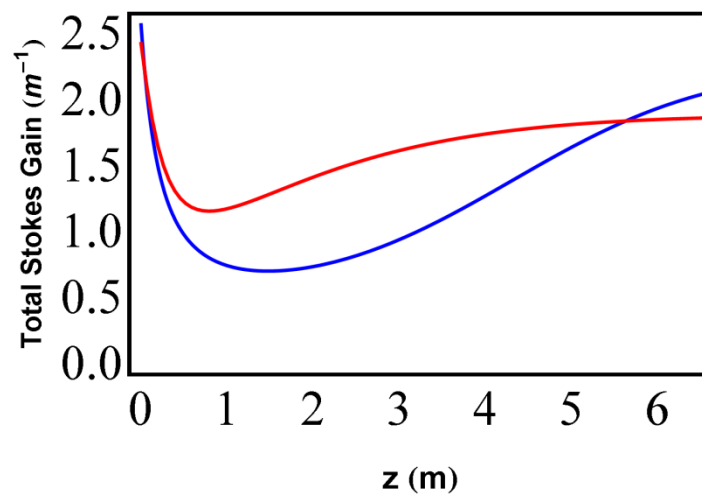


Figure 22. Total Stokes gain for the 1064 nm light for the two-tone (blue) and single-tone (red) cases. For the two-tone case the pump power is approximately 38 W which generated an output 1064 nm power of approximately 28 W (equal to the output at threshold in the single tone case).

4.3 NUMERICAL RESULTS (THREE-TONE SIMULATIONS)

In this section, SBS suppression through laser gain competition is extended to three-tone seeding. The gain fiber modeled in this case is the same as the preceding section so, for brevity, the parameters are not repeated here. In this case, the wavelength separation was chosen to be $\Delta\lambda = 4$ nm and the three seed wavelengths were chosen to be ($\lambda_1 = 1064$ nm, $\lambda_2 = 1060$ nm, $\lambda_3 = 1056$ nm). To maximize the power output for this case, the ratio of the seed powers $P_1 : P_2 : P_3$ was chosen to be 1:2.7:4. Recall, that there is no simple analytic expression to determine the optimal seed ratios. Here the ratios were determined by examining the total output power at SBS threshold for several different seed ratios.

Numerical results verified that FWM was small and was lower than the generated Stokes light at SBS threshold for this case. The oscillatory behavior of the inner sidebands as shown in Figure 23 is due to the fairly short phase-matching coherence lengths at this wavelength separation of the seed signals. The difference in coherence lengths between the two inner sidebands is due to dispersive effects as well as SPM and XPM. The outer sidebands exhibit similar behavior although this cannot be deciphered from the Figure. As shown in Figure 24, the total signal power was approx. 80 W (67 W of 1064 nm, 11 W of 1060 nm, and 2W of 1056 nm) at a pump power of 92 W. This is nearly three times more than the output from the one tone case which is also shown for comparison. Furthermore, there is an enhancement in the power of the 1064 nm light. In this case, the SBS suppression is due to laser action. As the signals propagate down the fiber, the population density of the upper state, N_2 decreases. The 1064 nm light has an appreciably lower absorption cross-section than the 1056 nm light leading to positive laser gain for the former and negative gain for the latter.

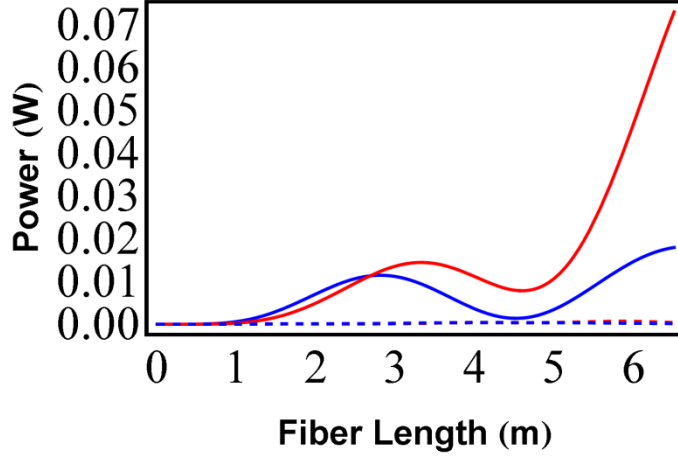


Figure 23. The FWM power generated in the inner and outer sidebands $[\omega_5=\omega_1+3\Delta\omega, \lambda_5\sim 1052nm]$ (solid blue), $[\omega_4=\omega_1-\Delta\omega, \lambda_4\sim 1068nm]$ (solid red), $[\omega_7=\omega_1+4\Delta\omega, \lambda_7\sim 1048nm]$ (dashed blue) and $[\omega_6=\omega_1-2\Delta\omega, \lambda_6\sim 1072nm]$ (dashed red) shown in Figure 7 for the three-tone amplifier. Due to the large wavelength separation FWM is much lower than the previous cases considered. ($\Delta\omega\sim 1THz, \Delta\lambda\sim 4nm$).

As described in the preceding section, this results in a lower integrated SBS gain for the 1064 nm light as compared to the single-tone case. It should also be clear from Figures 21 and 24 that the integrated area of the 1064 nm light is smaller in the multi-tone case. In terms of SBS, this is equivalent to a shorter effective fiber length and results in a higher SBS threshold for the multi-tone case. As the wavelength separation among the laser signals was increased, simulations indicated an increased enhancement in one of the signals. However, optimization of the output power required highly skewed ratios of the input powers. Alternatively, the possibility of having two of the signals with a relatively small wavelength separation, and a third signal having a relatively large wavelength separation was explored. In this case, only FWM effects due to the interactions between the closely

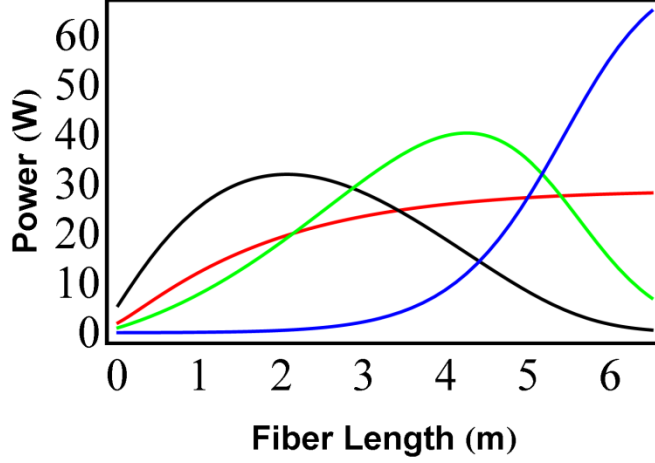


Figure 24. The signal power evolution of a three-tone amplifier compared with a single-tone amplifier using laser gain competition. The power of the $\lambda=1064nm$ single-tone case (red) reaches 28 W of output power before the SBS threshold is reached. The total output of the three-tone case with signals oscillating at $\omega_3=\omega_1+2\Delta\omega$, $\lambda_3\sim 1056nm$ (black), $\omega_2=\omega_1+\Delta\omega$, $\lambda_2\sim 1060nm$ (green) and $[\omega_1,\lambda_1=1064nm]$ (blue) was approx. 80 W. In the three-tone amplifier, the three signals are separated by $(\Delta\omega=1THz, \Delta\lambda\sim 4nm)$. In addition the 1064nm signal output at SBS threshold was over 60 W; more than twice the SBS threshold of the single-tone case. The seed ratios for the three-tone case are: $P_1:P_2:P_3=1:2.7:4$.

separated signals need to be considered if at all. However, as can be seen from previous simulations, FWM is small for a wavelength separation of 4 nm even when there were three evenly separated wavelengths (see Figure 23). For the following simulations, the seed wavelengths were chosen to be 1040 nm, 1044 nm, and 1070 nm. 1070 nm was chosen to explore the concept at a different wavelength than 1064 nm. The pump power at SBS threshold was 79 W. For this case the FWM gain coefficient $n^{(2)}$ was set to be zero in the code. This allowed one to numerically solve for the laser signals and their Stokes fields even though the wavelength separation was unequal. Recall that in the derivations described in Chapter 3 the wavelength separation was equal. The resulting field amplitudes as a function of z for the closely separated wavelengths were then used in the evolution equations describing the two inner sidebands without considering any interactions with the outer sidebands, as the latter should be extremely small in magnitude. This procedure confirmed FWM

effects were negligible. The output power for the laser signals is shown in Figure 25. The power output for the 1070 nm light is approximately 2.2 times greater than the one-tone amplification case. The optical efficiency of the amplifier at 1070 nm including the input seed powers was $\sim 72\%$ and 73% in the three-tone and single-tone configurations respectively.

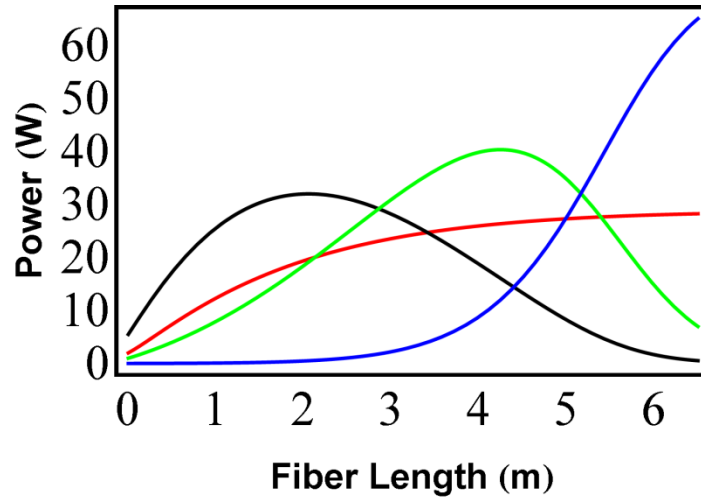


Figure 25. The signal power evolution of a three-tone amplifier compared with a single-tone amplifier using laser gain competition. The power of the $\lambda=1070nm$ single-tone case (red) reaches 28 W of output power before the SBS threshold is reached. The total output of the three-tone case with signals oscillating at $\lambda_3\sim 1040nm$ (black), $\lambda_2\sim 1044nm$ (green) and $\lambda_1=1070nm$ (blue) was approx. 75 W. In the three-tone amplifier, the 1070nm signal output at SBS threshold was over 60 W: 2.2 times the SBS threshold of the single-tone case.

A good measure to illustrate SBS suppression is to examine the Stokes gain as a function of position. The Stokes gain represents the total gain due to SBS and to laser action as can be seen from Eq. (3.10). Figure 26 shows the amplitude Stokes gain for the 1070 nm light in a three-tone configuration and for that same wavelength light in a one-tone configuration. For comparison purposes, the pump light for each case was adjusted such that both case had the same output power at 1070 nm. Note the reduced Stokes gain for the three-tone case, thus allowing for increased pump power.

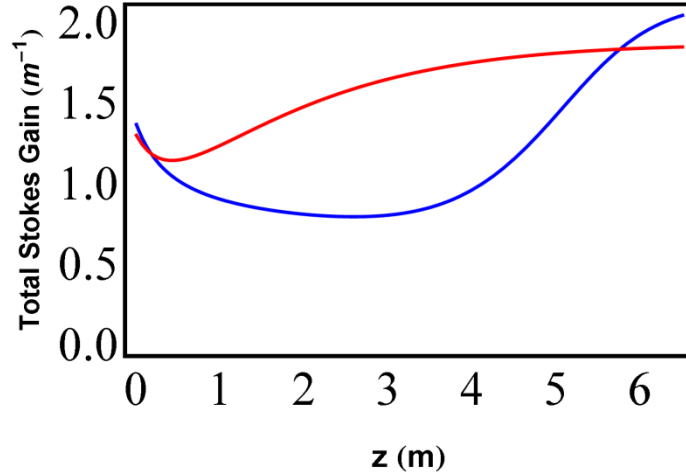


Figure 26. Total Stokes gain for the 1070 nm light for the three-tone (blue) and single-tone (red) cases. For comparison purposes, the pump light for each case was adjusted such that both case had the same output power at 1070 nm. Note the reduced Stokes gain for the three-tone case, thus allowing for increased pump power.

4.4 FIBER LENGTH AND COMPARISON TO COUNTER-PUMPING

In order to study the effects of SBS suppression with multi-tone amplification for a shorter length of fiber, a comparison was made between three-tone and single-tone amplification in a fiber of length 4.5 meters. In this case, the wavelengths, fiber type, etc. were the same as section 4.2. Due to the shorter length of the fiber, the SBS threshold is raised for both configurations allowing for higher pump powers. The pump power at SBS threshold for three-tone and single-tone was 110 W and 50 W, respectively. As shown in Figure 27, this corresponded to an output power in the 1070 nm wavelength of 83 W and 44.5 W for the three-tone and single tone configurations respectively. Therefore, the enhancement in the 1070 nm power is approximately 1.9. Thus, there is a slight reduction in the enhancement factor at the shorter length compared to the enhancement factor of 2.2 in the 6.5m fiber (see Figure 25); this point will be further discussed in Section 4.5.

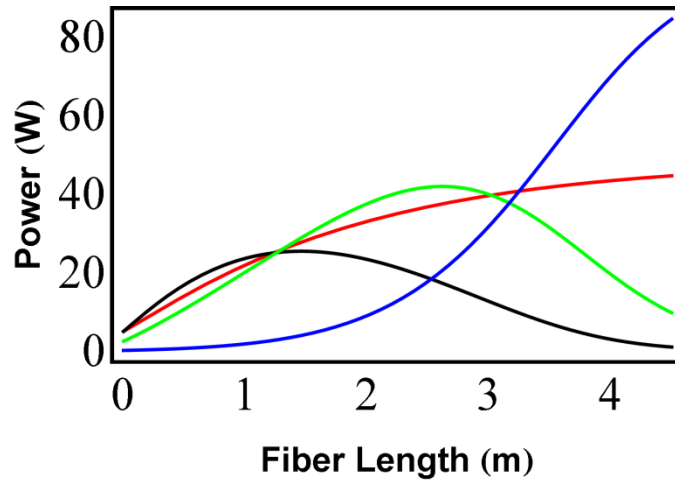


Figure 27. The signal power evolution of a three-tone amplifier compared with a single-tone amplifier using laser gain competition. The power of the $\lambda=1070nm$ single-tone case (red) reaches 44.5 W of output power before the SBS threshold is reached. The output signals of the three-tone case with signals oscillating at $\lambda_3 \sim 1040nm$ (black), $\lambda_2 \sim 1044nm$ (green) and $\lambda_1=1070nm$ (blue) is shown. In the three-tone amplifier, the 1070nm signal output at SBS threshold was approx. 83 W: ~ 1.9 times the SBS threshold of the single-tone case.

SBS suppression through multi-tone amplification will generally not offer an improvement in a counter-propagating pumping scheme in which all laser signals are propagating in the opposite direction to the pump light. This is due mainly to the fact that the concept relies on a high upper state population N_2 at the signal input end of the fiber. As described previously, this creates high laser gain for the lower wavelength signal in the first half of the fiber, and as the inversion density depletes the amplified signal becomes a secondary pump for the longer wavelength. In the case of a counter-pumped amplifier, the upper state population density is low at the input end of the fiber and thus sufficient energy transfer between the two signals does not occur. As shown in Figure 28, both a counter-pumped amplifier and the multi-tone scheme rely on inducing suppressed laser gain for the wavelength of interest in a good portion of the fiber, while allowing for a rapid rise in the signal at the output end of the fiber.

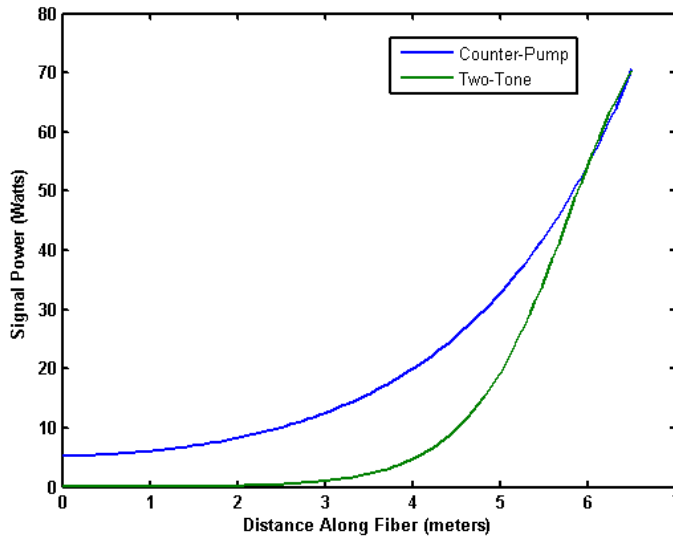


Figure 28. The signal power evolution of a two-tone amplifier and a counter pumped amplifier pumped to the SBS threshold. The pump power in this case was 92 W. Both amplifiers reach an output power of 77 W before the onset of the SBS threshold is reached and rely on SBS suppression through a rapid rise in the signal growth near the output end of the fiber.

In general, counter-pumping and three-tone seeding with all seed signals possessing narrow linewidth, will both lead to an improvement of 2-2.5 in output power (in the case of three-tone we are referring to improvement in the signal with the highest power). As will be discussed in Section 4.6, both techniques offer added SBS suppression through thermal gradients. However, an advantage that the multi-tone approach offers is that the amplifier can be constructed in an all-fiber system (ie. no free-space optics). As discussed in Ref.[46], all-fiber counter pumped amplifiers induce unwanted SBS and a reduction in amplifier performance since the high-signal light combined with the high intensity pump light can cause pump combiners to fail and signal light to leak into the pump diodes. In addition, the added delivery fiber can create a longer effective length of the SBS process minimizing the enhancement from a counter-pumped architecture [46]. For these reasons counter-pumped fiber amplifiers usually employ free-space optics to couple the pump light into the fiber.

4.5 SEEDING WITH BROAD-BAND AND NARROW-LINE SIGNALS

Although the three-tone approach with three single-frequency signals is an attractive way of increasing the SBS threshold for the tone of interest, it is more difficult than a two-tone system because it requires careful control over three wavelengths and three seed powers. Even if a 1x3 WDM is used to overcome the coupling of a third signal, SBS must still be considered all three signals. An alternative approach is to use a combination of signals possessing narrow and broad linewidths. In this case, the SBS in the broad linewidth signal is insignificant since here the linewidth of the laser is assumed to be orders of magnitude larger than the spontaneous Brillouin linewidth.

This concept is illustrated for a two-tone system with a single-frequency signal at $\lambda_1 = 1064$ nm and a broad linewidth signal at $\lambda_2 = 1040$ nm ($\Delta\lambda \sim .1nm$). The latter sees little SBS gain, thus providing an extra degree of freedom to elevate the threshold of the 1064 nm light. The equations derived in Section 3.2 can be used for this case with very little modification to the three-tone code. The input power for ω_3 (which represents the third signal seed) is set to zero. In addition, the SBS gain coefficient corresponding to the broadband signal is set to zero. The results for this case are shown in Figure 29. For a 6.5 meter fiber, the pump power at SBS threshold near optimal seed power ratio is 100 W leading to an output in the 1064 nm light of 74 W as compared to 28 W for the single-tone case. Accounting for total seed power and comparing optical efficiencies in the desired wavelength channel, this two-tone approach provides a conversion efficiency of 70% while the single-tone provides an efficiency of 83%. Of course, the output power in the former in the wavelength channel of interest is considerably higher (greater by approximately 2.6 times). These results are noticeably better than what was obtained for two-tone amplification with two narrow

linewidth signals as described Section 4.2. The reason for this is two fold: one, the output power is not limited by SBS in the broadband signal and two, the second wavelength was also lowered to 1040 nm, which has a higher absorption cross-section in Yb, and thus leads to more energy conversion into the 1064 nm signal. It should be noted that a similar enhancement could also be obtained using a 1070 nm signal as the single-frequency seed.

As shown in Figure 29, the power in the 1040 nm light peaks at a distance along the fiber of

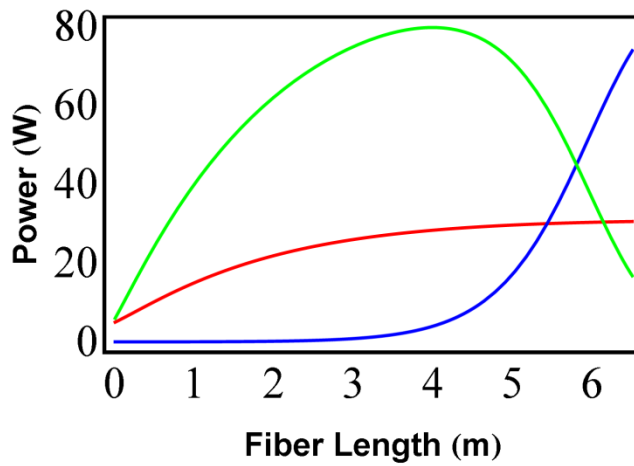


Figure 29. The signal power evolution of a two-tone amplifier compared with a single-tone amplifier using laser gain competition. The power of the $\lambda=1064nm$ single-tone case (red) reaches 28 W of output power before the SBS threshold is reached. The output signals of the two-tone case with signals oscillating at $\lambda_2\sim 1040nm$ (green) and $\lambda_1=1064nm$ (blue) is shown. In the two-tone amplifier, the 1064nm signal output at SBS threshold was approx. 74 W (2.6 times that of the single-tone case). The 1040 nm light possesses broad linewidth and the 1064 nm light is narrow.

Past that point, the power from this laser light, which has high intensity due to its confinement to the core, and the remaining pump light is transferred into the 1064 nm light. Therefore, the 1040 nm light acts essentially as a secondary “pump”. The maximum efficiency does not correspond to the maximum output power in the channel of interest. The efficiency of the amplifier can be improved through the seed power ratio to be in the range of 70%-80% at a cost of approximately 10% drop in power enhancement. The optimal efficiency obtained for the 1064 nm channel at this length of fiber

was 80%. For this case, the pump power was approximately 65W and the output signal in the 1064 nm channel was 56 W as shown in Figure 30.

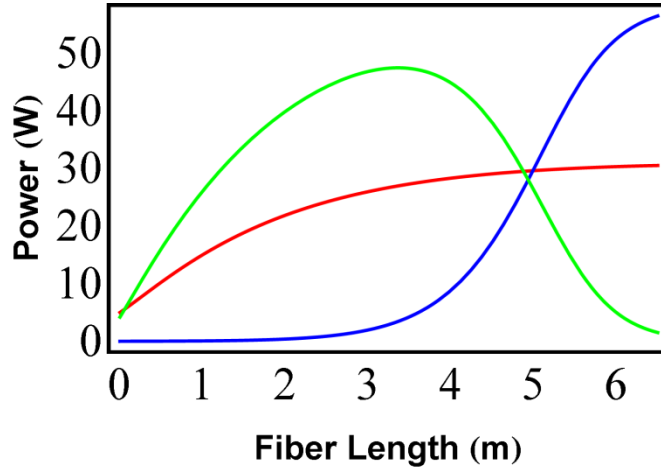


Figure 30. The signal power evolution of a two-tone amplifier (at optimal efficiency) compared with a single-tone amplifier using laser gain competition. The power of the $\lambda=1064nm$ single-tone case (red) reaches 28 W of output power before the SBS threshold is reached. The output signals of the two-tone case with signals oscillating at $\lambda_2\sim 1040nm$ (green) and $\lambda_1=1064nm$ (blue) is shown. In the two-tone amplifier, the 1064nm signal output at SBS threshold was approx. 56 W using approx. 200mW of 1064 nm seed.

In order to investigate other lengths a 4.5 meter fiber was simulated. The maximum power enhancement over the single case was slightly lower than in the case of the 6.5 meter fiber. In this case, the maximum power output was approximately 2.3 times greater. The amplifier efficiency was also optimized for this length of fiber. As shown in Figure 31, the power output near maximum conversion efficiency was 88 watts with an efficiency of 71%. The conversion efficiency for the single-tone case for this length of fiber was 79%, which is lower than the maximum conversion efficiency for the two-tone case at 6.5 meters. Furthermore, the output power was 11 W and 29 W less than the output power at 6.5 meters for the maximum conversion efficiency and the maximum output power cases, respectively.

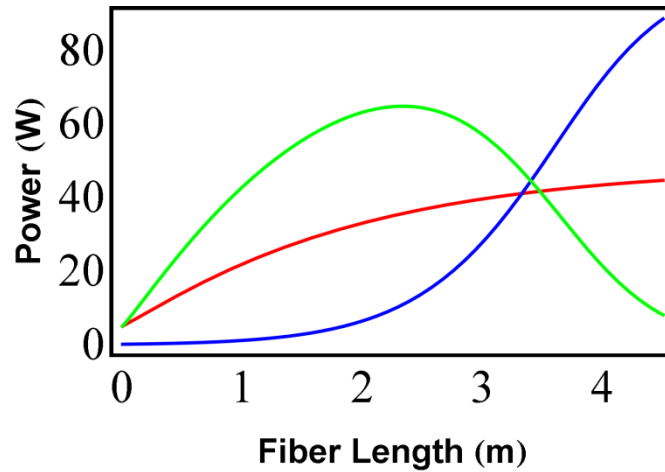


Figure 31. The signal power evolution of a two-tone amplifier at 4.5m near maximum efficiency (71%) compared with a single-tone amplifier (efficiency 79%) using laser gain competition. The power of the $\lambda=1064nm$ single-tone case (red) reaches approx. 40 W of output power before the SBS threshold is reached. The output signals of the two-tone case with signals oscillating at $\lambda_2\sim 1040nm$ (green) and $\lambda_1=1064nm$ (blue) is shown. In the two-tone amplifier, the 1064nm signal output at SBS threshold was approx. 88 W. The 1040 nm light possesses broad linewidth and the 1064 nm light is narrow.

As a further consideration of fiber length a 3 meter fiber was simulated. This fiber length allows for a pump power for single-tone amplification that is slightly above the 100 W pump power (104 W) used for the 6.5 meter long fiber for the case of two-tone amplification at maximum output power. The results of the simulations are shown in Figure 32. With an output power of approximately 72 W, the conversion efficiency for single-tone was 67%. For the two -tone case pumped near SBS threshold at 196 W with an input seed power ratio of 7:1, the output power and conversion efficiency in the 1064 nm channel were approximately 122 W and 61%, respectively. As mentioned above, the 6.5 meter fiber had a maximum conversion efficiency of 80% and a conversion efficiency of 70% near optimal output power for the two-tone configuration.

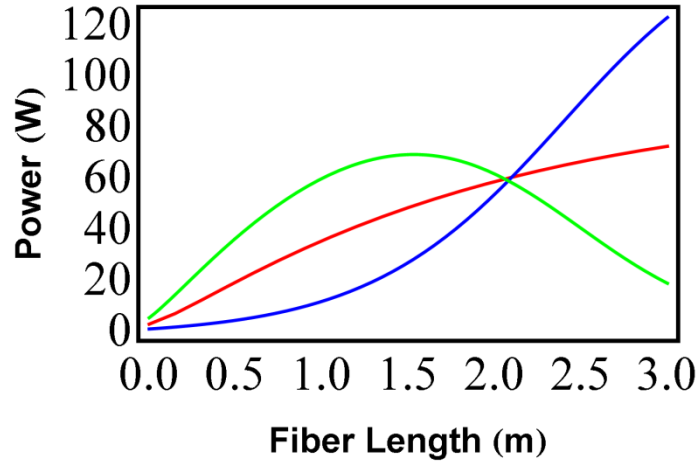


Figure 32. The signal power evolution of a two-tone amplifier at 3m near maximum efficiency (61%) compared with a single-tone amplifier (67% efficiency) using laser gain competition. The power of the $\lambda=1064nm$ single-tone case (red) reaches approx. 72 W of output power before the SBS threshold is reached. The output signals of the two-tone case with signals oscillating at $\lambda_2\sim 1040nm$ (green) and $\lambda_1=1064nm$ (blue) is shown. In the two-tone amplifier, the 1064nm signal output at SBS threshold was approx. 122 W. The 1040 nm light possesses broad linewidth and the 1064 nm light is narrow.

A summary of the efficiency and output power at the SBS threshold in the 1064 nm signal for the 6.5 m, 4.5 m, and 3 m fiber lengths is shown in Table 1.

Fiber Length (m)	1064 nm Output Power (W) Two-Tone/Single-Tone	Optical Efficiency % Two-Tone/Single-Tone
3.0	122/72	61/67
4.5	88/40	71/79
6.0	56/28	80/80

Table. 1 Summary of output power and optical efficiency at SBS threshold for the two-tone and single-tone cases for a 3.0 m, 4.5 m, and 6.0 m fiber length. In all cases the SBS threshold in the 1064 nm signal is higher for the two-tone case. As the fiber is made shorter the optical efficiency is lower for the two-tone case.

4.6 THERMAL EFFECTS

In this section the theoretical framework described in Section 3.2 is modified to include thermal effects in high-power fiber amplifiers. Since this analysis is restricted to the two-tone case with a large wavelength separation, the effects of FWM are also ignored. In this study, the

wavelengths considered are 1030 nm and 1080 nm for the broad-band and single-frequency seeds respectively. These specific wavelengths are chosen in order to maximize the induced thermal gradient at the output end of the fiber; created from the quantum defect heating that results when energy is transferred from the 1030 nm signal into the 1080 nm signal. Recall, that in Section 4.3 it was shown that FWM was negligible when the wavelength separation between the two signals was larger than 4 nm. To this end, the equations describing the evolution of the pump, signals, and Stokes fields are written as power equations. This model accounts for the shift in the resonance frequency of the phonons due to an optically induced or external thermal gradient. In addition, the previous treatment of the noise initiation of the Stokes process was to use a localized noise source at the back end of the fiber as shown in Eq. (3.13). Hilderbrandt et al. [47] have previously used a localized noise as described by Smith [48] to study the spatial evolution of the Stokes light in a conventional fiber amplifier with a thermal gradient. While the work of Boyd et al. [13] has shown that the localized and distributed noise models are generally equivalent in a passive and homogeneous medium of sufficient length, the use of a localized noise to describe amplifiers with thermal gradients suffers from the drawback that the location of the noise is determined a priori and the dependence of the noise on temperature (and thus the position) is ill-defined. This is not much of a problem in a passive fiber, but for a medium with laser gain and thermal gradient, a self-consistent treatment becomes problematic.

In order to model a thermal gradient, a spread in Stokes frequencies needs to be considered. The acoustic frequency in the fiber is temperature dependent and has the following form:

$$\Omega_B(x, y, z, T) = \Omega_B(T_0) + C_T \Delta T(x, y, z) \quad (4.1)$$

where $\Omega_B(T_0)$ and ΔT describe the acoustic frequency of some reference temperature and the difference between the reference temperature and the temperature in the fiber respectively. C_T is an

empirical constant, approximately equal to 2.0 MHz/C° in fused silica, that provides the shift in the center frequency due to the temperature difference. Since each acoustic frequency corresponds to a Stokes frequency, the thermal dependence of the acoustic frequency can be accounted for, in the steady-state, by discretizing the Stokes frequencies into bins $\omega_{s,i}$ of sufficient number to capture the temperature range. For the signal power, P_l , the following equation describing its evolution along the direction of propagation, z , is obtained:

$$\frac{dP_l}{dz} = \left[g(z) - \sum_i (g_{B,i}(z)P_{s,i} + \delta_i(z)) \right] P_l. \quad (4.2)$$

Where $P_{s,i}$ is the Stokes power of $\omega_{s,i}$, g and g_B represent the laser and Brillouin gain, respectively, and δ_i is the noise term due to spontaneous Brillouin. The laser gain and Brillouin gain are given by:

$$g(z) = \frac{\iint (\sigma^{(e)}N_2(x,y,z) - \sigma^{(a)}N_1(x,y,z)) |\varphi(x,y)|^2 dx dy}{\iint |\varphi(x,y)|^2 dx dy} \quad (4.3)$$

$$g_{B,i}(z) = \frac{\iint g_{B,i}(x,y,z) |\varphi(x,y)|^4 dx dy}{\left(\iint |\varphi(x,y)|^2 dx dy \right)^2} \quad (4.4)$$

Where φ is the lowest-order transverse modal profile, $\sigma^{(e)}$ and $\sigma^{(a)}$ are the emission and absorption cross sections, respectively, and where N_2 and N_1 are the populations of the upper and lower states, respectively. The dependence of the SBS gain on the temperature profile is dominated by the shift in the resonance acoustic frequency. It can be incorporated into $g_{B,i}(x,y,z)$ through:

$$g_{B,i}(x,y,z) = \frac{g_{B,\max}}{1 + 4 \left\{ [\Omega_B(T_0) + C_T \Delta T(x,y,z) - \omega_l + \omega_{s,i}]^2 / \Gamma_B^2 \right\}}. \quad (4.5)$$

The peak value of the Brillouin gain, $g_{B,\max}$, is given by:

$$g_{B,\max} = \frac{2\pi^2 n^7 p_{12}^2}{c\lambda_l^2 \rho_0 v_A \Gamma_B} \quad (4.6)$$

where n is the optical index of refraction, p_{12} is the longitudinal elasto-optic index, ρ_0 is the material density, and v_A is the acoustic velocity. Note that the variation of $g_{B,\max}$ with temperature is neglected in this analysis. Again, the dominant temperature-related effect on the Stokes gain is due to the shift in the resonance frequency. As mentioned earlier, the noise term can no longer be taken as local when thermal effects are considered. In this case, the distributed noise term is given by:

$$\delta_i(z) = \frac{\hbar\omega_{s,i}\Delta\omega \iint g_{B,i}(x,y,z)|\varphi(x,y)|^4 \left\{ \exp\left[\frac{\hbar(\omega_l - \omega_{s,i})}{KT(x,y,z)}\right] - 1 \right\}^{-1} dx dy}{2\pi \left(\iint |\varphi(x,y)|^2 dx dy \right)^2}, \quad (4.7)$$

where, $\Delta\omega = \omega_{s,i+1} - \omega_{s,i}$ is the bin size for the Stokes waves. For the Stokes light which propagates counter to the signal, the evolution is given by:

$$\frac{dP_{s,i}}{dz} = -\left(g(z) + g_{B,i}(z)P_{s,i}\right) - \delta_i P_i. \quad (4.8)$$

This is equivalent to injecting one photon per mode multiplied by the thermal average of the number of particles in the orbital as described by the Bose-Einstein distribution function. As in the previous analysis, the overlap integrals in the expression above account for the spatial distribution of the optical fields. In a co-propagating pump the spatial evolution of the pump power is given by:

$$\frac{dP_p}{dz} = \frac{d_{core}^2}{d_{clad}^2} \left(N_2 \sigma_p^{(e)} - N_1 \sigma_p^{(a)} \right) P_p \quad (4.9)$$

where $\sigma_p^{(e)}$ and $\sigma_p^{(a)}$ are emission and absorption cross sections at the pump wavelength, respectively, and where d_{core} and d_{clad} are the core and cladding diameters, respectively. Quantum defect heating

in the core provides the heat source. In a co-pumping configuration, the power balance equation takes the form:

$$Q(r \leq d_{core} / 2, z) = \frac{4}{\pi d_{core}^2} \left(-\frac{dP_p(z)}{dz} - \frac{dP_l(z)}{dz} \right)$$

$$Q(r > d_{core} / 2, z) = 0 \quad (4.10)$$

where Q is the heat generated per unit volume. This equation neglects the effect of the Stokes light on heating. This approximation is fairly accurate as long as the reflectivity is of the order of a few percent or less. To determine the temperature as a function of position, we use the steady state heat equation in an isotropic medium:

$$-k_{th} \nabla^2 T(r, z) = Q(z) \quad (4.11)$$

where k_{th} is the thermal conductivity. Noting that the variation of the temperature in the longitudinal direction in a fiber is much smaller than that in the transverse direction, and assuming azimuthal symmetry, one can express the heat equation as:

$$-k_{th} \frac{1}{r} \frac{\partial}{\partial r} \left(r \frac{\partial T}{\partial r} \right) = Q(z) \quad (4.12)$$

The equation above is subject to the boundary conditions of continuity of the temperature and heat flux $-k_{th} \nabla T$ across the fiber. In this analysis, it is assumed that the core and cladding of the fiber have the same thermal properties. At the outer layer of the fiber, which is typically comprised of a polymer coating, both convective cooling subject to Newton's law of cooling and radiative cooling subject to Stefan's law are taken into account:

$$k_{th} \frac{\partial T(r = r_{outer})}{\partial r} = h [T_c - T(r = r_{outer})] + e \sigma_{st} [T_c^4 - T^4(r = r_{outer})] \quad (4.13)$$

where r_{outer} represents the outer radius of the fiber, T_c is the coolant temperature (air in this case), h which lies in the range of 10-20 W/m²K is the convective cooling coefficient, $\sigma_{st} = 5.67 \times 10^{-8}$ W/m²K⁴ is the Stefan-Boltzmann constant, and e is the emissivity which is approximately 0.9 for the acrylate coating. As can be inferred from the equation above, radiative cooling which is typically neglected in thermal analysis of fiber amplifiers becomes substantial as the temperature difference approaches 100 °C.

The most significant limitation on power scaling of narrow linewidth fiber amplifiers that employ thermal gradients for SBS suppression is the interplay between thermal effects and the SBS process. Based on the operating temperature of the fiber coating and the heat management system, power scaling can be either thermally limited or SBS limited. [34] For conventional fibers, polymer material is also used for the outer cladding region in order to provide guiding for the pump light. These polymers are typically limited to around 150 °C.

A distinct advantage in terms of SBS suppression for a counter-pumped amplifier is the development of a steep temperature gradient at the output end where the signal is high. For a single-tone co-pumped configuration the temperature gradient is steepest at the input end where the signal is low. In comparison to these two cases, the temperature profile is more complex in a two-tone configuration. In this case, energy from the pump light is transferred into the two signals at the input end of the fiber leading to a drop in the temperature as the pump light is absorbed. However, this is followed by an increase in temperature as one of the signals (along with the pump) starts transferring its energy into the other signal. Eventually, the temperature drops again as the “pump” signal loses much of its energy.

To investigate this concept theoretically, a 6.5 meter long fiber with a core diameter of 25 μm and an MFD of 22 μm is considered. The inner cladding diameter used in the simulation is 400

μm . The outer cladding and fiber coating extend to $550 \mu\text{m}$ and are composed of a polymer material. An depiction of the cross-section of a fiber showing the core, cladding, and polymer jacket is shown in Figure 33.

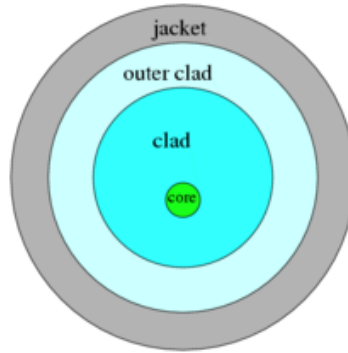


Figure 33. Skeleton diagram of fiber cross-section detailing the core, cladding, and polymer jacket surrounding a fiber.

The maximum operating temperature of the polymer is taken to be $150 \text{ }^\circ\text{C}$. The two input signals are chosen to be a broadband 1030 nm and a narrow-linewidth 1080 nm in order to obtain near optimal conditions for the thermal gradient developed through quantum defect heating. The system of equations describing the optical waves was integrated with Runge-Kutta Four (RK4) in conjunction with a relaxation algorithm until the boundary conditions for all optical fields was within 0.01% of the exact boundary conditions. Upon numerical investigations it was determined that approximately 50-100 channels of Stokes light, each of the order of several MHz, was required to achieve convergence whereby minimal change in the reflectivity was obtained by refining the resolution of the channels or by expanding the range of frequencies of the Stokes light. The heat equation was solved at 200 equally spaced points along the direction of propagation. In order to speed up this process, analytic functions were used to provide a three-dimensional temperature profile. This was made possible by utilizing the software Mathematica to provide physically viable algebraic solutions to the set of quartic equations described in Eqs. (4.10-4.13).

Figure 34 shows the evolution of the 1030 nm and 1080 nm signals indicating a factor of 5 enhancement in the output power from a co-pumped single-tone case. If one were to allow for a higher polymer temperature, the SBS threshold can be increased further. Figure 35 illustrates the temperature profile developed as compared to single-tone co-pumped and counter-pumped configurations. Note that for the single-co-pumped case the SBS process was turned off to allow for comparable pump powers. Therefore, when including the effects of the induced thermal gradient developed near the output end of the fiber through the quantum defect heating associated with the double-pump action of this two-tone concept, the expected SBS threshold enhancement relative to a single-tone amplifier can range between 2-5. Where the enhancement range depends on the wavelengths and seed ratios chosen and the added benefit of the induced thermal gradient (see Figure 35).

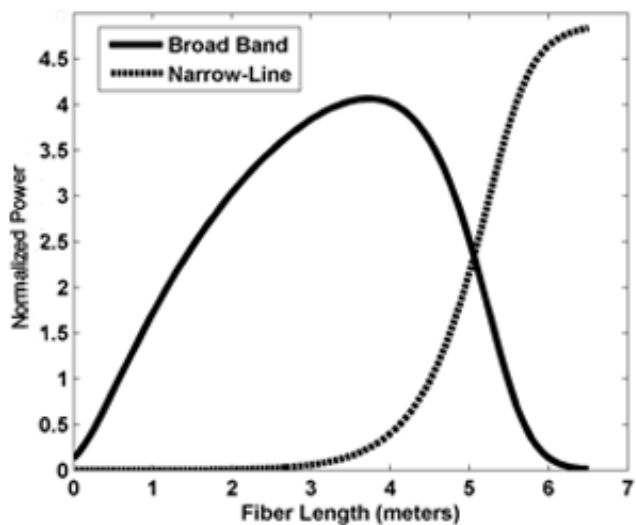


Figure 34. Spatial evolution of the 1030 nm (Broad Band) and 1080 nm (Narrow-Line) signals. Power is normalized to output power from co-pumped single tone at SBS threshold.

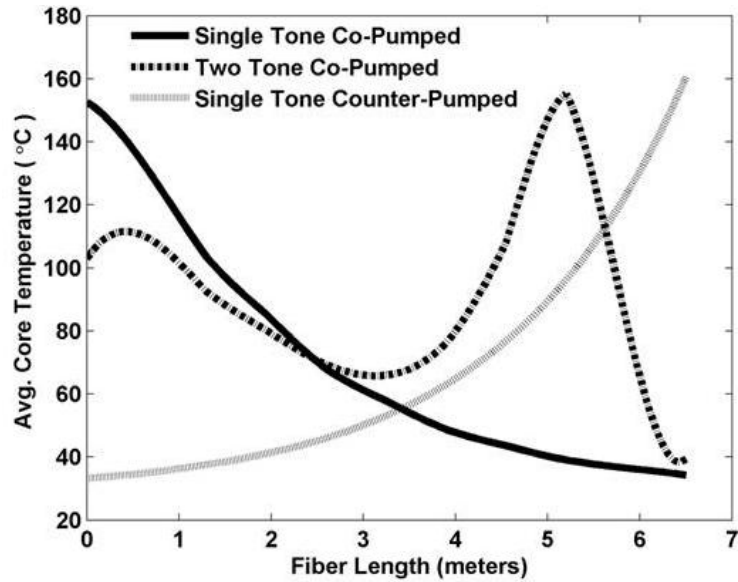


Figure 35. Temperature profiles for different configurations. SBS process turned off for single-tone co-pump to allow for comparable pumping power.

4.7 SUMMARY

In conclusion, this chapter demonstrated SBS mitigation theoretically through laser gain competition between signals in a monolithic co-pumped amplifier. The model used to study this concept included laser gain, SBS, and FWM. The large wavelength separation technique, which utilizes laser gain to suppress the SBS process, was shown to mitigate SBS and therefore enhance the power output of fiber amplifiers. This technique was also shown to mitigate FWM, which is an appreciable improvement over the concept presented in Chapter 3. For the two-tone amplification, an appreciable improvement is obtained when one of the signals possess a broad linewidth. This improvement is comparable to that obtained from counter-pumping while possibly being more suited for monolithic all-fiber designs since counter-pumped amplifiers rely on free-space optics. It was also shown that further power scaling can be achieved via quantum defect heating resulting from the secondary pump action of this two-tone concept. To that end, this technique provides a factor of 2-5 enhancement in the SBS threshold relative to a single-seeded fiber amplifier.

5 MULTI-TONE SEEDING (EXPERIMENTAL RESULTS)

5.1 INTRODUCTION

For a two-tone amplification approach employing broadband and narrow linewidth signals, it was shown theoretically in Chapter 4 that with appropriate selection of seed power ratio and wavelength separation, the SBS threshold can be increased to be in the range of 2-5 times that of a single-tone amplifier. This technique is suited for a co-propagating pump configuration and offers comparable SBS suppression to counter-pumping as both techniques induce reduced laser gain for a good portion of the fiber while allowing for a rapid rise in the signal of interest at the output end. In the counter-pump configuration, this rapid rise is due to the high intensity of the pump light at that end, while for two-tone it is due to the broad linewidth signal acting as a core-confined pump for the narrow linewidth signal. One benefit offered by the two-tone approach is improved compatibility with monolithic all-fiber designs as potential damage to the diode pumps is reduced. In this chapter, SBS suppression through laser gain competition in a multi-tone amplifier is investigated experimentally. The goal of this chapter is to demonstrate SBS suppression in a monolithic fiber amplifier in a laboratory environment. First, the concept is investigated at low powers ~ 10 W in a (10/125) μm Yb: doped fiber. In this low-power configuration the additional SBS enhancement due to the induced thermal gradient discussed in Chapter 3 is minimal. To that end, the expected SBS threshold enhancement relative to the single-tone case is 2-3. Next, the concept is demonstrated at high power ~ 200 W in a LMA (25/400) μm Yb: doped fiber. In this case, the additional SBS enhancement from both the induced thermal gradient via quantum defect heating and an external thermal gradient imposed on the fiber is explored to demonstrate the compatibility of this concept with thermally induced SBS suppression.

5.2 LOW-POWER DEMONSTRATION

5.2.1 EXPERIMENTAL SETUP

A monolithic fiber amplifier configuration, as shown in Figure 36, was used in these experiments. A narrow linewidth Koheras Boostik laser operating at 1064 nm with a maximum output of approximately 1 W provided the seed for one of the signals. The nominal linewidth of this laser was 10 KHz. An in-house built broad linewidth laser system operating at 1045 nm ($\Delta\lambda \sim 0.1nm$) provided the second seed signal. This laser system was comprised of a 100 mW diode-pumped fiber ring oscillator with a grating tuned to the desired wavelength, and a 3 m long gain fiber that allowed for amplification to the watt level. Two pigtail isolators protected the seed sources from back-scattered light. A wavelength-division multiplexer (WDM) was used to combine the two beams before they were coupled into the final stage amplifier which employed a 10 m long single mode polarization maintaining (PM) Yb-doped fiber with a core diameter of 10 μm and an inner cladding diameter of 125 μm . At a pump wavelength of 915 nm, the stated absorption of this fiber was 1.6 dB/m. In these experiments, an Alfalight diode stack operating near 976 nm was used to pump the amplifier. Measurements of the forward traveling signals were conducted using a 0.01% tap coupler and a WDM system, while the back-scattered light was measured using a 1% tap coupler and a WDM system. In addition, an optical spectrum analyzer (OSA) was used to monitor both forward and backward light. In one variant of the experiment, optical filters operating at the desired wavelengths to measure the output signals were used.

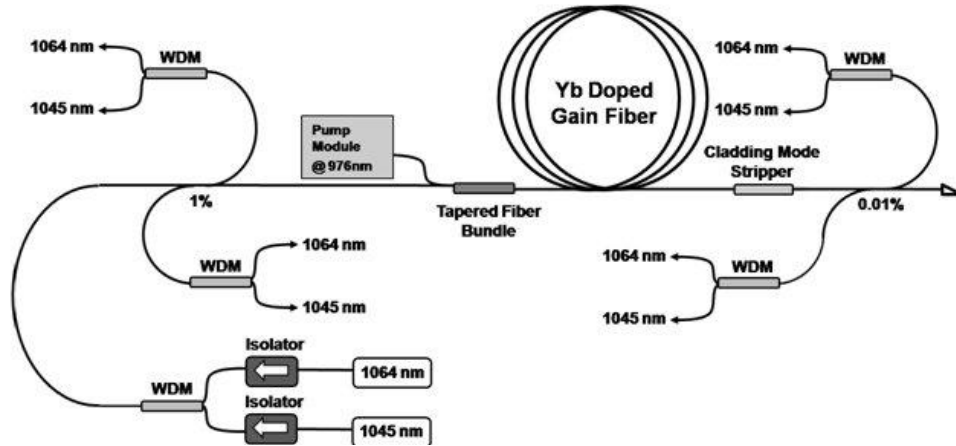


Figure 36. Experimental set-up. The 1045 nm laser was built in-house. The system of WDMs is used to combine or to separate the signals.

5.2.2 EXPERIMENTAL RESULTS AND ANALYSIS

With the 1045 nm seed laser turned off, the amplifier was seeded with 400 mW of 1064 nm. Both the output and back-scattered signal were recorded. The slope efficiency for this amplifier was slightly above 80%. Generally, for an active fiber the SBS threshold is defined as the signal output power where the reflectivity, defined as the output power over the backward power, departs from having a linear dependence on signal power. As shown in Figure 37, for this single-tone amplifier the SBS threshold was determined to be slightly above 3.5 W. The amplifier was also seeded at different powers of 1064 nm light lying in the range of 300-800 mW and this resulted in little variation in the SBS threshold. With the 1064 nm light turned off, the amplifier was seeded with the 1045 nm light. As expected from a broad linewidth signal, there was no associated Stokes light. According to the theoretical and computational analysis of two-tone amplification discussed previously, the seed power ratio of the signals is crucial to increasing the SBS threshold while maintaining good amplifier efficiency for the desired wavelength. To be certain, the maximum efficiency does not correspond to the maximum achievable power in the channel of interest.

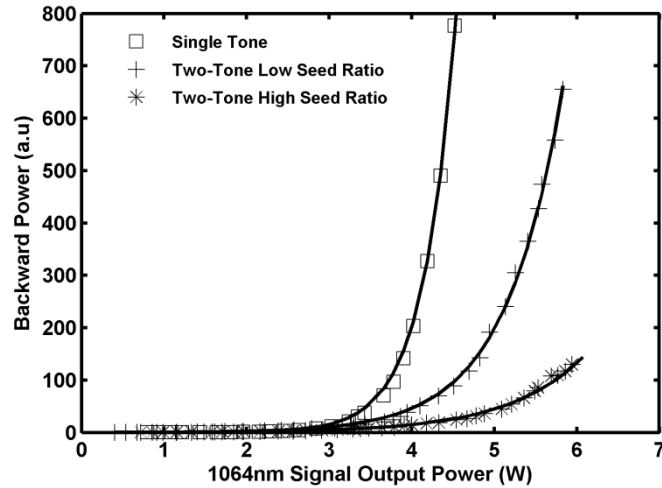


Figure 37. Stokes power vs. 1064 nm light power for single- and two-tone seeding showing increase in SBS threshold. The seed powers for these experiments were 800 mW for the single-tone case and (700/65) mW (high-ratio), (350/65) mW (low-ratio) in the (1045/1064) nm signals respectively.

The simulations for this fiber configuration indicated that the power in the 1045 nm seed should be slightly more than 10 times that in the 1064 nm seed in order to approximately double the SBS threshold, and yet suffer only a minimal decrease in the amplifier efficiency. In one set of measurements, the amplifier was seeded with 700 mW of 1045 nm light and 65 mW of 1064 nm which provided a seed power ratio (10.7:1), close to the theoretical prediction of (10:1) discussed above. In another set of measurements, the amplifier was seeded with 350 mW of 1045 nm light and 65 mW of 1064 nm light which according to the theoretical analysis would provide a lower SBS threshold. For both sets of measurements, the OSA was scanned for any distinguishable sign of four-wave mixing (FWM) due to the third-order nonlinear interaction of the two input signals. No associated FWM sidebands were detected which can be attributed to the large wavelength separation of the two signals as discussed in Chapter 4.

As shown in Figure 37, both seed ratios provided an appreciable increase in SBS threshold over the single-tone. For the small seed ratio case, the SBS threshold occurred at approximately 5 W. As

expected, the SBS threshold for the large seed ratio case was even higher. In fact, we were able to obtain more than 6 W of 1064 nm light without encountering the SBS threshold and were limited by the available pump power from achieving even higher power. The spectral content of the backscattered light of the two-tone configuration at 6 W is shown in Figure 38; which clearly indicates that the backward light was still dominated by Rayleigh light. The amplifier efficiency was also investigated for the two-tone technique. At the highest output power, the power in the 1045 nm light was less than 200 mW. As shown in Figure 39, the slope efficiency is approximately 78% which is slightly below that of the single-tone case. These results are in excellent agreement with the theoretical predictions discussed previously. At low power without additional enhancement from a thermal gradient, the expected threshold increase for the optimal configuration was expected to be between 2-3. In these experiments, the SBS threshold increase was 1.4 in the low seed ratio case and larger than 1.7 in the high seed ratio case (here the results were pump limited). The next section will explore this concept at high power to demonstrate further SBS suppression by using the two-tone concept in conjunction with a thermal gradient.

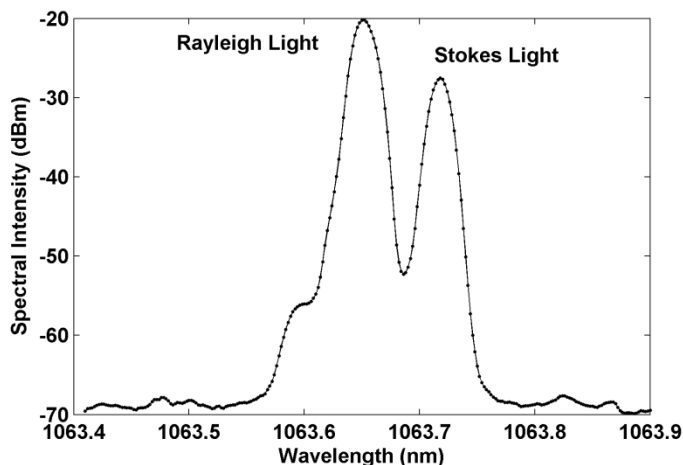


Figure 38. Spectral content of backward light for two-tone configuration for high seed ratio case. Stokes light below the Rayleigh light indicates operation below the SBS threshold.

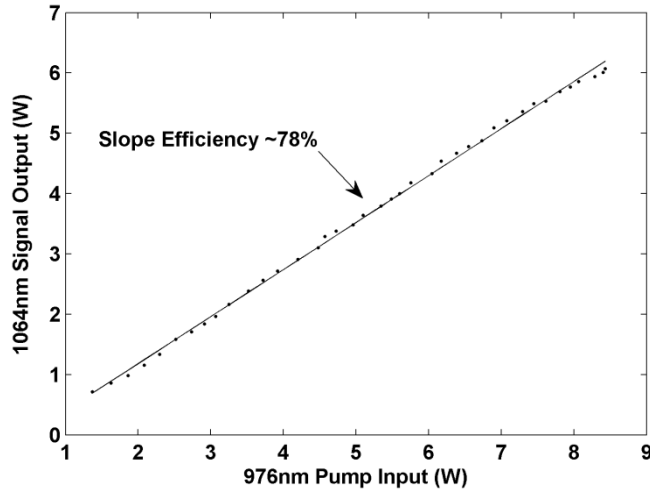


Figure 39. Power output of 1064 nm signal vs. input pump power for two-tone. Efficiency is comparable to single-tone seeding.

5.3 HIGH-POWER DEMONSTRATION

5.3.1 EXPERIMENTAL SETUP

The experimental setup is shown in Figure 40. A Novawave laser operating at 1065 nm with a maximum output of 1 W and a nominal linewidth <100 KHz was used to provide the single-frequency seed. In an effort to explore various wavelengths for the broadband seed laser, a Keopsys 2 W tunable laser ($\sim 1035\text{nm}-1045\text{nm}$) was used. The spectral bandwidth of this laser is ~ 0.1 nm over the tuning range making it sufficiently broad such that the SBS process at this wavelength was completely suppressed. The measured spectral content of the seed laser operating at 1035 nm, 1040 nm, and 1045 nm showed broad amplified spontaneous emission (ASE) from 1045 nm-1080 nm of 5%, 2%, and 1%, respectively. Since the single-frequency wave was to be seeded at low power, it was imperative that a considerable amount of the ASE be removed. Otherwise, the broadband signal would transfer a significant amount of optical power into the ASE thus reducing the amplifier efficiency in the channel of interest (the 1065 nm single-frequency wave). A tunable (1030nm-

1080nm) Agilitron all-fiber PM filter with a 1 nm wide bandwidth was used to suppress this unwanted noise. The measured spectral content after the filter was well over 99% for the three laser wavelengths. After loss from the 1064nm isolator, ASE filter, and splices the measured output power was approximately 500 mW from 1035-1045nm. The broadband signal was sent through an intermediate amplifier comprised of a Nufern PM 10/125 fiber. The intermediate amplifier provided us with up to 6 W of power from 1035-1045 nm. The single-frequency and broadband signals were then combined through a 10 W all-fiber WDM into a mode field adapter (MFA). The MFA was spliced onto a (6+1)x1 tapered fiber bundle (TFB) which was comprised of six 50 W wavelength stabilized 976 nm Limo pump modules.

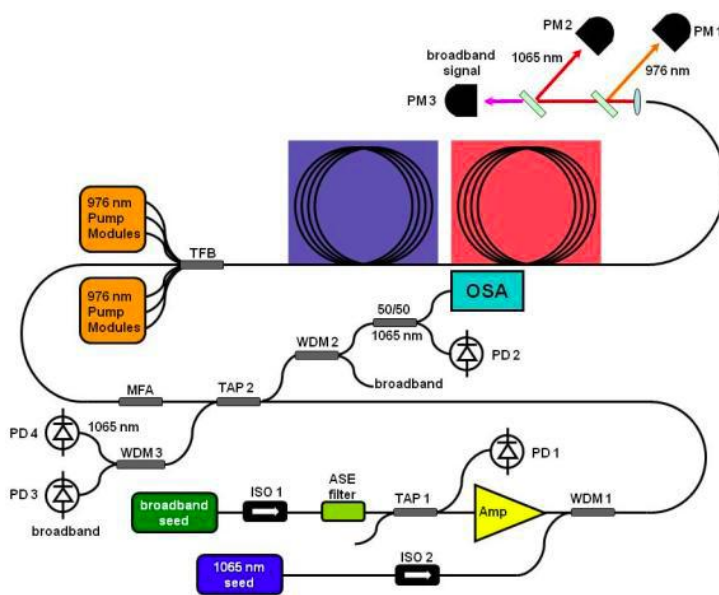


Figure 40. Experimental set-up of monolithic two-tone fiber amplifier system. PD 1, PD 2, PD 3, and PD 4 are photodiodes. ISO 1 and ISO 2 are isolators. PM 1, PM 2, and PM 3 are power meters.

The measured pump power after the TFB with full current on the diode banks was ~281 W. The TFB was then spliced onto 7 meters of a Nufern large mode area (LMA) PM (25/400) fiber with an absorption of 1.7-1.8 dB/m for 976 nm pump light which corresponds to a calculated dopant

concentration of $7-7.5 \times 10^{25} \text{ m}^{-3}$. The numerical aperture of the core and cladding was 0.06 and 0.46 respectively. The estimated loss at this splice was 0.3 dB yielding a maximum available pump power of approximately 260 W. A 0.01% tap coupler was spliced onto the output of the WDM to monitor the forward and backward propagating light. The forward and backward tap legs were then spliced onto WDMs operating in a reverse configuration to separate the 1065 nm light from the broadband light which allowed measurements of the instantaneous forward and backward propagating signals on photodiodes. In addition, the backward 1065 nm tap was spliced onto a 50/50 splitter to allow simultaneous monitoring of the power of the backward light on a photodiode and its spectral content on a 0.01 nm resolution bandwidth optical spectrum analyzer (OSA). Two dichroics were used at the output: a dichroic to separate and measure the unused 976 nm pump light and a dichroic to separate and measure the two signals.

In an effort to investigate this technique in conjunction with a thermal gradient, three different thermal configurations were employed. In one configuration, the fiber was wrapped entirely on a cold spool held at 12 °C in order to measure the SBS suppression due to the two-tone concept without benefit of the thermal gradient. In the second configuration, 6 m of the fiber was coiled on the cold spool with the final one meter coiled in air and left to cool under ambient conditions. This configuration was used to experimentally verify the theoretical prediction discussed in Chapter 4 that a steep thermal gradient would develop at high power in the two-tone amplifier near the output end of the fiber leading to further SBS suppression. The third configuration used was similar to that above except that the last meter of fiber was coiled around a hot spool held at 80 °C. The manufacturer of the fiber, Nufern, suggested that the low index polymer coating used in the fiber should be kept below 100 °C to prevent thermal damage and ensure long-term reliability. The

coiling diameter for all these configurations was approximately 30 cm to allow for near single mode operation.

5.3.2 EXPERIMENTAL RESULTS AND ANALYSIS

Experiments were conducted at 1040 nm and 1035 nm. Seed wavelengths above 1040 nm were not investigated since preliminary tests showed insufficient transfer of energy (<70%) from the amplified broad-band signal light into the 1064 nm signal. The output power was scaled in these experiments until the Stokes light was ~10 dB higher than the Rayleigh light on the OSA except for the cases that were pump limited. There appeared to be a strong correlation among an exponential rise in the reflectivity, a reflectivity value of 0.05%-0.1%, and the 10 dB relative difference between the Stokes and Rayleigh light. For a fair comparison among the various configurations, 0.05% reflectivity was used as a measure of the SBS threshold. The reflectivity was defined as the backward power normalized to the output power in the single-frequency channel. For the single-tone amplifier with the entire fiber wrapped around the cold spool, approximately 43 W of output power was obtained near SBS threshold. The seed power for this case was 1 W. It should be note that little variation in SBS threshold was observed as the seed power was varied for the single-tone case.

For the set of experiments with the two-tone amplifier wrapped around the cold spool, the SBS thresholds were approximately twice as high as the single-tone case at slope efficiencies comparable to the single-tone case (~70%). The broadband to single frequency seed ratios used for these experiments were generally greater than 15:1. While an increase in threshold beyond the factor of 2 was attainable, the amplifier efficiency dropped in agreement with the conclusions of Chapter 4. The 1035nm configuration gave the higher output powers at 90 W, while the 1040 nm configuration provided approximately 7 W less.

For the second configuration, little enhancement over the first thermal configuration was obtained for the single-tone amplifier. This was expected, as in this case, the steep thermal gradient would develop at the input end of the fiber (see Figure 35). For the two-tone configuration, both the 1035 nm and 1040 nm cases showed increased output, with the former showing appreciably more power. The output power near SBS threshold of the single frequency 1065 nm signal was approximately 130 W. This can be attributed to the steep thermal gradient developed at the output end of the fiber due to the optical power transfer from the 1035 nm and into the 1065 nm light as shown in Figure 35. Figure 41 provides the reflectivity as a function of the single-frequency signal output when the broadband seed laser was set to a wavelength of 1035 nm for both thermal configurations and also, for comparison, the reflectivity for the single-tone case. As can be inferred from the plots, the SBS threshold was approximately 3.2 dB (x2) and 4.8 dB (x3) higher for the first and second two-tone configurations, respectively.

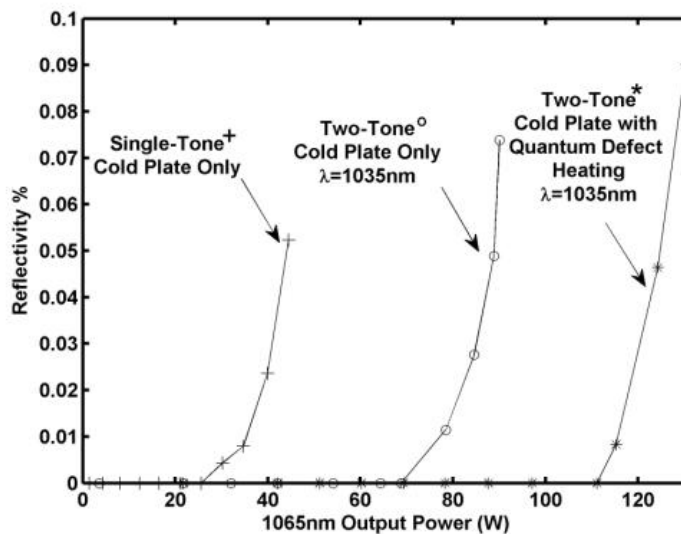


Figure 41. Reflectivity vs. 1065nm signal output power for monolithic amplifier in different thermal configurations : single tone all on cold spool, 1035 nm two-tone all on cold spool, and 1035 nm two tone with 6 m on cold spool and 1 m left to cool in air under ambient conditions (thus utilizing quantum defect heating).

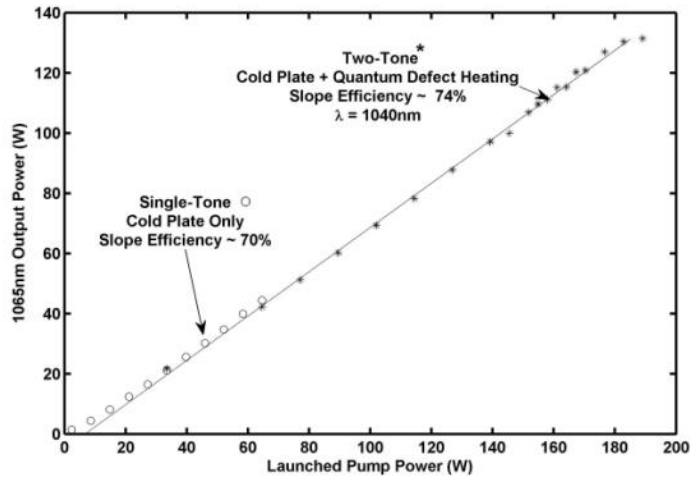


Figure 42. Comparison of output power in the single frequency 1065 nm channel versus launched power for single tone and the two-tone thermal configuration utilizing quantum defect heating. The broadband seed for the latter operated at 1035 nm.

For the second configuration, the amplifier efficiency was approximately 74%. The increased slope efficiency was mainly a result of the Limo pumps, which are optimized to tune to 976 nm at high pump power. The signal at 1065 nm versus the launched pump power is shown in Figure 42 and compared to the single-tone case.

As a final consideration we employed the use of hot and cold spools to further scale the output power of this amplifier. As stated above, in this configuration we put 6 meters of gain fiber on the cold spool and the last meter was wrapped around a hot spool fixed at 80° C. Experiments were again performed considering 1040 nm and 1035 nm signals as the broadband seed. For the former, high power output and high efficiency in the single frequency channel required a seed ratio of roughly 50:1. Figure 43 shows the results of the amplifier operated with 4.5 W of 1040 nm seed and 110 mW of 1065 nm seed. In this case, as much as 182 W of 1065 nm output power at 77% slope efficiency was generated but no exponential turn in the power of the backward traveling light was observed.

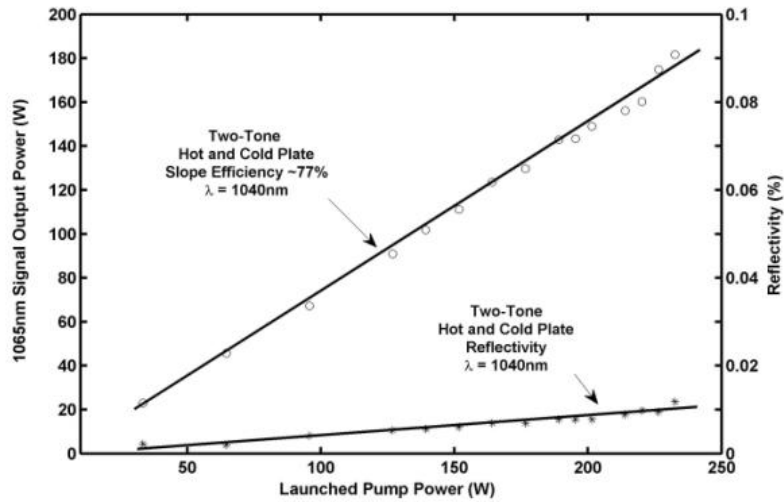


Figure 43. Output power as a function of launch power and reflectivity the for cold plate hot plate configuration with the broadband seed operating at 1040 nm.

The measured unabsorbed power at the highest pump power was 8 W and 9 W in the 1040nm and 976nm signals, respectively. In addition, the spectral content of the backscattered light showed that the Stokes peak was approximately 5 dB below the Rayleigh peak; further confirming that operation below the SBS threshold. The forward spectrum indicated an amplified spontaneous emission suppression of ~40 dB.

For the 1035 nm case, the optimal seed ratio was roughly 100:1. The difference in optimal seed ratios between the 1035 nm and 1040 nm wavelengths can be attributed to the difference in the absorption cross sections. Using the 1035 nm broadband seed at 5 W and the 1065 nm seed at 40 mW, the Limo pumps were pushed to the absolute limit of available power. The slope efficiency, shown in Figure 44, was 80% with a maximum output of 203.5 W. The simulated results using Eqs. (4.1-4.13) for this fiber are also shown for comparison. In this case, the measured unused 1035 nm and 976 nm light were 10.6 W and 11W, respectively and the ASE suppression was ~32 dB.

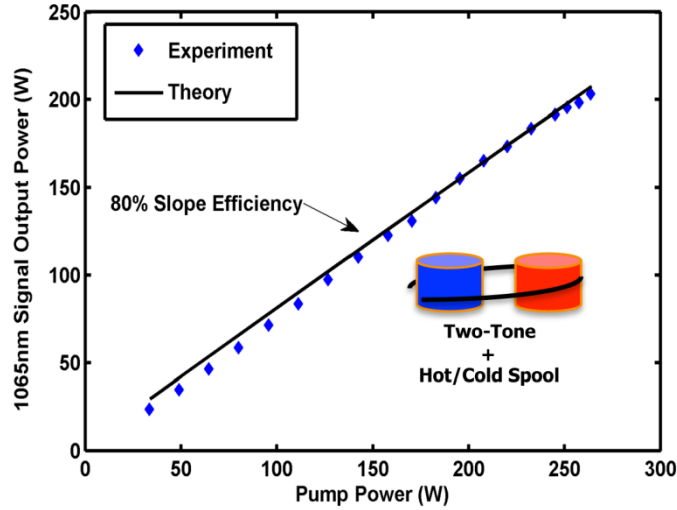


Figure 44. Output power as a function of launch power and reflectivity the for cold plate hot plate configuration with the broadband seed operating at 1035 nm. The theoretical results using the equations developed in Chapter 4 are shown for comparison.

At the 203 W level, the reflectivity was linear with the signal power; indicating operation below the SBS threshold. Figure 45 shows the spectral content of the backward light at different output powers for the single-frequency signal. Note that at 203 W, the Stokes peak is only 3 dB above the Rayleigh peak. Figure 46 further underscores that the system is operating under the SBS threshold. In this case, the backward power vs. signal output power is shown along with the simulated results using Eqs. (4.1-4.13). The experimental data shows a linear growth indicating operation below the SBS threshold.

At this time, this power level is the highest reported in the literature for a monolithic Yb-doped PM single-frequency amplifier. The estimated SBS threshold (based on the nonlinear turn of the simulation) for this amplifier is approximately 220 W as shown in Figure 46. Moreover, it is estimated that further power scaling to the 300 W at >70% efficiency can be achieved by reducing the amplifier length to ~5 m and optimizing the length of fiber on the cold spool. A similar

procedure should also provide a substantial power increase for the second configuration wherein quantum defect heating was utilized.

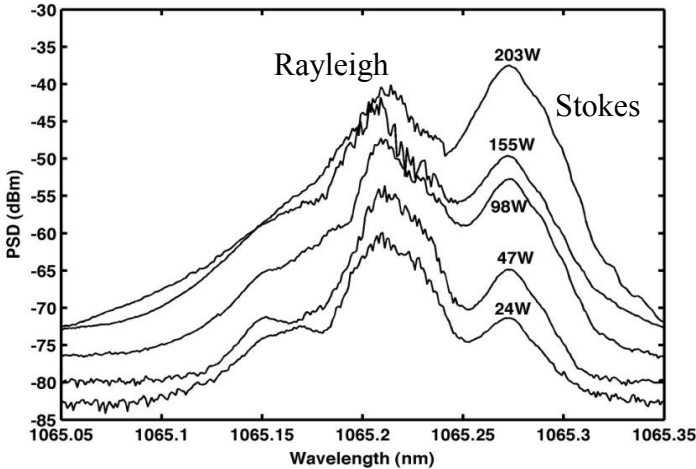


Figure 45. Spectral content of the backscattered light at various signal output powers for the hot plate cold plate configuration.

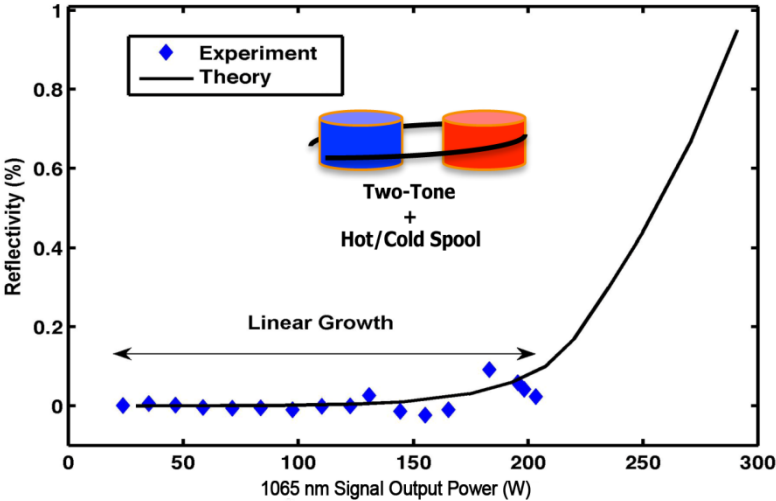


Figure 46. Reflectivity vs. signal output power for two-tone configuration with 1035 nm broad-band signal and hot and cold plate. The numerical simulations of integration of Eqns. (4.1-4.13) are also shown for comparison.

5.4 SUMMARY

In conclusion, this chapter demonstrated experimentally, SBS mitigation through laser competition between two signals in a monolithic co-pumped amplifier leading to output power >200

W in the single-frequency channel. It was shown that this concept works in conjunction with both intrinsic and external thermal gradients. In addition, numerical simulations of the fiber considered in these experiments using the theory developed in Chapter 4 were found to be in excellent agreement with the experimental results. These experiments represent the first demonstrations of SBS suppression through laser gain competition.

6 TIME DEPENDENT SBS WITH PHASE MODULATION

6.1 INTRODUCTION

In recent years, researchers have used phase modulation as a means of suppressing the SBS process in optical fibers [49-51]. The general thinking is that the SBS process is suppressed due to the spectral broadening of the pump. Recent demonstrations of a kW class amplifier with a measured linewidth of 11 GHz only increased the SBS threshold by a factor of ~ 30 [52]. Previous works have suggested that under specific conditions the SBS threshold should increase linearly with the ratio of the pump spectral linewidth to the Brillouin gain bandwidth [53,54]. This means that for an 11 GHz linewidth continuous-wave (CW) pump and a spontaneous Brillouin linewidth ~ 60 MHz the SBS threshold increase should be approaching a factor of 200; well above the suppression factor obtained in the experimental work of Ref. [52]. The goal of this chapter is to reconcile this discrepancy and characterize the SBS suppressing effects of phase modulation by solving the three-wave interaction of the SBS process using a time-dependent model.

Time-dependent SBS was previously treated numerically in a passive fiber [13]. Furthermore, an analytical solution for the Stokes light in the long-time limit in the case of an undepleted pump has also been developed [13,55]. However, the study did not consider the effects of phase modulation on the input pump field. The SBS process has also been examined in the Fourier domain under phase modulated conditions [17]. This model assumes that the fiber length is long $L > 1km$ and the separation among optical modes is large $\Delta\omega > 1MHz$. With these assumptions, the phase-mismatched terms arising from interactions among Stokes sidebands created from the phase modulation may be neglected. In most fiber amplifiers the interaction length of the SBS process is, ($L < 10m$) so these approximations are questionable. In this chapter, the time-dependent approach is extended to study the effects of phase modulation with no assumption on fiber length or separation

between optical sidebands. The geometric layout of a fiber and the three-wave interaction of the SBS process is shown schematically in Figure 47. Here the pump field refers to the optical field propagating in the forward direction, the acoustic field is a material wave that propagates in the forward direction in the fiber, and the Stokes field is the optical field that propagates in the backward direction as a result of scattering between the pump and acoustic field.

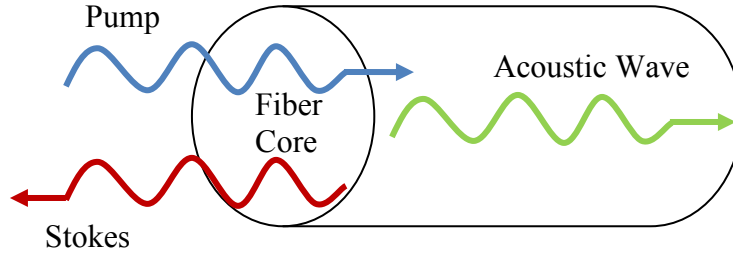


Figure 47. Three-wave interaction between optical pump, Stokes, and acoustic wave in an optical fiber.

6.2 THEORETICAL FRAMEWORK

In accordance with Ref. [13], the three-wave interaction, which describes the SBS process, consists of two optical fields and an acoustic field. The optical fields are represented as time-harmonic waves:

$$\tilde{E} = \tilde{E}_L(z, t) + \tilde{E}_S(z, t) \quad (6.1)$$

$$\tilde{E}_L = E_L(z, t)e^{i(k_L z - \omega_L t)} + c.c. \quad (6.2)$$

$$\tilde{E}_S = E_S(z, t)e^{i(-k_S z - \omega_S t)} + c.c. \quad (6.3)$$

$$\tilde{\rho} = \rho_o + \left[\rho(z, t)e^{i(qz - \Omega t)} \right] + c.c. \quad (6.4)$$

where \tilde{E}_L , \tilde{E}_S and $\tilde{\rho}$ represent the pump, stokes, and acoustic fields respectively. k_L, k_S and q represent the pump, stokes, and acoustic wave-vectors, where $q = k_L + k_S$. Likewise, ω_L, ω_S and Ω

represent the pump, stokes, and acoustic frequencies where $\Omega = \omega_L - \omega_s$. Implicit in the fields given in Eqs. (6.2-6.4) is the assumption that the transverse variation of the fields may be neglected, which is known to be highly accurate for single-mode optical fibers. The non-linear wave equation:

$$\nabla^2 \tilde{E} - \frac{n^2}{c^2} \frac{\partial^2 \tilde{E}}{\partial t^2} = \frac{1}{\epsilon_o c^2} \frac{\partial^2 \tilde{P}_{nl}}{\partial t^2} \quad (6.5)$$

describes the propagation of the optical fields in the medium where $\tilde{P}_{nl} = \gamma_e \tilde{\rho} \tilde{E} / 4\pi\rho_o$ describes the non-linear polarization associated with the SBS process and where γ_e represents the electrostrictive constant of the medium. The acoustic field is described by the acoustic wave equation:

$$\frac{\partial^2 \tilde{\rho}}{\partial t^2} - \frac{\Gamma_B}{q^2} \nabla^2 \frac{\partial \tilde{\rho}}{\partial t} - v_s^2 \nabla^2 \tilde{\rho} = \nabla \cdot g + \tilde{f} \quad (6.6)$$

where the driving force $\nabla \cdot g$ is given by:

$$\nabla \cdot g = -\frac{1}{2} \epsilon_o \gamma_e \nabla \langle \tilde{E}^2 \rangle \quad (6.7)$$

and we have introduced the phonon decay rate $\Gamma_B = 1/\tau_p$, where τ_p is the phonon lifetime. Here, v_s denotes the velocity of sound in the medium and n is the optical index of refraction. The second term on the right hand side of Eq. (6.6) initiates the SBS process and is described by a Langevin noise source [13]:

$$\begin{aligned} \langle f(z, t) f^*(z, t) \rangle &= Q \delta(z - z') \delta(t - t') \\ Q &= kT \rho_o / v_s^2 A \end{aligned} \quad (6.8)$$

Where Q describes the strength of the fluctuations. We express \tilde{f} as [13]:

$$\tilde{f} = -2i\Omega f(z, t) e^{i(qz - \Omega t)} + c.c \quad (6.9)$$

Plugging Eq. (6.1) into Eq. (6.5), making the slowly varying envelope approximation, and keeping only phase-matched source terms for the non-linear polarization yields the equations which describe the evolution of the optical field amplitudes in the fiber:

$$\frac{c}{n} \frac{\partial E_L}{\partial z} + \frac{\partial E_L}{\partial t} = \frac{i\omega\gamma_e}{2n^2\rho_o} \rho E_S \quad (6.10)$$

$$-\frac{c}{n} \frac{\partial E_S}{\partial z} + \frac{\partial E_S}{\partial t} = \frac{i\omega\gamma_e}{2n^2\rho_o} \rho^* E_L \quad (6.11)$$

where $\omega \approx \omega_L \approx \omega_S$. Phase modulation effects are including through the boundary and initial conditions of the electric field at the input end of the fiber:

$$\begin{aligned} E_L(0,t) &= E_L^0 e^{i\varphi(t)} \\ E_L(z > 0, 0) &= 0 \\ E_S(z, 0) &= E_S(L, t) = 0 \\ \rho(z, t \leq 0) &= \rho' \end{aligned} \quad (6.12)$$

Where ρ' is the solution to Eq. (6.6) excluding the electrostrictive driving term and the second order derivative, which is insignificant without the driving force. E_L^0 and $\varphi(t)$ denote the input electric field amplitude and phase modulation function, respectively. It should be noted that implicit in the derivation of Eqns. (6.10-6.11) is the assumption that the higher order terms arising from the second derivative of the non-linear polarization in the case of phase modulation are small. Specifically, this is justified as long as $\omega_{FM} \ll \omega$, where ω_{FM} is the modulation frequency.

Focusing now on the phonon equation, the phase-matched driving term of Eq. (6.7) for the fields in Eqns. (6.2-6.3) is:

$$\nabla \cdot g = \varepsilon_o \gamma_e q^2 \left[E_L E_S^* e^{i(qz - \Omega t)} + c.c \right] \quad (6.13)$$

Substitution of Eqns. (6.4), (6.9) and (6.13) into Eq. (6.6), keeping only the phase matched terms and ignoring the spatial variation of the phonon field in the medium, the equation describing the evolution of the acoustic disturbance is:

$$\frac{\partial^2 \rho}{\partial t^2} + (\Gamma_B - 2i\Omega) \frac{\partial \rho}{\partial t} + (\Omega_B^2 - \Omega^2 - i\Omega\Gamma_B) \rho = \varepsilon_o \gamma_e q^2 E_L E_S^* - 2i\Omega f \quad (6.14)$$

where the resonant acoustic frequency of the medium may be approximated as [1] :

$$\Omega_B = 2nv_S \omega_L / c \quad (6.15)$$

In the absence of external effects such as temperature variation, stress, fiber impurities, and other sources of variation for the acoustic velocity, only acoustic frequencies at or near the resonant frequency of the medium contribute significantly to the growth of the acoustic wave. Keeping this in mind, Eq. (6.14) is solved at resonance $\Omega = \Omega_B$:

$$\frac{\partial^2 \rho}{\partial t^2} + (\Gamma_B - 2i\Omega_B) \frac{\partial \rho}{\partial t} - i\Omega\Gamma_B \rho = \varepsilon_o \gamma_e q^2 E_L E_S^* - 2i\Omega_B f \quad (6.16)$$

The second order derivative term in Eq. (6.16) is typically neglected since it is normally insignificant compared to the other terms. However, this approximation can break down when the modulation frequency becomes proportional to the acoustic frequency. Since the driving term on the right-hand side of Eq. (6.16) is proportional to E_L and the electric field carries a time-varying phase it is natural to assume that the phonon amplitude also carries a time-varying phase. To that end,

when $\frac{\partial \rho}{\partial t} \propto \omega_{FM} \propto \Omega_B$ the first and second order derivatives on the left-hand side of Eq. (6.16) can

become comparable: $\frac{\partial^2 \rho}{\partial t^2} \propto (\Gamma_B - 2i\Omega_B) \frac{\partial \rho}{\partial t}$, and the higher order term should be included.

Equations (6.10), (6.11), and (6.16) completely describe the three-wave interaction including the effects of noise initiation.

6.3 NUMERICAL APPROACH

Equations (6.10), (6.11) and (6.16) are solved numerically using the method of characteristics. The characteristics for the laser, Stokes, and phonon fields are: $dz/dt = c/n$, $-c/n$ and 0 respectively. To that end, these equations at resonance take the form:

$$\frac{dE_L}{dt} = i\sigma\rho E_S \quad (6.17)$$

$$\frac{dE_S}{dt} = i\sigma\rho^* E_L \quad (6.18)$$

$$\frac{\alpha}{\Gamma_B} \frac{d^2\rho}{dt^2} + (\alpha - i) \frac{d\rho}{dt} - i \frac{\Gamma_B}{2} \rho = \chi E_L E_S^* - if \quad (6.19)$$

where $\chi \equiv \varepsilon_o \gamma_e q^2 / 2\Omega_B$, $\alpha \equiv \Gamma_B / 2\Omega_B$, $\Gamma_B \equiv 1/\tau_p$, $\sigma \equiv \omega\gamma_e / 2n^2\rho_o$, and τ_p is the phonon lifetime. As noted earlier, the higher order derivative of Eq. (6.19) could be significant in the limit that the phase modulation frequency ω_{FM} approaches Ω_B . In this work, modulation frequencies up to $\omega_{FM} = 30\Gamma_B \ll \Omega_B$ are considered. To that end, the higher order term may be neglected in this analysis. However, the accuracy of this approximation was checked numerically and it was determined that the term played no significant role over the modulation frequencies investigated. The system of equations is solved using the modified Euler method. In the discrete case, the boundary and initial conditions take the form:

$$\begin{aligned} E_L(0, t_j) &= E_L^0 e^{i\varphi(t_j)} \\ E_L(z_i > 0, 0) &= 0 \\ E_S(z_i, 0) &= E_S(L, t_j) = 0 \\ \rho(z_i, t_j \leq 0) &= \rho'_{i,j} \end{aligned} \quad (6.20)$$

where

$$\rho_{i,j} = \sqrt{\frac{nQ}{c\Gamma_B}} R_{i,j} \quad (6.21)$$

Here $R_{i,j}$ is a complex Gaussian random distribution function with zero mean and unit variance. The spatial grid is determined from the characteristic $\Delta z = \frac{c}{n} \Delta t$. The simulation time is taken over more than 30 transit times of the fiber. In the discrete case, the amplitude of the noise term used in Eq. (6.19) is given by:

$$f_{i,j} = \sqrt{\frac{Q}{\Delta t \Delta z}} R_{i,j} \quad (6.22)$$

where i, j describe the grid points of intersection along the three characteristics in space and time, respectively.

6.4 MODEL VALIDATION

In an effort to characterize the numerical stability and accuracy of the solver, Eqns. (6.17-6.19) were solved using both the Euler and the modified Euler method. Since, for all practical purposes, the Stokes and laser frequencies are equal, the quantity

$$\langle |E_L(z,t)|^2 \rangle - \langle |E_S(z,t)|^2 \rangle = C, \quad (6.23)$$

which describes conservation of photons, should be constant [1]. Here the brackets indicate the time-averaged power in the long time limit where $\Gamma_B t \gg 1$. Figures 48 and 49 show a comparison of Eq. (6.24) normalized to unity for both methods for different reflectivity using the parameters listed in Table 2. For both techniques it is clear that in the low reflectivity limit Eq. (6.23) is conserved across the fiber length. However, both methods indicate variation near the input end of the fiber where the reflectivity is highest. The modified Euler technique has a maximum variation less than 1% compared to a 6% variation using just the one-step Euler method. All results presented hereafter are

done with the modified Euler technique. In addition, this study is concerned with SBS threshold calculations (ie. $R \sim 1\%$) and as can be inferred from these figures both methods indicate conservation of photons over the fiber length in this regime.

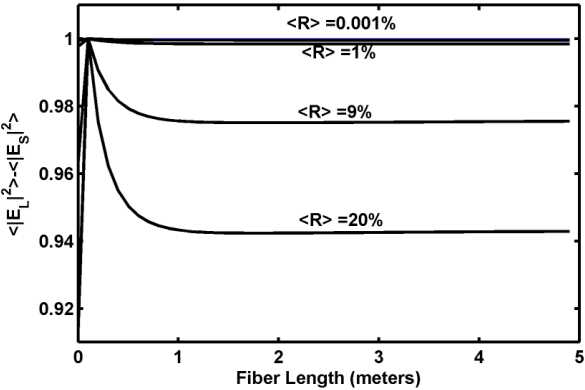


Figure 48. Normalized power difference along fiber length for different reflectivity using one-step Euler Method. $\langle R \rangle$ defines the time-averaged reflectivity over several transit times in the long time-limit $\Gamma_B t \gg 1$.

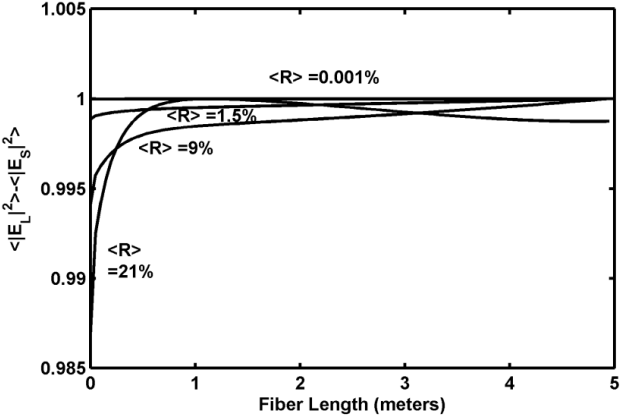


Figure 49. Normalized power difference along fiber length for different reflectivity using Modified Euler Method. $\langle R \rangle$ defines the time-averaged reflectivity over several transit times in the long time-limit $\Gamma_B t \gg 1$.

ρ_o	$2201 \text{ kg} / \text{m}^3$	v_s	$5.9 \times 10^3 \text{ m} / \text{s}$
ω	$1.77157 \times 10^{15} \text{ rad} / \text{s}$	A	$7.85 \times 10^{-11} \text{ m}^2$
γ_e	1.95	Ω_B	$10.1 \times 10^9 \text{ rad} / \text{s}$
n	1.45	L	5 m
T	300 K	τ_p	17.5 ns

Table 2. Fiber simulation parameters. These parameters are based on approximate values for fused silica at room temperature and a pump wavelength of 1064nm.

The accuracy of the numerical solver can be tested by comparing the SBS reflectivity to the analytic approximation in the low-SBS gain limit for an un-modulated pump: [13]

$$R = \left(\frac{\gamma_e \omega_S}{2 \rho_o n c} \right)^2 \frac{QL}{\Gamma} e^{G/2} [I_o(G/2) - I_1(G/2)], \quad (6.24)$$

where $G = g_o I L$, $I = 2n\epsilon_o c |E_L|^2$, and L is the fiber length. Additionally, g_o describes the SBS gain factor:

$$g_o = \frac{\gamma_e^2 \omega_S^2}{\rho_o n c^3 v_s \Gamma}. \quad (6.26)$$

Figure 50 shows the results of this comparison for the fiber parameters listed in Table 2 using a spatial grid of 100 points. It is clear from the figure that in the limit where single-pass SBS gain is small ($G < 20$), there is excellent agreement between the analytic approximation and the numerical integration of the coupled system. For the numerical solution, logarithmic growth is observed in the reflectivity over the entire gain range and there is a strong departure from the undepleted pump approximation near $G \sim 25$ which is in good agreement with previous results. [13]

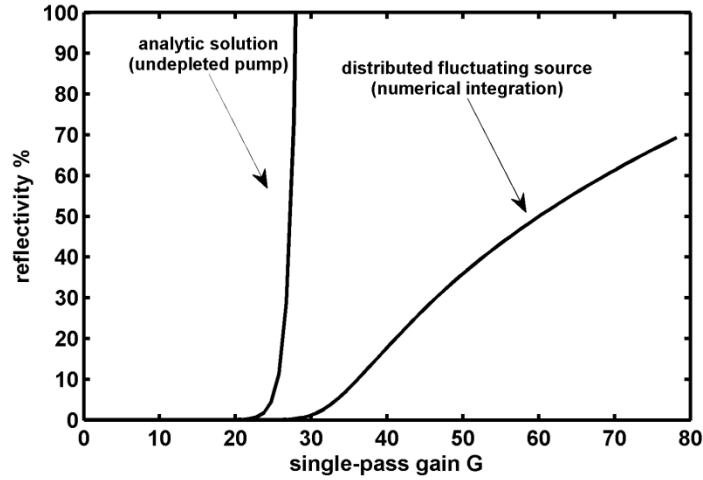


Figure 50. Comparison between analytic reflectivity of Eqn. (6.24) for undepleted pump and numerical integration of the equations using a distributed fluctuating noise source. The reflectivity in the case of the numerical integration is averaged over several transit times in the long time limit $\Gamma_B t \gg 1$. The analytic solution shows a strong exponential growth near $G \sim 25$ while the numerical integration shows logarithmic growth over the entire range. These results are in excellent agreement with those discussed in previous works. [13]

Another useful comparison to measure the accuracy of the discrete noise term and the numerical integration is to compare the full width at half maximum (FWHM) of the output stokes radiation to the analytic, undepleted approximation: [13]

$$S(\omega) = \frac{8\pi\hbar\omega_s(\bar{n} + 1)}{ncA} \left[\exp\left(\frac{G(\Gamma/2)^2}{\omega^2 + (\Gamma/2)^2} \right) - 1 \right]. \quad (6.27)$$

In Figure 51 the normalized ($\text{FWHM} = \Delta\omega / \Gamma$) is compared to the results of the numerical integration using Eq. (6.27). In the case of the numerical routine, the (FWHM) is computed using the power spectral density of the stokes radiation at $z = 0$. It is evident from the figure that in the low SBS gain limit there is good agreement with Eq. (6.27) and a departure from the analytic approximation as the single-pass SBS gain is increased. This is to be expected since Eq. (6.27) is only valid for an undepleted pump. It should also be noted that the numerical integration is able to

resolve the spontaneous Brillouin linewidth Γ_B in the case of low SBS gain, and shows that the Stokes radiation exhibits considerable narrowing as the single-pass gain increases. This is in excellent agreement with previous results for a passive fiber. [13]

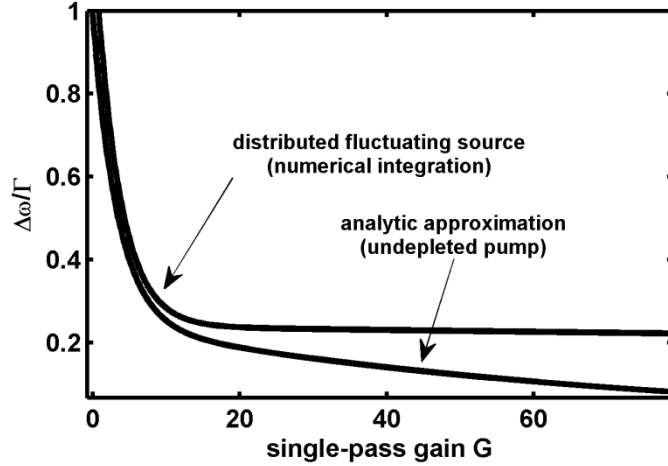


Figure 51. Comparison between analytic linewidth for undepleted pump shown in Eqn. (6.27) and numerical integration of the equations using a distributed fluctuating noise source. The normalized (FWHM= $\Delta\omega/\Gamma$) of the Stokes radiation is computed using the power spectral density of the Stokes field at $z=0$. The analytic solution shows a strong departure from the numerical solution as the single-pass SBS gain is increased. We also observe an asymptotic convergence of the line-width in the numerical solution. These results are in excellent agreement with those discussed in. [13]

6.5 PHASE MODULATION SCHEMES AND SBS THRESHOLD EFFECTS

6.5.1 SINGLE-SINUSOIDAL MODULATION

In this section the SBS suppression of a pump field phase-modulated with a single-frequency sinusoidal modulation function with modulation amplitude γ and modulation frequency ω_{FM} is explored. The modulation function is given by

$$\varphi(t) = \gamma \sin(\omega_{FM} t) \quad (6.28)$$

Eqns. (6.17-6.19) are integrated for various combinations of phase modulation amplitudes and frequencies in order to characterize the SBS threshold. In all cases, the SBS threshold is defined as

the input field power for which the time-averaged reflectivity over several transit times, where the transit time is given by $\tau_{RT} = nL / c$, is $\sim 1\%$.

In order to capture the effects of phase modulation, a temporal grid whose grid spacing is $\Delta t = 0.0125 \times 2\pi / \omega_{FM}$ or $\Delta t = \tau_p / 50$ is employed, where the lesser of the two values is chosen. The latter restriction is imposed to capture the time scale of the phonon lifetime and was also verified by studying the convergence of the modified Euler technique for the unmodulated case. In addition, the total simulation time encapsulated at least 20 transit times of the fiber length, $\Delta t N_t \geq 20\tau_{RT}$. The SBS threshold enhancement normalized to the un-modulated threshold is shown in Figure 52 for various combinations of γ and ω_{FM} using the parameters shown in Table 2. The x-axis in the figure is normalized to the spontaneous Brillouin linewidth $\Delta\nu_B = \Gamma_B / 2\pi$. Also shown in this figure is the analytic solution provided in Ref. [17] using formulism in the frequency domain. In this limit the Stokes modes resulting from the phase modulation of the optical field act independently ($\Delta\nu_{FM} \gg \Delta\nu_B$) the SBS threshold should be determined by the highest amplitude Stokes band. To that end the SBS gain is [17]:

$$g_{eff} = g_0 \left(\Gamma_B / 2 \right) L \int_{-\infty}^{\infty} \frac{I(\omega) d\omega}{\left(\Gamma_B / 2 \right)^2 + (\omega - \omega_s - \Omega_B)^2} = \frac{g_0 I_L^{\max} L}{\Gamma_B / 2} \quad (6.29)$$

where $\omega = \omega_{\max}$ is the frequency corresponding to the maximum intensity I_L^{\max} and

$g_0 = \gamma_e^2 \omega_s^2 / \rho_0 n c^3 v_s \Gamma_B$ is the small-signal SBS gain. Since the gain is linearly proportional to the SBS threshold, in the large separation limit the expected threshold increase is:

$$P_{th} = P_{th}^0 \frac{I_L^0}{I_L^{\max}} = \frac{P_{th}^0}{J_{n,\max}^2(\gamma)} \quad (6.30)$$

where P_{th}^0 is the SBS threshold of the unmodulated field, I_L^0 is the total intensity of the input field, and $J_{n,\max}(\gamma)$ is the the Bessel function of the 1st kind which describes the amplitude of the sideband with the maximum value.

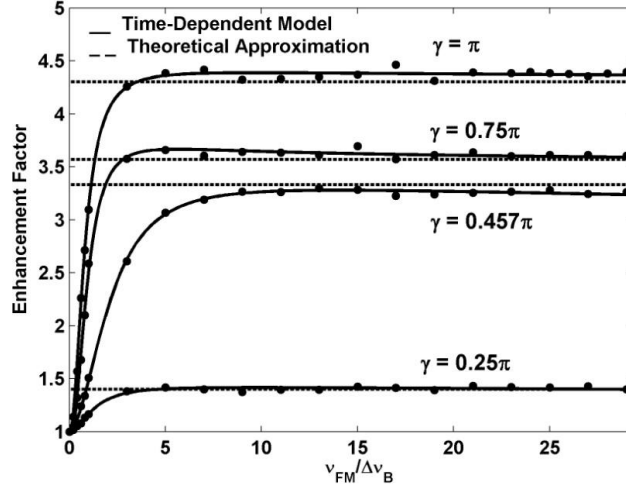


Figure 52. Results of SBS threshold enhancement factor vs. modulation frequency $\nu_{FM} = \omega_{FM} / 2\pi$ for various modulation amplitudes. As expected, the results indicate asymptotic convergence to the theoretical approximation of Eq. (6.30) in the large modulation frequency limit where the separation between optical modes is large compared to the spontaneous Brillouin linewidth.

When considering modulation frequencies within the Brillouin line width $\omega_{FM} / \Gamma_B \ll 1$ little enhancement is expected regardless of modulation amplitude due to a large degree of overlap between the SBS spectra in the sidebands. We see from Figure 52 that the expected enhancement in this regime is minimal for all modulation amplitudes. For the range of modulation frequencies $0.5\Gamma_B \leq \omega_{FM} \leq 5\Gamma_B$ the SBS threshold increases with modulation frequency. This regime also describes the transition from strong to weak overlap among the SBS in the optical sidebands. When considering even larger modulation frequencies: $\omega_{FM} > 5\Gamma_B$ additional enhancement in SBS suppression is minimal since in this regime the Brillouin gain overlap among the Stokes sidebands is

very small. As expected, in the large modulation frequency limit, the threshold enhancement approaches the approximation of Eq. (6.30).

Qualitatively, this can be seen by comparing the SBS spectra near SBS threshold at $\gamma = 1.435$ for $\omega_{FM} = 2\Gamma_B$ and $\omega_{FM} = 20\Gamma_B$. The power spectral density of the optical and Stokes fields for these two cases are shown in Figure 53. For simplicity, the spectra are normalized about their respective DC components. In this case, the optical pump spectrum contains three equal amplitude lines. If overlap is present, the two inner sidebands will feed the central Stokes and so for the case $\omega_{FM} = 2\Gamma_B$ the central Stokes is higher than the two inner bands by 12dB. On the contrary, in the case where the pump bands are separated by $\omega_{FM} = 20\Gamma_B$ the overlap is minimal and the Stokes spectrum closely resembles that of the pump with three equal intensity sidebands. In this case the difference is less than 1.5 dB.

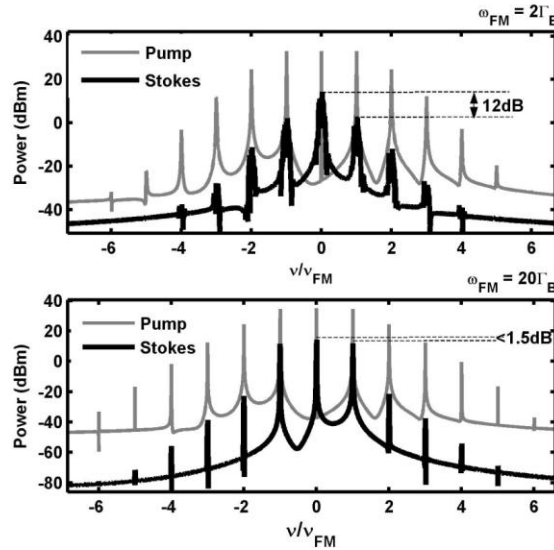


Figure 53. Results of the power spectral density (PSD) of the pump and Stokes fields near SBS threshold for the case $\gamma = 1.435$, with $\omega_{FM} = 2\Gamma_B$ (upper) and $\omega_{FM} = 20\Gamma_B$ (lower). Both curves are normalized about their respective DC components. The results clearly show that in the small modulation regime interactions among the various sidebands tend to feed the central DC term leading to a higher central Stokes mode. When the modulation frequency is large the Stokes spectrum closely follows that of the pump with three approximately equal side bands.

6.5.2 WHITE-NOISE MODULATION

One way to broaden the linewidth of a laser is through white-noise modulation [56]. A schematic of this technique is shown in Figure 54. A white-noise source (WNS) is sent through a filter with a pass band control mechanism to shape the bandwidth of the RF driving signal. The amplified RF signal drives an electro-optic modulator (EOM) which increases the laser linewidth producing a broadband CW output whose linewidth may be controlled by the pass band filter and the gain of the RF amplifier. In order to model the effects of phase modulation with the white-noise modulation scheme shown in Figure 54, we must construct the boundary and initial conditions shown in Eq. (6.20).

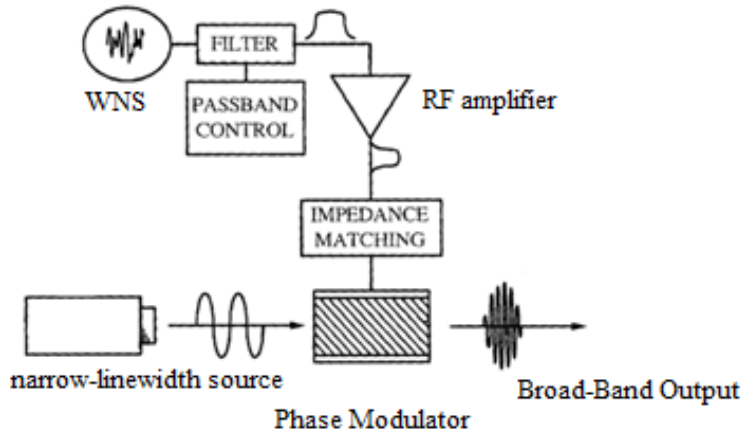


Figure 54. Schematic of white-noise driven phase modulation to broaden and control the linewidth of a laser source. A white noise source is sent through a filter and pass band control to shape the bandwidth of the RF driving signal. The filtered response is amplified and set to match the impedance of the electro-optic modulation (EOM). When the EOM is driven with the noise-filtered signal the laser linewidth is broadened. [56]

In this case, the initial WNS is assumed to be delta correlated in the sense that:

$$\begin{aligned} \langle \varphi_i(t) \varphi_i(t') \rangle &= \gamma_0 \delta_{i,j} \delta(t - t') \\ \langle \varphi_i(t) \rangle &= 0 \end{aligned} \tag{6.31}$$

where γ_0 describes the small-signal modulation depth and the RF signal has a finite bandwidth of 10 GHz. To shape the spectrum into a Lorentzian with full-width half maximum (FWHM) $\Delta\nu_{FWHM}$ in the range [0-10] GHz the RF signal is convoluted with a Sinc function:

$$\varphi_f(t) = \varphi_0(t) \otimes \text{Sinc}(\Delta\nu_{FWHM}t). \quad (6.32)$$

In Fourier space, this is equivalent to passing the RF signal through a band-pass filter of width $\Delta\nu_{FWHM}$. Next, one determines the appropriate RF gain G_{RF} needed to appropriately create a Lorentzian lineshape such that:

$$\varphi(t) = G_{RF} \varphi_f(t) \quad (6.33)$$

and

$$E_L(\omega) = \mathfrak{F} \left\{ E_L^0 e^{i\varphi(t)} \right\}, \quad (6.34)$$

where \mathfrak{F} represents the Fourier transform. Numerically, this is done by computing the discrete Fourier transform (DFT) of $E_L(t)$ for various G_{RF} until a suitable fit to a Lorentzian lineshape with $\Delta\nu_{FWHM}$ is achieved. To this end, a root-solving technique with the merit function being the FWHM of the resultant Lorentzian lineshape was employed. In all cases the FWHM of the resultant lineshape was within 1% of $\Delta\nu_{FWHM}$. A suitable temporal grid is chosen such the smallest time step determined by the following set of constraints is chosen: $\Delta t = \tau_p / 50$, $\Delta t N_t \geq 20\tau_{RT}$, and $\Delta t \leq 1 / (2 \times 10 \Delta_{FWHM})$. The latter requirement is made to satisfy the Nyquist–Shannon sampling theorem for a maximum frequency of 10 times the linewidth of the pump. In these cases, the fiber parameters are the same as those listed in Table 2 with the exception that the fiber length is varied and the fiber area was changed to incorporate a $(25/400)\mu\text{m}$ large-mode area (LMA) fiber. Figure

55 shows the SBS enhancement vs. the normalized pump linewidth $\Delta\nu_{FWHM} / \Delta\nu_B$ for several different fiber lengths. Here the enhancement is normalized to the unmodulated case for each fiber length. Substitution of a Lorentzian lineshape into the analytic approximation of Eq. (6.29) and evaluating at line center gives an expected threshold enhancement of:

$$P_{th} = P_{th}^0 \left(1 + \frac{\Delta\nu_{FWHM}}{\Delta\nu_B} \right). \quad (6.35)$$

which is also plotted in the figure for reference.

From Figure 55 it is clear that in the limit where the fiber length becomes large the expected enhancement factor closely resembles that of Eq. (6.35), but in short fibers the enhancement factor is much lower. Furthermore, Figure 56 shows that the slope of the enhancement relative to the pump linewidth increases for larger fiber lengths and approaches unity for long fibers also in agreement with Eq. (6.35). The discrepancy at short fiber lengths is attributed to interactions among Stokes frequencies. Eq. (6.35) is often used as the basis for estimating the SBS threshold in fiber amplifiers possessing a broad linewidth. Recent results of a kW class amplifier whose linewidth was broadened using a WNS contradict Eq. (6.35). [31] Figure 57 shows the experimental results of Ref. [31] along with the prediction using Eq. (6.35). It is clear that Eq. (6.35) overestimates the SBS threshold in fiber amplifiers. This discrepancy is not surprising given that Eq. (6.35) is derived using Eq. (6.29) which was formulated in the Fourier domain under the assumption that the longitudinal mode spacing was large ($\Delta\nu > 10MHz$) and the fiber was long ($L \geq 1km$).[17]

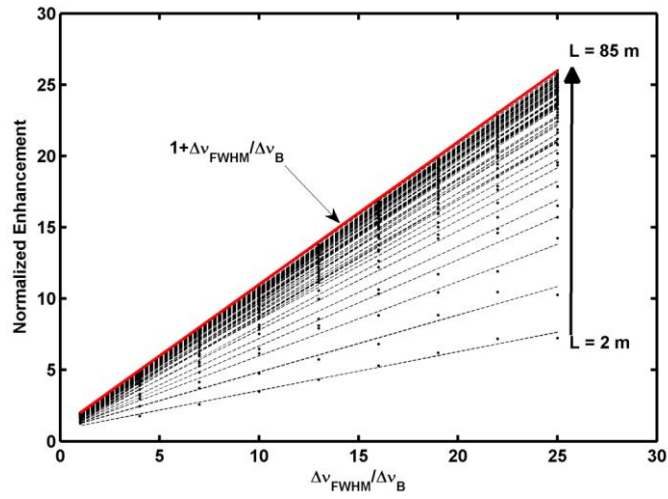


Figure 55. Normalized enhancement factor vs. normalized pump linewidth for fiber lengths ranging from 2m-85m. As the fiber length is increased the enhancement factor closely resembles Eq. (6.35).

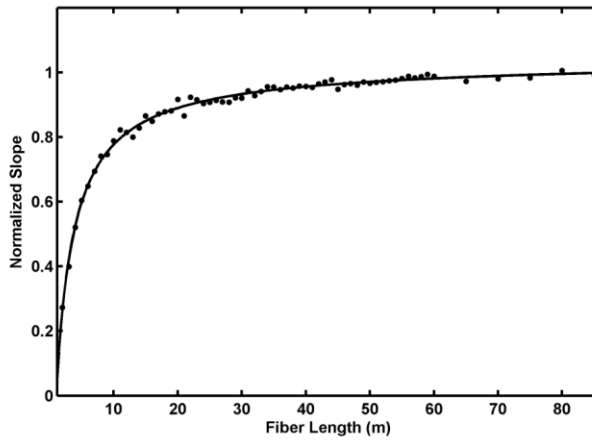


Figure 56. Normalized slope vs. fiber length. For long fiber lengths the slope approaches unity in agreement with Eq. (6.35).

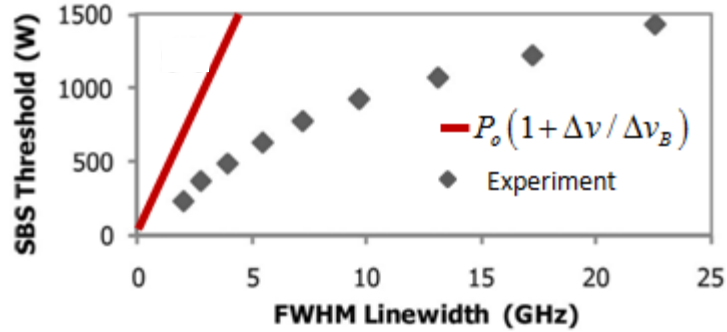


Figure 57. Experimental data of SBS threshold vs. seed linewidth using Ref [31]. The SBS threshold predicted from Eq. (6.35) is also shown and clearly indicates a severe discrepancy with the experimental data.

Under the aforementioned approximations, the phase-mismatched terms describing the interactions of the longitudinal Stokes modes created from the phase modulation may be ignored and Eq. (6.35) would predict the correct SBS threshold. However, in short fibers these interactions are important and cannot be neglected. Furthermore, for a WNS the longitudinal mode spacing of the Stokes frequencies is ill-defined since the resultant power spectral density (PSD) is a continuous distribution of frequencies. In this case, the cross-diagonal terms neglected in the derivation of Eq. (6.29) and SBS gain interactions among the Stokes frequencies are responsible for a reduction in the threshold enhancement with respect to that predicted by Eq. (6.29). The reduction as a function of length is clearly evident in the results shown in Figures 55 and 56. Thus, the time-dependent approach is well suited for describing the SBS threshold enhancement due to phase modulation in fiber amplifiers since the time-dependent equations encapsulate cross-interactions among the Stokes frequencies and thus the temporal approach is not limited to long fibers.

6.6 SUMMARY

In summary, a time-dependent model was developed to study the effects of phase modulation on stimulated Brillouin scattering. Two phase modulation schemes were examined: a single-

sinusoidal modulation and a WNS modulation. It was shown that, in the case of a single-sinusoidal phase modulated pump, the SBS threshold increases with modulation amplitude. Furthermore, for large modulation frequencies the threshold is uniquely determined by the largest amplitude sideband and closely follows Eq. (6.30). The SBS process was also examined for a pump phase modulated using a WNS to broaden the linewidth. The SBS threshold vs. pump linewidth was characterized for several fiber lengths. Here, it was determined that the expected SBS threshold enhancement is dependent on the length of fiber, and only in the long fiber limit, follows the often quoted threshold enhancement of Eq. (6.35). A theoretical explanation for this discrepancy was provided that showed how the approximations used to derive Eq. (6.29) break down for fiber amplifiers when the fiber length is short (and/or) the longitudinal mode spacing is small. The discrepancy was resolved using a time-dependent approach which clearly showed that the SBS threshold depends on the longitudinal mode spacing created from the phase modulation scheme and the fiber length.

7 CONCLUSION

7.1 SUMMARY

This dissertation addressed several aspects of the SBS process in fiber amplifiers seeded with multiple signals and when a single seed is phase modulated. Throughout this investigation detailed models of the SBS process were developed in both the steady-state and transient regimes. In the first theoretical study, multiple signals with frequencies separated at twice the Brillouin shift were input into the fiber amplifier. For this case, non-linear coupling between the signals and Stokes fields is created such that the SBS gain is reduced in the highest frequency seed leading to an enhancement of the SBS threshold that scales linearly with the number of input seeds. Analytic expressions describing the optimal seed ratios to achieve maximal SBS suppression were developed and compared well with previous experiments [7] and numerical simulations. In addition, FWM was characterized for this novel technique and found to be significant; making this concept impractical for applications requiring single-frequency output.

Next, a novel concept was developed that suppresses the SBS process through laser gain competition among multiple signals in a fiber amplifier. For this case, the frequency separation between the amplifier seeds was on the order of nm or greater. It was shown that for this case, FWM effects were negligible up to 100's of watts of output power and in addition could be completely ignored for wavelength separations $\Delta\lambda > 4nm$ while simultaneously providing an SBS threshold increase of twice that of the single-tone case. In addition, thermal aspects of this concept were also explored theoretically and it was found that, for specific wavelength separations, a large thermal gradient develops near the output end of the fiber due to quantum defect heating which further increases the SBS suppression. In this case, the SBS threshold was increased up to a factor of 5 relative to the same amplifier seeded with only one seed.

To demonstrate the concept experimentally several tests were carried out in Yb doped fibers for the case of an amplifier seeded simultaneously with a broad-band ($\Delta\lambda \sim .1nm$) and single-frequency ($\Delta\nu < 100KHz$) laser. In the lower power demonstrations over 6 W of single-frequency output was obtained resulting in an SBS threshold increase of 1.7. In this case, the result was pump limited. Several high power experiments were also conducted with various thermal configurations. In one case a portion of the output fiber was cooled in ambient conditions to experimentally verify the theoretical prediction that this technique would form an intrinsic thermal gradient due to quantum defect heating thus increasing the SBS threshold beyond a factor of 2. In this configuration over 120 W of single-frequency light was generated demonstrating an SBS threshold enhancement of 3.3 times the single tone case. In the highest power result, a 203 W fiber amplifier was constructed by employing this two-tone concept in conjunction with an externally applied thermal gradient yielding the highest reported output power of a co-pumped Yb doped, PM single-frequency amplifier.

Finally, a detailed theoretical investigation of the SBS process in an optical fiber with a phase modulated signal was explored. A theoretical framework was developed that represents transient effects of the SBS process in both gain and passive fibers under phase modulated pump conditions. Using this model, the SBS threshold was characterized for both a single-sinusoidal phase modulation function and one generated by a WNS. In the former it was concluded that the SBS threshold closely resembles the analytic approximation of [17] in the case of large modulation frequency but fails when the modulation frequency is smaller than the spontaneous Brillouin linewidth. For the latter, it was shown that the analytic approximation of [53] fails to accurately

predict the SBS threshold for short fibers and that the SBS threshold enhancement of a broad-band pump depends strongly on the length of fiber.

7.2 SUGGESTIONS FOR FUTURE WORK

Several concepts could be explored which build and expand on the ideas presented in this dissertation. First, concepts, which address the FWM problems inherent in the SBS mitigation concept of mutli-tone seeding at twice the Brillouin shift, could be investigated. One possible solution would be to employ the concept in a highly dispersive optical fiber which would reduce phase matching of the FWM sidebands. Additionally, one could study the suppression of FWM in specialty fibers such as photonic-band gap fibers which could be manufactured to create frequency selective guiding. Second, one could investigate using the SBS suppressing concept of laser gain competition in conjunction with other SBS suppressive techniques. In this work, only combined SBS suppression with a thermal gradient was explored. Some other techniques to mitigate SBS include acoustic tailoring of the fiber core, phase modulation of the single-frequency seed, and application of stress to the fiber surface. The combination some or all of these concepts in conjunction with laser gain competition could allow for further power scaling in fiber amplifiers. Finally, the time-dependent model of the SBS process could be used to characterize the SBS threshold for several phase modulation schemes not discussed in this work such as sawtooth, square-wave and random bit sequences. A comparative study of the different schemes could be useful in determining the optimal modulation scheme for maximum SBS suppression with minimal linewidth broadening. In addition, other nonlinear effects such as FWM and laser gain could be incorporated into this model to further study how these effects interact with phase modulation to determine the SBS threshold.

References

1. Robert W. Boyd, *Nonlinear optics*, Second edition, Academic press, (2003).
2. Jeffrey P. Koplow, David A. V. Klimer, and Lew Goldberg, "Single-mode operation of a coiled multimode fiber amplifier," *Opt. Lett.* **25**, 442-444 (2000).
3. Y. Jeong, J. Nilsson, J. K. Sahu, D. N. Payne, R. Horley, L. M. B. Hickey, and P. W. Turner, *IEEE J. Sel. Top. Quantum Electron.* **13**, 546 (2007).
4. S. Gray, A. Liu, D. T. Walton, J. Wang, M. Li, X. Chen, A. B. Ruffin, J. A. Demeritt, and L. A. Zenteno, "502 Watt, single transverse mode, narrow linewidth, bidirectionally pumped Yb-doped fiber amplifier," *Opt. Express* **15**, 17044-17050 (2007).
5. C. Robin, I. Dajani, and F. Chiragh, "Experimental studies of segmented acoustically tailored photonic crystal fiber amplifier with 494 W single-frequency output," *Fiber Lasers VIII: Technology, Systems, and Applications*, Proc. of SPIE Vol. **7914**, 79140B (2011).
6. Anping Liu, "Stimulated Brillouin scattering in single-frequency fiber amplifiers with delivery fibers," *Opt. Express* **17**, 15201-15209 (2009).
7. P. Weßels, P. Adel, M. Auerbach, D. Wandt, and C. Fallnich. "Novel suppression scheme for Brillouin scattering." *Opt. Express*, **12**, 4443-4448 (2004).
8. Y. Jeong, J. K. Sahu, D. N. Payne, and J. Nilsson, "Ytterbium-doped large-core fiber laser with 1 KW of continuous-wave output power," *Electron. Lett.* **40**(8), 470-472 (2004).
9. T. R. O'Meara, "The multidither principle in adaptive optics," *J. Opt. Soc. Am.*, **67**(3), 306-315 (1976).
10. F. J. Kontur, I. Dajani, Y. Lu, and R. J. Knize, "Frequency-doubling of a CW fiber laser using PPKTP, PPMgSLT, and PPMgLN," *Opt. Express* **15**(20), 12882-12889 (2007).
11. C. A. Denman, P. D. Hellman, G. T. Moore, J. M. Telle, J. D. Drummond, and A. L. Tuffli,

- “20 W CW 589 nm sodium beacon excitation source for adaptive optical telescope applications,” *Opt. Mater.* **26**(4), 507–513 (2004).
12. E. Rochat, K. Haroud, and R. Dändliker, “High power Nd-doped fiber amplifier for coherent intersatellite links,” *J. Quantum Electron.* **35**(10), 1419–1423 (1999).
 13. R. W. Boyd, K. Rzazewski, and P. Narum. “Noise initiation of stimulated Brillouin scattering,” *Phys. Rev. A* **42**, 5514 (1990).
 14. S. A. Akhmanov, K. N. Drabovich, A. P. Surkhorukov, and A. S. Chirkin, *Zh. Eksp. Teor. Fiz.*, **59** (1970), 485; *Sov. Phys. JET*, **32** (1971), 266.
 15. V. I. Bespalov, A. A. Betin, G. A. Pasmanik, and A. A. Shilov, *Pis'ma Zh. Eksp. Teor. Fiz.* **31**, 668 (1980); [*Sov. Phys. JETP Lett.* **31**, 630 (1980)]; [M. V. Vasil'ev, A.L. Gyulameryan, A. V. Mamaev, V. V. Ragul'slioi, P. Semenov, and V. G. Sidorovich, *ibid.* **31**, 673 (1980) [*ibid.* **31**, 634 (1980)]; and N. G. Basov, I.G. Zubarev, A. B. Mironov, S. I. Mikhailov, and Y. Yu. Okulov, [*ibid.* **31**, 685 (1980)][*ibid.* **31**, 645 (1980)].
 16. E. Lichtman , A. A. Friesem, R. G. Waarts, and H. H. Yaffe, “Stimulated Brillouin Scattering excited by two Pump Wave in Single-Mode Fibers,” *JOSA B* **4**, 1397-1403 (1987).
 17. E. Lichtman , R. G. Waarts, and A. A. Friesem, “Stimulated Brillouin Scattering Excited by a Modulated Pump Wave in Single-Mode Fibers,” *Journal of Lightwave Technology* **7**, 171-174 (1989).
 18. B. Ya. Zel'dovich, N.F. Pilipetskii, and V. N. Shkunov, “Principles of Phase Conjugation.” (Springer-Verlag, Berlin, 1985).
 19. G. C. Valley, “ A review of stimulated Brillouin scattering excited with a broad-band pump laser,” *IEEE J. Quantum Electron.* **QE-22**, 704. (1986).

20. R. Bernini, A. Minardo, and L. Zeni, "An accurate high-resolution technique for distributed sensing based on frequency-domain Brillouin scattering," *IEEE Photon. Technol. Lett.* **18**, 280-282 (2006).
21. Minardo, Aldo, Testa. Genni, Zeni. Luigi, and Romeo Bernini. "Theoretical and Experimental Analysis of Brillouin Scattering in Single-Mode Optical Fiber Excited by an Intensity and Phase-Modulated Pump. *Journal of Lightwave Technology.* **28**, 193-200. (2010).
22. Kovalev. V.I, Kotova. N. E., and R.G. Harrison. "'Slow Light' in stimulated Brillouin scattering: on the influence of the spectral width of pump radiation on the group index." *Opt. Express.* **17**. 17317-17323. (2010).
23. Aldo Minardo, Romeo Bernini, and Luigi Zeni, "Comment on: "Slow Light" in stimulated Brillouin scattering: on the influence of the spectral width of pump radiation on the group index," *Opt. Express* **18**, 1788-1790 (2010).
24. Aldo Minardo, Romeo Bernini, and Luigi Zeni, "Comment on: "Slow Light" in stimulated Brillouin scattering: on the influence of the spectral width of pump radiation on the group index," *Opt. Express* **18**, 1788-1790 (2010).
25. V. I. Kovalev, N. E. Kotova, and R. G. Harrison, "'Slow Light" in stimulated Brillouin scattering: on the influence of the spectral width of pump radiation on the group index: Reply," *Opt. Express* **18**, 1791-1793 (2010).
26. Willems. F.W. , Muys. W., and J.S. Leong. "Simultaneous Suppression of Stimulated Brillouin Scattering and Interferometric Noise in Externally Modulated Lightwave AM-SCM Systems." *IEEE Photonics Tech. Lett.* **6**. 1476-1478. (1994).

27. F. W. Willems, J.C. van der Plaats, and W. Muys, "Harmonic distortion caused by stimulated Brillouin scattering suppression in externally modulated lightwave AM-CATV systems." *IEEE Electron. Lett.* **30**, 343-345. (1994).
28. P. Gabla and E. Leclerc, "Experimental investigation of stimulated Brillouin scattering in ASK and DPSK externally modulated transmission systems," *European Conf. Optical Commun. ECOC. ThC10-5*. 657-660. (1993).
29. J. Yang, Z. Guo, and K. Zha, *Chinese J. Lasers (in Chinese)* **28**, 439. (2001).
30. Y. Liu, Zhiwei Lü, Y. Dong, and Q. Li. "Research on stimulated Brillouin scattering suppression based on multi-frequency phase modulation." *Chinese Optics Letters*. **7**. 29-31. (2009).
31. Goodno. G. D. McNaught. S.J. , Rothenberg. J.E. et al. "Active phase and polarization locking of a 1.4kW fiber amplifier." *Opt. Lett.* **35**, 1542-1544. (2010).
32. D. Marcuse, *Theory of dielectric waveguides*, Academic press, 1991.
33. Iyad Dajani, Clint Zeringue, and T.M. Shay,"Investigation of nonlinear effects in multi-tone driven narrow linewidth high power amplifiers", *IEEE J. Sel. Top. Quantum Electron.* **15**(2), 406-414 (2009).
34. Iyad Dajani, Christopher Vergien, Craig Robin, and Clint Zeringue, "Experimental and theoretical investigations of photonic crystal fiber amplifier with 260 W output," *Opt. Express* **17**, 24317-24333 (2009).
35. P. C. Becker, N. A. Olsson, and J. R. Simpson, *Erbium-doped fiber amplifiers, Fundamentals and technology*, Academic Press, 1999.
36. K. Lu and N.K. Dutta,"Spectroscopic properties of Yb-doped silica glass", *J. Appl. Phys.* **91**, 576 (2002).

37. F. Patel, *Ph.D. Dissertation*, University of California, Davis (2000).
38. J. Anderegg, S. Brosnan, E. Cheung, P. Epp, D. Hammons, H. Komine, M. Weber, and M. Wickham, "Coherently coupled high power fiber arrays," *Proc. SPIE* **6102**, 61020U (2006).
39. J. E. Kinsky, C. X. Yu, D. V. Murphy, S. R. Shaw, R. C. Lawrence, and C. Higgs, "Beam control for a 2D polarization maintaining fiber optic phased array with a high-fiber count," *Proc. SPIE*. **6306**, 63060G (2006).
40. V. Daneu, A. Sanchez, T. Y. Fan, H. K. Choi, G. W. Turner, and C. C. Cook, "Spectral beam combining of a broad-stripe diode laser array in an external cavity," *Opt. Lett.* **25**, 405- 407 (2000).
41. T. H. Loftus, A. M. Thomas, P. R. Hoffman, M. Norsen, R. Royse, A. Liu, and E. C. Honea, "Spectrally beam-combined fiber lasers for high-average-power applications," *IEEE J. Sel. Top. Quantum Electron.* **13**, 487-497 (2007).
42. L. G. Cohen, "Comparison of single-mode fiber dispersion measurement techniques," *J. Lightwave Technol.* LT-3, 958 (1985).
43. M. Li, X. Chen, J. Wang, S. Gray, A. Liu, J. Demeritt, A. B. Ruffin, A. M. Crowley, D. T. Walton, and L. A. Zenteno, "Al/Ge co-doped large mode area fiber with high SBS threshold," *Opt. Express* **15**, 8290-8299 (2007).
44. S. Gray, A. Liu, D. T. Walton, J. Wang, M. Li, X. Chen, A. B. Ruffin, J. A. Demeritt, and L. A. Zenteno, "502 Watt, single transverse mode, narrow linewidth, bidirectionally pumped Yb-doped fiber amplifier," *Opt. Express* **15**, 17044-17050 (2007).
45. M. D. Mermelstein, M. J. Andrejco, J. Fini, C. Headley, and D. J. DiGiovanni, "11.2 dB SBS Gain Suppression in a Large Mode Area Yb-Doped Optical Fiber," *Fiber Lasers V: Technology, Systems, and Applications*, *Proc. SPIE* **6873**, 68730N (2008).
46. Anping Liu, "Stimulated Brillouin scattering in single-frequency fiber amplifiers with delivery fibers," *Opt. Express* **17**, 15201-15209 (2009)

47. M. Hildebrandt, S. Büsche, P. Wessels, M. Frede, and D. Kracht, “Brillouin scattering spectra in high-power single-frequency ytterbium doped fiber amplifiers,” *Opt. Express* **16**(20), 15970–15979 (2008).
48. R. G. Smith, “Optical power handling capacity of low loss optical fibers as determined by stimulated Raman and Brillouin scattering,” *Appl. Opt.* **11**(11), 2489–2494 (1972).
49. Yingfan, L., Zhiwei, L., Yongkang, D., and Qiang, L., “Research on stimulated Brillouin scattering suppression based on multi-frequency phase modulation,” *Chin. Opt. Lett.* **7**, 29-31 (2009).
50. Yang, J., Guo, Z., and Zha, K., *Chinese J. Lasers (in Chinese)* **28**, 439 (2001).
51. Willems, F.W., Muys, W., and Leong, J.S., “Simultaneous Suppression of Stimulated Brillouin Scattering and Interferometric Noise in Externally Modulated Lightwave AM-SCM Systems,” *IEEE Photonics Tech. Lett.* **6**, 1476-1478. (1994).
52. Goodno. G.D, McNaught. S.J., Rothenberg. J.E, et. al, “Active phase and polarization locking of a 1.4 kW fiber amplifier,” *Opt. Lett.* **35**, 1542- 1544 (2010).
53. Agrawal, G., [Nonlinear Fiber Optics], Academic Press, (2007).
54. Gabla, P.M., and Leclerc, E., “Experimental investigation of stimulated Brillouin scattering in ASK and DPSK externally modulated transmission systems,” *European Conf. Optical Commun., ECOC, ThC10-5*, 657-660 (1993).
55. Raymer, M.G. and Mostowski, J., “Stimulated Raman scattering: unified treatment of spontaneous initiation and spatial propagation” *Phys. Rev. A* **24**, 1980-1993 (1981).
56. Williamson III, R.S., “Laser Coherence Control Using Homogeneous Linewidth Broadening.” U.S. Patent No. 7,280,568, Oct. 9 (2007)

